

# Porosity and surface controls of porous carbon materials by multistep activation and pore-size-selective surface modification

兪, 瑤

<https://hdl.handle.net/2324/4110530>

---

出版情報 : Kyushu University, 2020, 博士 (工学) , 課程博士  
バージョン :  
権利関係 :

多段階賦活および細孔径選択的 surface 改質による  
多孔質炭素材料の細孔および表面制御

**Porosity and surface controls of porous  
carbon materials by multistep activation  
and pore-size-selective surface  
modification**

2020 年 9 月

九州大学

総合理工学府

量子プロセス理工学専攻

指導教員：宮脇 仁

**MIYAWAKI Jin**

俞 瑶

**YU Yao**

# Contents

<b>Contents</b> .....	2
<b>Abstract</b> .....	3
<b>Abstract (Japanese)</b> .....	6
<b>Chapter 1 General introduction</b> .....	8
1.1 From the ordered graphite to disordered porous carbons .....	8
1.2 Porous carbon materials .....	12
1.3 Activated carbon (AC) .....	18
1.4 The porosity of porous carbons .....	22
1.5 The surface properties of porous carbons .....	27
1.6 Scope and objectives of this thesis .....	32
<b>Chapter 2 The porosity tuning of activated carbons by multistep activation</b> .....	35
2.1 Introduction .....	35
2.2 Experimental .....	36
2.3 Results and discussion .....	39
2.4 Conclusion .....	49
2.5 Future work .....	49
<b>Appendix for Chapter 2</b> .....	52
<b>Chapter 3 Pore-size-selective control of surface properties of porous carbons by molecular masking</b> .....	62
3.1 Introduction .....	62
3.2 The proposed strategy for pore-size selective surface modification .....	63
3.3 Experimental .....	64
3.4 Results and discussion .....	67
3.5 Conclusion .....	72
<b>Chapter 4 The controllability of size-selective-modifications by various pre-masking agent and heating temperature</b> .....	75
4.1 Introduction .....	75
4.2 Experimental .....	79
4.3 Results and discussion .....	82
4.4 Conclusion .....	91
4.5 Future work .....	91
<b>Appendix for Chapter 3 and Chapter 4</b> .....	93
<b>Chapter 5 General conclusions</b> .....	101

# Abstract

Porous carbon is a big family of indispensable materials in modern-day environmental & energy-related technologies, chemical industry and electronics field. Besides the common merits of carbon materials as high thermal stability, good electrical & thermal conductivity, the porous structure gives it excellent adsorption abilities, making it a versatile material as sorbents and storage media, catalyst/ catalyst supports, electrodes materials of energy storage and conversion devices, and so forth.

Among the many factors, porous texture and surface chemistry are the two pivotal aspects that largely condition the adsorption properties of porous carbons.

As for the porosity, the controlling the specific surface area, pore volume, and more importantly, the pore size distribution (PSD) are the keys to improve the performance in many applications. One of the most famous porous carbon, activated carbons (AC) are usually produced by the activation of natural coals and chars, the latter can be the artifacts by carbonizing of biomass or polymers. Although the improvement of surface area and pore volume, as well as the adjustment of average pore size of ACs, are available, besides the effective porosity, there are still large number of unserviceable pores whose size are too wide or too narrow in ACs. The reason of such a usually broad PSD in AC can be attributed to the inhomogeneous gasification/removal of carbon during activation process. In typical activation process, the char and activation agent react with each other at the set temperature for once, and the incomplete contact and the local temperature differences easily happened.

Synergistically with the porosity, surface chemistry governs the performance especially for porous carbons working as catalyst support/catalyst and adsorbents. The surface property is determined by the types, amount, and the distribution of surface functional groups. In spite of the extensive body of literature describing entire-surface modifications by introducing and removing surface functionalities, only one report was related to the pore-size-selective surface modification utilizing the molecular sieving effect of porous materials to selectively modify the surface of certain pores.

In this thesis, aiming at improving the performance and exploiting new functionalities of porous carbons, porosity and surface controls by multistep activation and pore-size-selective surface modification were trialed: (1) Pore size distribution (PSD) narrowing by multistep activation by physical and chemical activations; (2) Pore-size-selective surface modification based on molecular pre-masking; (3) Arbitrary controllability of the proposed size-selective surface modifications.

The conclusions of this study are briefly summarized as follows:

In **Chapter 1**, starting from the hierarchical structure carbon materials, the disordered turbostratic structure of porous carbons (activated carbon) was introduced. The specific structure of certain porous carbon decides the parameters, which can be classified into porosity and surface chemistry, thus its bulk properties and the resulting performance in applications. Based on the structure, the porosity and surface chemistry, as well as the corresponding tuning methods were discussed.

**Chapter 2** tried stepwise activation process under various mixing/reaction conditions to obtain narrower PSD by trials of homogeneous activation. A once-activated carbon was chosen as the starting material. As the activation agent for second-step activation, physical activation using steam or CO<sub>2</sub> and chemical activation with KOH were adopted. The physical second-step activation didn't see further development in porosity nor observable narrowing in PSD. However, two factors in the KOH second-activation narrowed the PSD of AC; one was to slow down the heating rate during KOH activation, and the other was to mix the activating agent and starting carbon material by solution impregnation before the activation. Both approaches were applied to induce uniform distribution of activating agent on overall carbon surface in already introduced micropores of once-activated starting sample. Experimental results demonstrated that either single or combined usage of these two approaches was effective to narrow the PSD. By carefully adjusting the mixing and activation conditions in second activation, development of AC with narrow PSD centered at optimized average pore size, which exhibits maximized effective adsorption amount, is highly expected.

In **Chapter 3**, a new strategy incorporating three sequential treatments—molecular pre-masking, surface modification, and unmasking—is proposed for pore-size-dependent control of the surface properties of porous carbon materials. The method was experimentally validated by wide-pore-selective hydrophilization. *n*-Nonane was physically adsorbed into the prepared wide PSD activated carbon with both micropores and mesopores for the pre-masking, followed by room-temperature ozonation for surface modification. With the unchanged porosity indicated by the N<sub>2</sub> adsorption and desorption isotherms at 77 K, different amounts of oxygen-containing functional groups were introduced into samples with and without pre-masking shown by the elemental analysis results. The result of H<sub>2</sub>O adsorption and desorption isotherms at 298 K further confirmed that oxygen-containing functional groups were not introduced into the pre-masked narrow pores, but only to the exposed wide pores without pre-masking. Thus, the wide-pore-selective hydrophilization was

achieved, with no loss in porosity, by applying the aforementioned three-step surface-treatment protocol.

**Chapter 4** further investigated the controllability of the proposed 3-step pore-size-selective surface modification methods explained in detail in **Chapter 3**. It was expected that by adjusting the degree of pre-masking, that is, low pre-masking degree will further expose the narrow pores that should be pre-masked under high pre-masking degree, the pore size range within which the pores are selectively modified should be tunable. Based on this hypothesis, 1) The various vacuum-heating temperature ( $T_{VH}$ ) in pre-masking step for removal of excess adsorbed *n*-nonane; 2) Other pre-masking agents with different boiling point (inter-molecular interaction) were tried in this chapter. As a conclusion, higher  $T_{VH}$  or pre-masking agent with lower boiling point (weaker inter-molecular interaction) led to lower pre-masking degree. By adjusting the pre-masking degree, the pore-size-selective surface modification was verified to be controllable. This 3-step strategy was also applied to commercial microporous activated carbon, and similar effectiveness and the controllability were demonstrated in these samples. The flexibility and universality of this molecular pre-masking-based pore-size-selective surface modification method were well demonstrated here.

**Chapter 5** as the general summary of this thesis was given.

# Abstract (Japanese)

多孔質炭素材料は、炭素材料が有する化学的および熱的安定性、高い電気および熱伝導性に加え、優れた吸着特性を併せ持つ。そのため、分離精製・貯蔵用吸着材、触媒担体、電極材など、多岐に亘る用途で用いられている。その吸着性能を左右するのは、発達した細孔構造とその表面特性である。細孔構造因子の中では、細孔発達度の指標となる比表面積や細孔容量と共に、細孔径とその分布の制御が高機能化・高性能化のカギとなる。代表的な多孔質炭素材料である活性炭は、原料の炭素化・賦活工程を経て調製される。平均細孔径は調整できるものの細孔径に広い分布があり、有効利用できない不要な狭すぎる細孔または逆に広すぎる細孔が含まれている。活性炭の細孔径分布が広い原因の一つとして、賦活工程における炭素化物のガス化が均一に進行しないことが考えられる。通常の賦活工程では、炭素化物と賦活剤を所定の賦活温度で一度に反応させるが、賦活剤との接触や局所温度に差が生じうる。一方、表面特性は表面官能基の種類や量、そして分布に大きく依存する。多孔質炭素材料に存在する全ての細孔の表面について表面官能基を導入・除去する手法は多数あるが、細孔径選択的な表面制御法の報告例はこれまで分子篩効果を用いた一つしかない。

本研究では、多孔質炭素材料の高機能化を目的とし、細孔径分布および表面制御のため（１）多段階賦活処理による細孔径分布狭隘化法の開発、（２）分子マスキング法による細孔径選択的な表面特性改質法の開発、（３）開発した細孔径選択的な表面改質法における制御任意性の向上、に関する研究を行った。本研究における知見は、以下のように纏められる。

第１章では、多孔質炭素材料の用途および製造法、そして多孔質炭素材の機能性と細孔および表面構造の関係について述べた。

第２章では、二段階目以降の賦活条件の影響を精査するためマイクロ孔のみを有する市販の球状活性炭を出発原料に用いて、多段階賦活法による細孔径分布狭隘化について検討した。二段階目以降の賦活手法として、賦活剤に水蒸気または二酸化炭素を用いた物理賦活および KOH を用いた化学賦活を検討したところ、物理賦活ではいずれの条件においても効果的な細孔発達がなされず、また細孔径分布の狭隘化もなされないことを確認した。一方、KOH 賦活においては、賦活昇温速度の低速度化による KOH の細孔深部への拡散性向上または溶液含浸による KOH の細孔内分散性の向上を図ることで、賦活剤である KOH と炭素表面の均一な反応を誘導し、二段階賦活により細孔発達度を高めつつ細孔径分布の狭隘化が可能であることを見出した。

第３章では、細孔径選択的な分子マスキング・表面改質・マスキング剤除去の３ステップからなる、多孔質炭素材料の細孔径選択的な表面改質法を新たに提案し、その実証を行

った。マイクロ孔からメソ孔までの広い細孔径分布を有する疎水性活性炭を用い、分子マスキング剤として  $n$ -ノナン、表面改質法として室温オゾン処理法を採用して、狭い細孔は疎水性表面を広い細孔は親水性表面を有する多孔質炭素材料の調製を試みた。77 K 窒素吸着等温線解析の結果、3ステップのいずれの処理によっても元の活性炭の細孔構造はほとんど変化しないことが確認されたのに対し、元素組成分析により室温オゾン処理が酸素含有表面官能基を導入したことが示された。さらに、298 K 水蒸気吸着等温線測定の結果、分子マスキングにより狭い細孔は疎水性のまま保持されたのに対し、広い細孔は酸素含有表面官能基が導入されて親水的表面となったことがわかった。つまり、提案した3ステップ法により、活性炭の細孔径選択的 surface 改質が可能であることを明らかにした。

第4章では、開発した3ステップ法における細孔径選択の制御性について検討した。低いマスキング程度であればより狭い細孔だけが、高いマスキング程度であればより広い細孔までがマスキングされると予想した。つまりマスキング程度を調整できれば表面改質の細孔径選択性も制御できると考え、1) マスキング時のマスキング分子の部分脱着温度、および2) マスキング分子の種類、を変化させて検討を行った。その結果、例えば、部分脱着温度を高くするまたは分子間相互作用が弱いマスキング分子を選択することで低いマスキング程度が誘導でき、逆に部分脱着温度を低くするまたは分子間相互作用が強いマスキング分子を選択することで高いマスキング程度が誘導できた。さらに、マスキング程度を調整することで表面物性の細孔径選択的制御が可能であることを見出し、開発した3ステップ法の汎用性を明らかにした。

第5章では、本研究で得られた主な成果について総括した。



# Chapter 1 General introduction

## 1.1 From the ordered graphite to disordered porous carbons

As one of the most abundant elements in earth and universe, carbon has the astonishing ability to bond with each other in three different hybrid orbitals, and  $sp$ ,  $sp^2$  and  $sp^3$ , each also shows various possibilities for accepting foreign atoms to form linear, planar, and tetrahedral bonding arrangements; thus, producing various carbon materials.

Most carbon materials (natural and artifacts) used in our lives and industries are mainly composed of the basic C-C bond with  $sp^2$  hybrid. Carbon elements bond each other to form two types of layers/structures, as shown in **Figure 1.1**; the flat planar (graphene) that considered as a part cut from the indefinite planar hexagons is the typical and the most “perfect” structure, and the curved planes/structures contain the pentagon or a heptagon entrapped by hexagons—not both contiguously, which is a necessary condition for the growth of curved  $sp^2$  structures. The curved  $sp^2$  structures form the fullerenes, carbon nanotubes, nanohorns, etc.; known as nanocarbons.

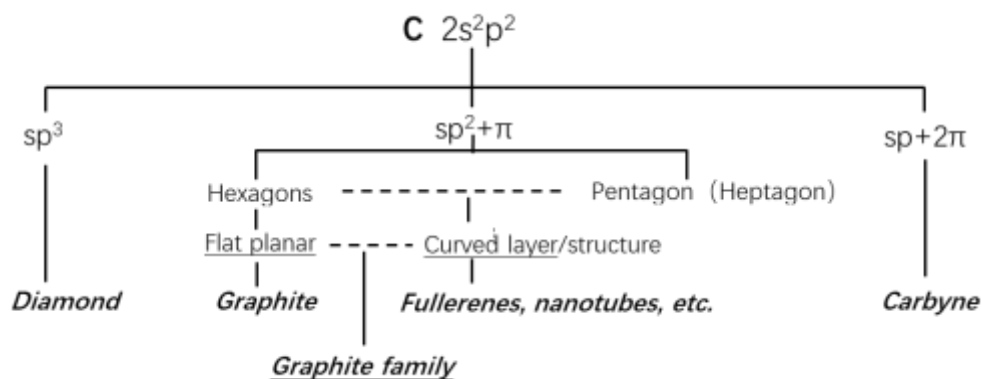


**Figure 1.1.** Classification of carbon materials based on C-C bond nature [1].

**Figure 1.2** summaries the hierarchical structure models of graphite family proposed based on experimental observations. To some extent, they answered the question that how single layer of planar compose the diversified members of graphite family; and what are their differences in nature.

### 1) Single layers to stacking structures

The most “perfect” order that the flat layers are stacked parallel by using  $\pi$ -electron clouds with a regularity of ABAB (the bonds in the layer are covalent and those between the layers are van der Waals-like), which belongs to a hexagonal crystal, and ABCABC stacking to a rhombohedral crystal system, with the latter the can be considered as an extended stacking fault in hexagonal graphite (**Figures 1.2** and **1.3**). The less order ones are the turbostratic stackings with some regularity displaced and rotational structures as shown in **Figure 1.3**.

The layers in these stacking are not necessary to be “perfect” hexagonal structure, but can also be curved, and/or defective ones with vacancies, as shown in **Figure 1.4**. Usually, the defective curved layer in Figure 1.4 contains heteroatoms like oxygen, nitrogen, sulfur and hydrogen etc.

When the stacking order further reduces, no regularity of stacking can be observed; more defective curved layers randomly assembled together even without an observable “laminar” stacking structure; the size of single layers becomes smaller. As a consequence, a wide range of structures from pure ABAB stacking to a completely turbostratic structure with gradually decreasing degree of order is possible.

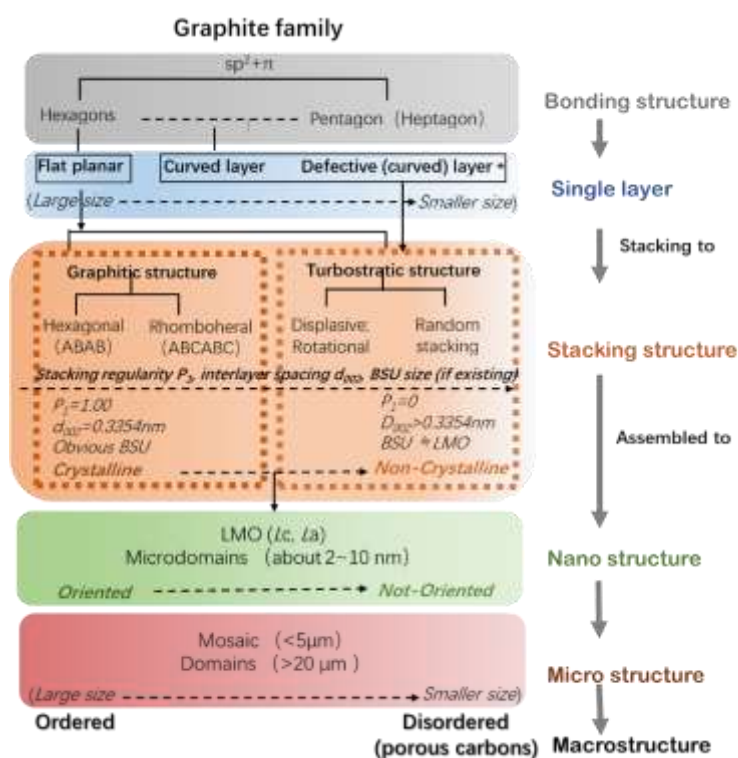


**Figure 1.2.** The structure of graphite carbons.

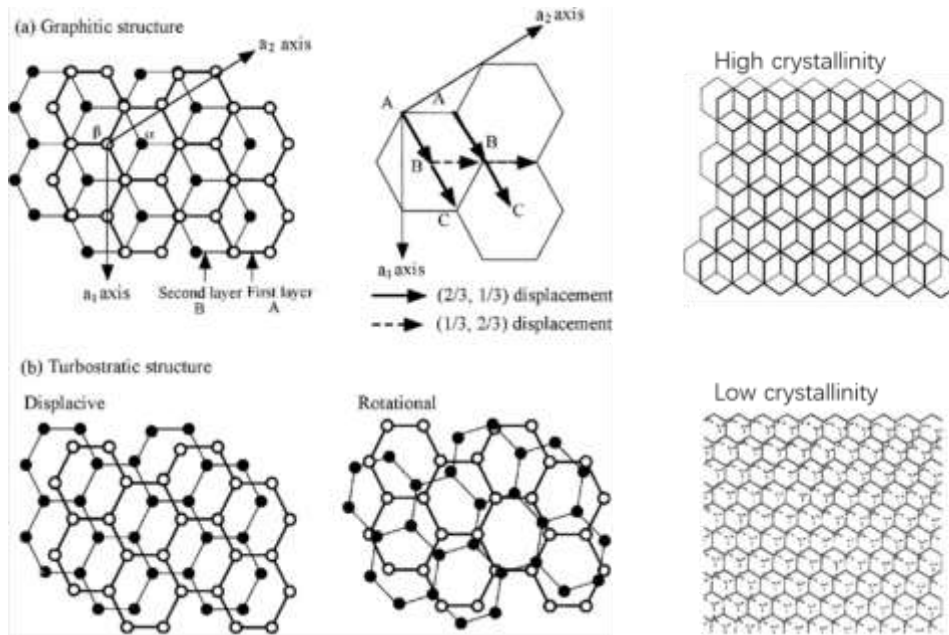


**Figure 1.3.** Graphitic and turbostratic structures shown by stacking of two hexagonal carbon layers [1].

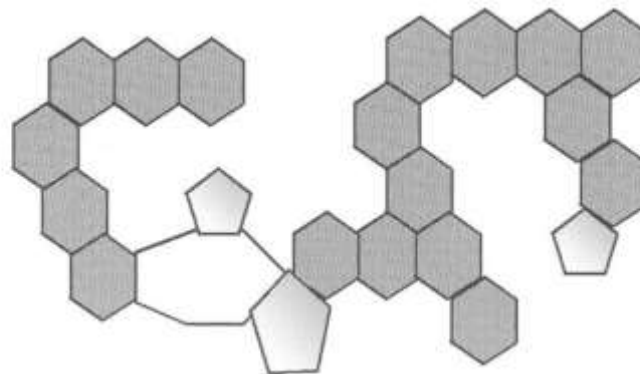


**Figure 1.4.** The basics of the model of a defective graphene layer (non-planar) showing vacancies, and five- and seven-membered ring systems [2].

## 2) From stacking structure to nanostructures

The stacking structures, or be termed in some models as basic structural unit (BSU), assemble each other isotropously/in the same orientation to form the local molecular orientation (LMO), as shown in **Figure 1.5**. The LMOs itself or assembled to form various anisotropic areas. For disordered structures, the size of BUS becomes similar to that of LMO.

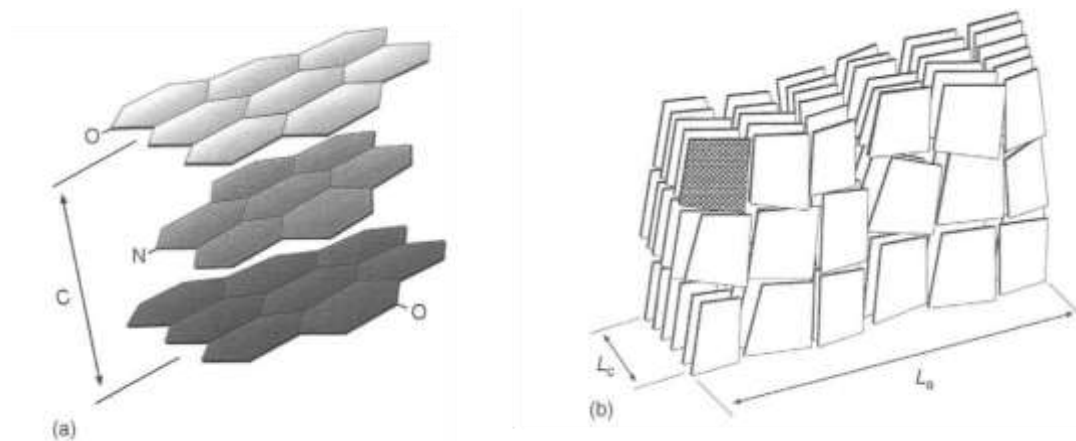


**Figure 1.5.** The model of Basic Structural Unit (BSU) (a), and Local Molecular Orientation (LMO) (b) [3].

### 3) From nanostructures to microtexture

Originated from the common ancestry, “graphite layer”, the graphitic family-derived various textures in different scales depending on the order. The members of “graphitic family” can be ranked according to a continuous decrease in the degree of order. The order here, applies to different scales: from a single layer (perfect hexagonal to curved and/ defective ones), to how these layers are stacked, which can be graphic and turbostratic, to form BSU; how these BSUs assemble together to form LMO or microdomains; and how they further assemble to form microstructures as a mosaic (< 2–5  $\mu\text{m}$ ) and domain (>20  $\mu\text{m}$ ). These microstructures form the macro/bulk carbon materials.

The more graphitic the carbon is, the larger the sizes of the anisotropic areas are. The smaller sizes are being termed mosaics (< 5  $\mu\text{m}$  in size) and the larger sizes are named domains (> 20  $\mu\text{m}$  in size) [3]. To bridge the nanostructures to microstructure, the concept of “microdomain” was proposed by Shiratori *et al.* [4] which can also be taken as a BSU to assemble the domain.

The wide range of graphite carbon artifacts are related to the graphite lattice in some way with each form of carbon representing one of an infinite number of assembled defective graphene layers, some very defective. From the single-crystal hexagonal graphite, progressively, carbons exist in which the graphene layers abandon the ABAB stacking, they become smaller and more defective, to disordered porous materials, until eventually, the existence of identifiable graphene layers is almost lost, as happens with the glassy carbons [3].

Such differences in structure of each scale are originated from the precursors of materials, and largely influenced by the details of the corresponding production processes, in which the temperature may play an important role. Roughly speaking, there are three basic routines to production carbon materials: solid-phase carbonization, liquid-phase carbonization and gas-phase carbonizations. The graphite carbons can be briefly classified into non-graphitizable carbons and graphitizable carbons depending on their graphitization degree after high-temperature heat

treatment ( $> 2400^{\circ}\text{C}$ ). The non-graphitizable carbons were supposed to have a random stacking as shown in **Figure 1.6**.

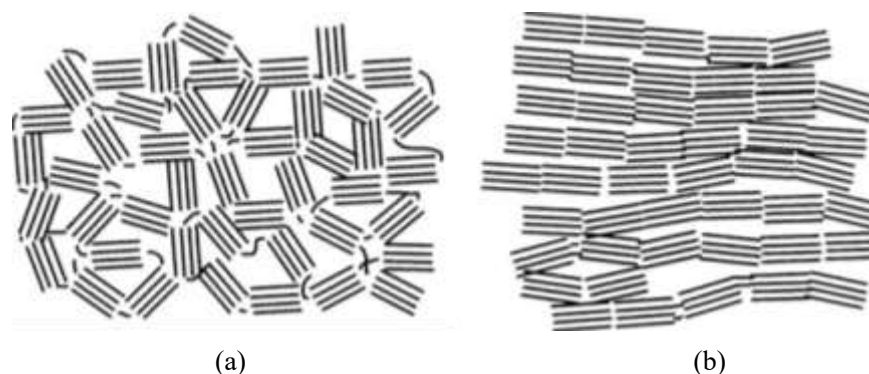


**Figure 1.6.** The Franklin models of (a) non-graphitizable carbons (b) graphitizable carbons [5].

The same origin led to common advantages in bulk properties of carbon materials, like good electrical and thermal conductivities, high resistance to corrosive and toxic environments and chemical stability, high lubrication, the various possibility of macroscopic shaping and the corresponding diverse physical properties (the variety of forms like powders, fibers, cloths, felts, monoliths...), etc. Each property can find its origin and explanations in the structure; similarly, the desired properties can also be obtained by tuning one or more levels of these structures.

More importantly, these abundant varieties in bonding-, nano- and micro- structures led to unique properties of each carbon materials; making the family of carbon materials an indispensable and versatile existence in human society, for example, as electrodes, conductivity materials, lubricant, pigments, carbon fiber reinforced composite, etc.

## 1.2 Porous carbon materials

### 1.2.1 The concept of porous carbons, their applications and classifications

The porous carbon materials, directly, from its name, refers to the carbons that having a porosity resulted from the “disordered” structures. When talking about porous carbon materials, the first impression are charcoals and activated carbons (ACs) and their applications to clean water and remove harmful gases. Besides that, there are many other applications in modern-day environmental & energy-related technologies, chemical industry, electronics field and bio-pharmaceuticals, for example, air and water quality improvement; gas storage and separation; electrodes/catalyzing in secondary battery, fuel cell, EDLC; adsorption heat pump, etc. All these applications can be classified into two main aspects, one is taking advantage of the adsorption properties (gas-phase and liquid-phase) and work as adsorbents., the other is in the field of heterogeneous catalysis working as supporters, or as catalysts itself.

Besides the common merits of carbon materials, porous carbons are benefiting from porous texture and thus the surface chemistry, the two pivotal aspects of porous material that largely condition the applications and the corresponding performance. Porous carbons have many specific features such as high surface area, thermal and chemical stability, and hydrophobic surface properties [6].

In the applications with adsorption phenomenon, these two pivotal aspects: porosity and surface properties, influence the adsorption properties like adsorption and desorption speed, the adsorption heat, and more importantly, the effective adsorption amount. By adjusting the porosity and surface chemistry, we can get better adsorption performance. Similarly, in catalyst field, the separation of catalysts onto the porous surface and catalytic activity are also deeply influenced by both factors.

Porous carbons have been in constant development with increasing members, as listed in **Table 1.1**. from the early charcoal, activated carbons (ACs), to later carbon gels (aerogels, xerogels, cryogels), carbon nanotubes, carbon nanofoams, and hierarchically porous carbons fabricated by molecular design and template methods, etc. also, partially oxidized fullerenes, nanotubes and nanohorns with “window” opened on the “walls” can also be taken as porous materials.

Among them, the traditional activated carbons, activated carbon fibers, and part of template carbons can be grouped together and named as “activated carbon (ACs)”. From the name, the term activated carbon refers to carbon materials manufactured by the activation of natural coals and chars, the latter can be the artifacts by carbonizing of biomass or polymers. The chars are pyrolyzed by high-temperature (from 773 to 1273 K) of various vegetative residues (*i.e.*, wood chips, peat, coal, nutshells and pits, etc.) as well as pitch and polymer substances, namely, carbonization process, and followed by activation to create desirable porous structure of the target materials. All these processes can be taken as the removal of carbon atoms.

The AC is a typical and one of most famous members in porous carbons. It’s still the workhorse nowadays in industry (the principal products and incomes for carbon industries) and our daily life because of its versatile applications and low cost. It has a high specific surface area, well-developed micropores, complex interconnected porosity. What’s more, its tunable porosity and surface chemistry makes it an attractive porous carbon material.

**Table 1.1.** The typical members in porous carbon family.

Classification of carbons	Porous carbons	Activated carbons (ACs)
Classic carbons (~ 1960)	Charcoal	
	Traditional activated carbons	⊙
New carbons (1960~)	Carbon gels	
	Activated carbon fibers (ACFs)	⊙
	Template carbons (uniform/ hierarchically structure)	⊙ (part of)
Nano carbons (~1985)	Carbon nano foams	
	Nanotubes/ Oxidized nanotubes	
	Oxidized nanohorns	
	Oxidized fullerenes	

**Figure 1.7** show the schematic pore images of ACs. Usually, there are three kinds of pores defined by different pore-size-ranges: micro-, meso- and macro pores.

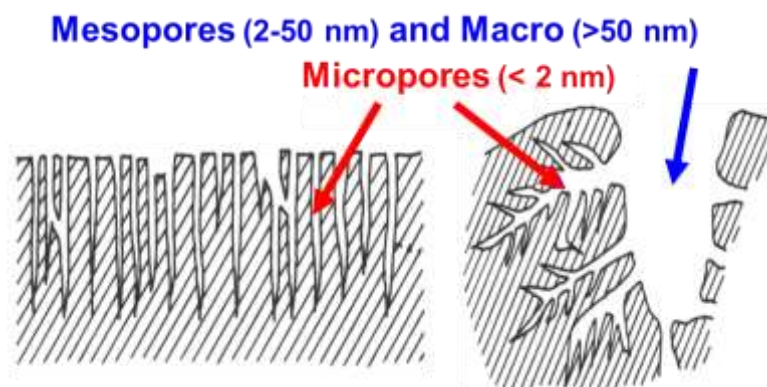


**Figure 1.7.** Schematic microstructure (pore images) of activated carbon fibers (ACFs) (left) and activated carbons (right).

## 1.2.2 The types of the porosity and their roles in applications

The directly observed data by transmission electron microscopy (TEM), scanning electron microscopy (SEM), and scanning tunneling microscopy (STM) together with the various models of pores enable us to make some classification of the pores.

1. Based on their shape, the pores can be basically divided into three types: slit, cylinder and irregular ones (**Figure 1.8**).

The pore shape, together with the pore size, also plays an important role in (selective) adsorption and storage. For example, the bottle-neck pores attribute to special adsorption phenomenon (during desorption). In gas storage filed, it was pointed out that AC have slit-shaped pores, displays the effect of pore size and shape on the packing density of spherical molecules such as those of methane [3].

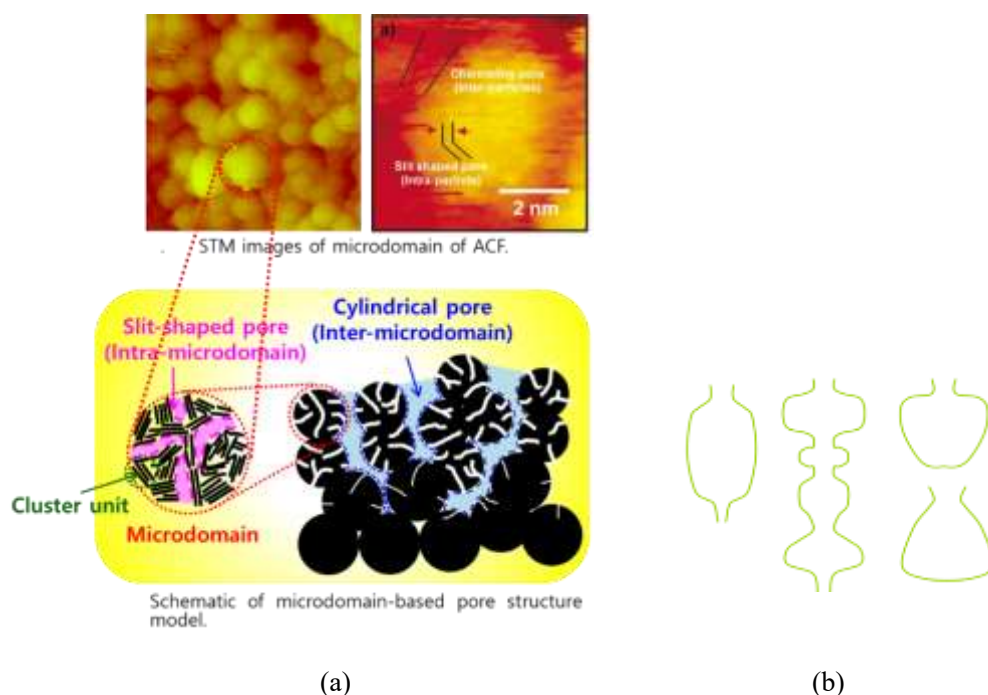


**Figure 1.8.** (a) The schematic of slit-shaped and cylinder pore based on the microdomain-based pore structure model [4], and (b) The schematic of irregular pores (bottle-neck pores).

2. As mentioned in **Section 1.2.1 (Figure 1.7)**, we can divide the porosity according to its size as listed in **Table 1.2**. The corresponding applications of these pores were also briefly summarized in **Table 1.2**.

**Table 1.2.** The different pore size range of ACs and its corresponding specific applications.

Pore types based on size	Size	Applications/Roles [1, 7]
Micropores	< 2 nm: ultra-micropores (< 0.7 nm) super-micropores(0.7–2.0 nm).	Molecular sieving carbons, gas phase adsorption (small gas molecules) , adsorption of atoms, ions, gases, odors
Mesopores	2–50 nm	Gas-phase adsorption (VOCs and etc.), liquid-phase adsorption (polymer, dye or vitamin, even bacteria), small virus, protein molecular; hosts for enzyme immobilization, bulky pollutants, as electrodes for EDLCs and fuel cells.
Macropores	> 50 nm	Virus, Bacteria, macromolecular

\*Size here: for slit-shaped pores, the size means pore width; while for cylinder-shaped pores, the size here refers to pore diameter.



3. Depending on whether the pores are accessible or not, they are divided as open pore and closed pores (latent pores).

The schematic images of open and closed pores are given in **Figure 1.9**.

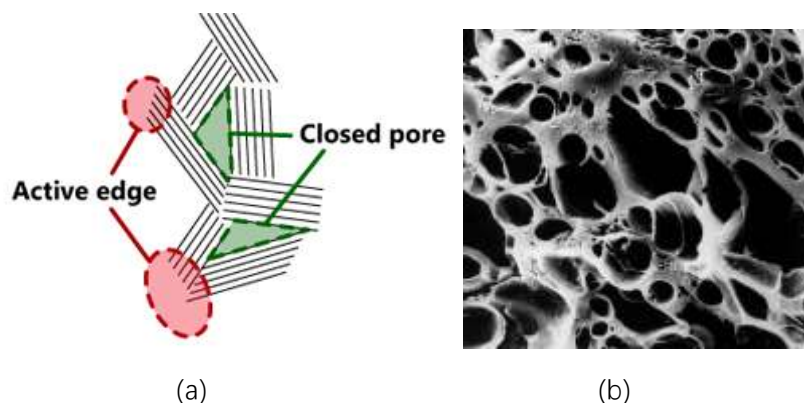


**Figure 1.9.** (a) Schematic pictures of closed pores [8], (b) Open pores directly observable [9].

### 1.2.3. The origin of porosity and surface chemistry in porous carbons

The two key factors: porosity and surface properties of porous carbons, especially ACs are tunable to improve the performance and exploit new applications as aforementioned. To well-control these two aspects, it's necessary for us to know where are the porosity and surface properties come from.

For the porous nanocarbons (**Table 1.1**) like nanotubes, where the porosity comes from the space “encapsulated” by the curved walls; similarly, the porosity of graphite porous carbons (ACs) originates from its structure.

For traditional porous carbons, like activated carbons (ACs), based on the original (porous) structure of precursors, and the further removal of carbon atoms by carbonization and mainly by activation process leads to the final connectively complex porosity within ACs. To some extent, AC can be taken as the porosity (space) enclosed by carbon atoms.

Let's return back to the well-known hierarchical structure models detailed introduced in **Section 1.1**. As shown in **Figure 1.10**, the perfect graphite layers which are planar and hexagonal, stack together to form the basic structural unit (BSU); then these units assemble together to form the local molecular orientations (LMO) composed nano structures. Each level of this model is highly-ordered for a perfect graphite.

The porous carbons (ACs) show a similar hierarchical structure but quite disordered in each level. As a highly “disordered” non-graphitized composed of turbostratic structures, the precursor structure and the carbon removal within each hierarchical level may contribute to the porosity.

Structurally, if we look into the hierarchical structure of porous carbon as shown in **Figure 1.10**, the carbon layer is curved with defects, voids, and heteroatoms like O, N, H, and S. These defective layers stack in a less-ordered way, in some real porous carbon, we may not tell such an obvious “laminar” stacking structure, but quite turbostratic ones. And these units of layers will be assembled randomly without orientations.

The vacancies within defective carbon layers (①), the enlarged distances between stacking layers (②), the voids or encapsulated space within the assemblies of BSU (③ closed and open), microdomains and domains can all become part of the porosity. Especially, for ACs, the complex interconnectivity within the porosity system make it an attractive also riddling material. Therefore, the porosity in porous carbons can result from each of these levels shown here.

As for the surface properties, if we look close into one single layer the edges of porous carbon in **Figure 1.10**, the defects and heteroatoms all-together compose the active sites. The surface chemistry of these active sites is largely decided by the position/environment where it is. In this study, we will focus on the surface functional groups composed of heteroatoms.

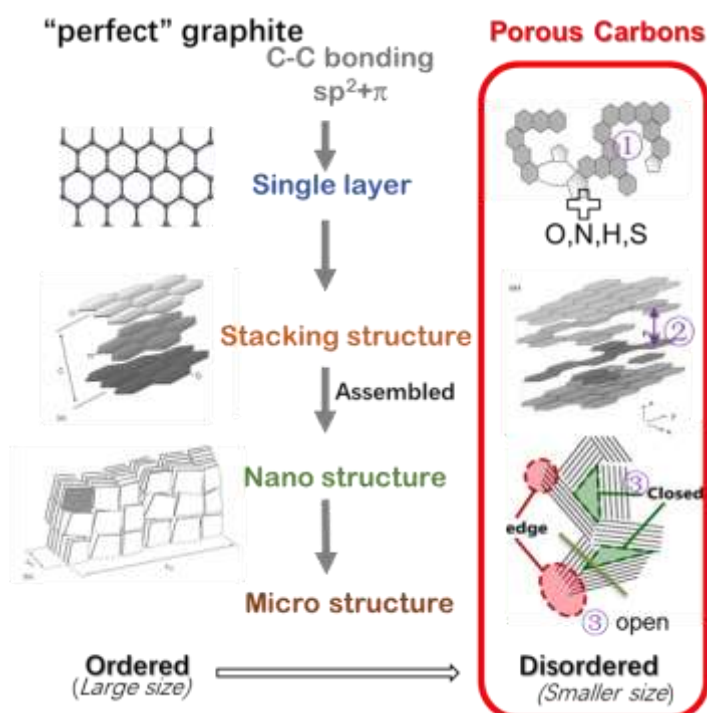


**Figure 1.10.** The structural origin of porosity in porous carbons [10].

#### 1.2.4 The relationship of porosity surface properties both originated from the structure and the macroscopic properties

For porous carbons, both the precursor and the production process determine the its basic structures. Originated from the structure, appear porosity and surface properties, the most important

two aspects as the “expressions” of the basic structure (**Figure 1.11**). These two aspects synergistically decide main bulk properties of porous carbons as adsorbents, carbon molecular sieves, and catalyst support/catalyst.

By analyzing and tuning these factors/parameters, it helps us to understand how they influence the corresponding bulk properties; we can thus predict or explain certain properties of one porous carbon material using these parameters. What’s more, by selecting the proper precursor and designing the reaction process, we can tune these parameters to improve/ get the desirable bulk properties for a target application.

The parameters and bulk properties can be obtained qualitatively and quantitatively by various characterization methods and assessments, as listed in **Figure 1.11**. Also, the nano- and micro-scale analyses, together with the virtual models created by computer simulations, facilitating and enriching our understanding of the structures and the properties/possibility of porous carbons.

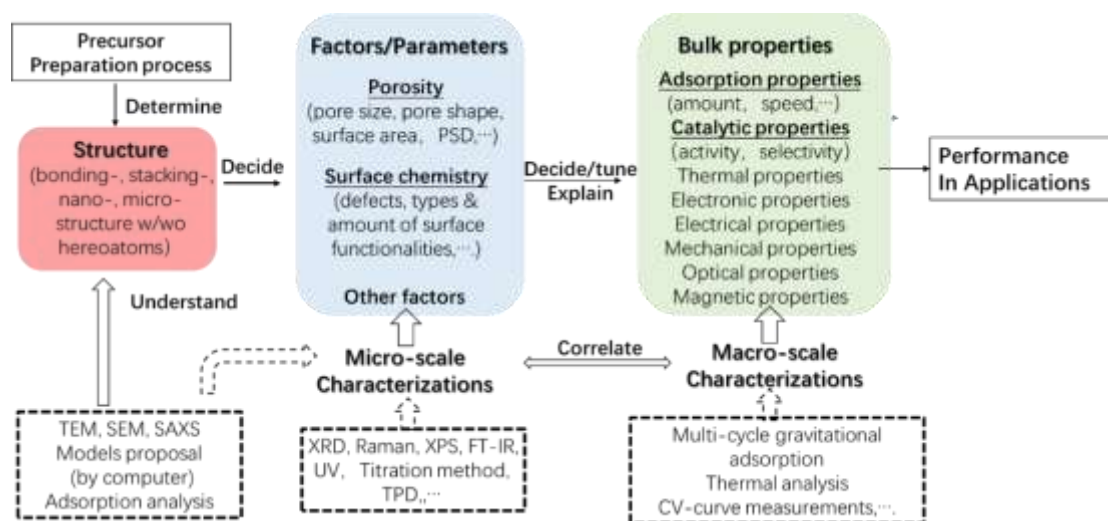


**Figure 1.11.** How the structure influences on the factors and thus bulk properties of porous carbon materials, and the common characterization methods to quantitatively/quantitatively obtain these parameters and properties.

## 1.3 Activated carbon (AC)

### 1.3.1 The production of porous carbons

In porous carbon preparation, solid-phase carbonization is used for charcoal and AC preparations, Liquid-phase carbonizations for ACF preparation and in template-method, while the gas-phase carbonizations for nanocarbons and pyrolytic carbons [3], the mechanism involved are significantly different.

**Table 1.3** shows the main methods for porous carbon preparation. For the production of activated carbons (AC), although the template method can give a uniform or well-designed porosity, the cost and the complexity largely limited its application in mass industrial production. On the other hand, the more traditional activation method, the synthesis of uniform porous carbon materials (a narrow pore size distribution) has been very challenging [11].

**Table 1.3.** Preparation methods of porous carbon materials [12].

Method	Process and agent			Carbon precursor	Characteristics of preparation	Characteristics of porous carbon	
Carbonization method	Pyrolysis under oxygen-poor atmosphere			Wood, bamboo, coal, organic waste	Exothermic reaction	Charcoal	Smaller pore size than activated carbon
Activation method	Activation agent	Gas	Steam, carbon dioxide, air	Charcoal from wood, fruit shell, coal, resin	Endothermic reaction	Activated carbon	Microporous
		Dehydrator	Zinc chloride, phosphorus acid	Sawdust	Simultaneous reactions of carbonization and activation		Mesoporous
		Alkali	Potassium hydroxide, sodium hydroxide	Charcoal, mesocarbon microbeads, coconut shell charcoal	High activation yield		High specific surface area
Template method	Template	Silica gel, zeolite, mesoporous silica, layered clay, surfactant micelle		Organic polymer, organic monomer	Dissolution of template materials after carbonization	Pore size dependent on template	
Heat elimination method	Elimination gas	Hydrochloric acid gas, hydrofluoric acid gas		Vinyl chloride resin, vinylidene chloride resin, saran	Only heat treatment	Narrow pore size distribution	
Polymer blend method	Pore formation material	Polyethylene glycol, urethane, poly (vinyl butyral)		Poly ( para-phenylene pyromellitimide), polyamide, phenolic resin	Evaporation of pore formation materials during carbonization	Large pore size	
Vapor-phase growth method	Gasification method	Low-pressure arc, laser evaporation, catalytic CVD, torch arc, vacuum arc		Graphite, graphite containing metal catalyst	High temperature treatment, Low production efficiency	Carbon nanotube, Carbon nanohorn	
Sol-gel method	Condensation catalyst	Sodium carbonate		Resorcinol-formaldehyde solution	Super-critical drying, Freeze drying	Mesoporous and microporous	

### 1.3.2 Activation mechanism for structure formation and surface properties

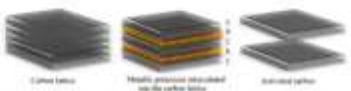
As mentioned before, the porosity (also the surface chemistry) of activated carbons is originated from original porosity of the precursor, also the production process in which a part of the carbon atoms was moved from the precursor by activation reactions.

In this section, the activation mechanism will be introduced to discuss the porosity formation process. The selections of precursors are also mentioned.

During the endothermic physical activation by steam and CO<sub>2</sub>, the most reactive amorphous components are burned off, which is taken as selective reaction. Another approach, chemical activation, consists of heat treatment in the presence of alkali (KOH, NaOH), inorganic acids (H<sub>2</sub>SO<sub>4</sub>, H<sub>3</sub>PO<sub>4</sub>), or salts (ZnCl<sub>2</sub>, K<sub>2</sub>S) in an inert atmosphere at temperatures from 873 K to 1073 K; which can be taken as non-selective removal of carbon atoms catalyzed by the activating agent or their decomposed products. The gasification mechanism and metal intercalation mechanism for alkali hydroxyls (KOH, NaOH) were proposed.

**Table 1.4** briefly summarizes the mechanism of physical activation (steam and CO<sub>2</sub>) and chemical activation (KOH) and the porosity development during activations. For gas activation, through the endothermic reactions between carbon and activation gas, the porosity was developed by selectively gasification to removal part of the carbon atoms. The porosity development can be summarized in three aspect. For KOH activation, similar to gas activation in physical activation, one of the main mechanisms of KOH activation is catalyzed non-selective gasification. The other mechanism of KOH activation, is the intercalation happened when the temperature is higher than 700°C. The formed metallic potassium can diffuse into the vapor phase and was movable during the high-temperature activation process, which was also shown by Marsh and Mochida [13]. As a synthetic effect of these two mechanisms, the porosity development of KOH activation can be attributed to the gasification process, and also, the fast removal of intercalates and enlarged lattice due to intercalation.

**Table 1.4.** The reaction mechanism and the porosity development process of physical and chemical (KOH) activation. [3, 14].

Two types	Physical (gas) activation	Chemical activation
Typical agents	Steam, CO <sub>2</sub> , and their mixture	KOH (NaOH)
Mechanism	<b>Endothermic selective gasification</b> of carbon by steam/CO <sub>2</sub> (mainly at 800-1000°C)	<p><b>Catalyzed non-selective gasification</b> of carbon by oxidative gases (H<sub>2</sub>O, CO<sub>2</sub>, CO) formed during KOH &amp; C reactions (catalyzed by alkali metals and salts)</p> $2\text{KOH} \rightarrow \text{K}_2\text{O} + \text{H}_2\text{O} \quad (\text{a})$ $\text{C} + \text{H}_2\text{O} \rightarrow \text{CO} + \text{H}_2 \quad (\text{b})$ $\text{CO} + \text{H}_2\text{O} \rightarrow \text{CO}_2 + \text{H}_2 \quad (\text{c})$ $\text{CO}_2 + \text{K}_2\text{O} \rightarrow \text{K}_2\text{CO}_3 \quad (\text{d}) \quad [15]$ <p><b>Intercalation (&gt; 700°C)</b> Penetration of free metal into inter-layer space of graphitic layers</p> $\text{K}_2\text{O} + \text{H}_2 \rightarrow 2\text{K} + \text{H}_2\text{O} \quad (\text{e})$ $\text{K}_2\text{O} + \text{C} \rightarrow 2\text{K} + \text{CO} \quad (\text{f}) \quad [15]$
How porosity developed	<p><b>Gasification:</b></p> <ul style="list-style-type: none"> <li>(I) Opening of previously inaccessible pores</li> <li>(II) Creation of new pores by selective gasification</li> <li>(III) Widening of existing pores</li> </ul>	<p><b>Gasification:</b> (I) (II) (III) in the left</p> <p><b>Intercalation (micropores):</b></p> <ul style="list-style-type: none"> <li>1) Rapid removal of layers and intercalation</li> <li>2) Expansion of lattice</li> </ul> 

Main factors that influence the activation process for physical activations are: reaction temperature, partial pressure of the reacting gas and heating rate. For KOH/NaOH activation, similarly, the reaction temperature, activation agent concentration (KOH:C weight ratio), heating rate, flow rate of inert carrier gas (usually N<sub>2</sub>) will play a role. The initial state of the dispersion of KOH/NaOH is important to maximize the contact between activation agent and the carbon surface. By controlling these influence factors, the porosity tuning during activation is available.

One of the merits of chemical activation is that for biomass-originated precursors, the carbonization and activation are finished in one-step. Usually, the pores formed within ACs has a wide range of pore size, there is a trade-off between narrow pore size distribution (PSD) and developed porosity. The other important advantage of chemical activation, especially KOH activation gives an uniform pore structure, namely, narrow (PSD) with rather developed porosity.

### 1.3.3 The selection of precursor

As discussed previously, except the preparation process, the porosity development of porous carbon is also largely dependent on the precursor. Not only the porosity, surface properties of AC, can also originated from both the precursors and the activation process [17].

When we select or molecular design a precursor, the reactivity at activation/production process, target applications and required porosity like pore framework/ density, and surface properties need to be taken into consideration.

Biomass provides an economic environmental choice, however, collection from separated areas, transportation, bulk availability and seasonal variations in quality and availability are reasons why these resources are not widely used in production. In this study, spherical phenol resins as-supplied BEAPS series (ASAHI YUKIZAI CORPORATION, Japan.), (**Figure 1.12**) were chosen as the precursor out of its stable properties as the precursor and less ash content of the final production, which facilitate the comparison of experimental conditions. In addition, it keeps the spherical shape after the carbonization and activation as it does not melt at high temperatures. Apparently as-supplied BEAPS shows orange color and some bubbles were observed inside of the particles. It may be expected to form during the manufacturing the BEAPS.



**Figure 1.12.** The pictures of spherical phenol resins.

### 1.3.4. Classification of ACs

The general classification of ACs based on particle size divides them into Powder type of Activated Carbon (PAC) (a typical particle size of less than 0.1 mm and the common size of the

particle ranges from 0.015 to 0.025 mm), Granular type of Activated Carbon (GAC) (size between 0.6 to 4 mm), and Activated Carbon Fibers (ACF). These carbon artifacts are related to each other with the defective micro-graphene layer that is the totally central to the structure of AC. These graphene-like layers in ACs can have defects, contain heteroatoms, or foreign species chemically bonded, whose arrangements and coordination of carbon atoms determine the type of nanostructure.

Beside the precursor and the preparation process, the shape of the activated carbon affects its pore structure, properties and performance [18].

## 1.4 The porosity of porous carbons (representative: activated carbons)

### 1.4.1 The characterization of the porosity

Table 1.5 summarized the methods to investigate the porosity. Figure 1.13 gives the detectable scales of usual experimental methods to get the information of porosity. Among them, only the gas adsorption/desorption isotherms, using molecules such as N<sub>2</sub>, Ar, CO<sub>2</sub>, and He as probes, can provide the information of porosity. Small-angle X-ray scattering (SAXS) is the only way to directly assess the closed pores.

**Table 1.5.** The ways to investigate the porosity.

Classifications			Obtained Information
<b>Experimental characterization</b>	Adsorption	Gas adsorption/desorption isotherm using probe molecules (N <sub>2</sub> , Ar, CO <sub>2</sub> , He): N <sub>2</sub> @77 K, Ar@87 K, CO <sub>2</sub> @298 K	Overall porosity: Surface area, average pore size, micropore volume, external surface
		Interaction with surface: <sup>129</sup> Xe-NMR	The average pore size (chemical shift)
	SAXS		Only way to assess closed pores
	Direct observation	HR SEM	Observed range (Local part); the graphic information
HR TEM			
STM			
Computational simulations		Based on the experimental results/ observations.	Try to investigate pore connectivity in porous carbon, especially activated carbons, which can't be obtained by above methods.

For ACs, the N<sub>2</sub> adsorption/desorption isotherms measurement at 77 K is a routine for porosity analysis. To obtain the parameters like, specific surface area, average pore size, pore volume and pore size distributions (PSD). For activated carbon, the  $\alpha_s$ -plot analysis (Figure 1.14) and quenched solid density functional theory (QSDFT) are adopted in this thesis.

QSDFT is a modified version of the non-local density functional theory (NLDFT). Taking into consideration of surface roughness and heterogeneity, it eliminated the drawbacks of NLDFT which assumes a flat graphitic surface structure of pore walls.

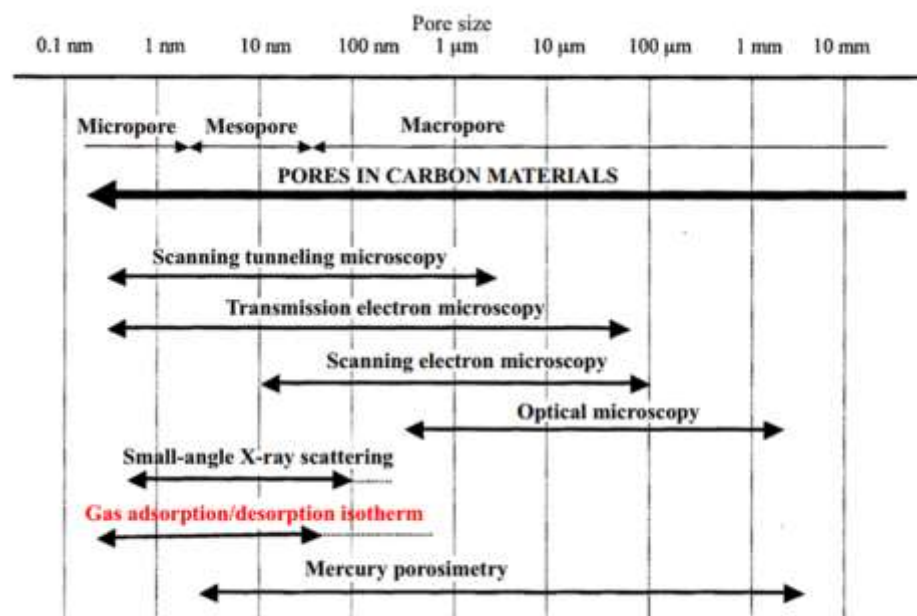


Figure 1.13. Pores in carbon materials and their characterization techniques [19].

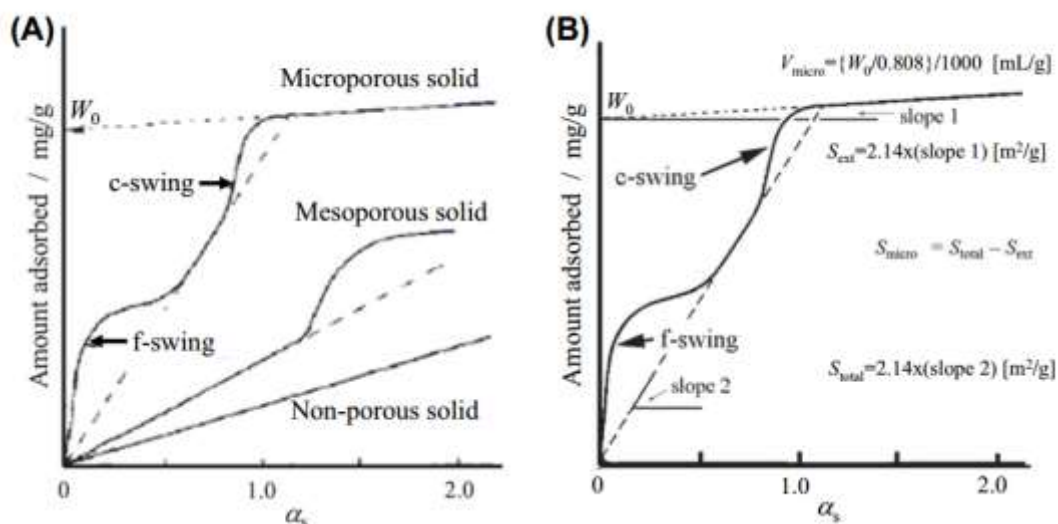


Figure 1.14. Schematic  $\alpha_s$  plots of the isotherms of adsorption branch of  $N_2$  at 77 K. (A) Schema for nonporous, mesoporous and microporous solids and (B) scheme for microporous carbon with calculation procedure of pore parameters [19].



## 1.4.2 The importance of porosity and its tuning

As shown in **Figure 1.11**, the porosity is the most basic character of porous carbon. Based on it, the physical and chemical properties of pore surface enable porous carbon to be an indispensable and promising materials as electrode for electric double layer capacitor (EDLC), adsorbents (environmental and gas storage), and catalyst supports. These pores possess intense van der Waals force-originated interaction potentials (from the near proximity of carbon atoms) and these are responsible for the adsorption process.

In carbon molecular sieves for gas separation, the 0.1-nm difference in pore size will lead to 10 times difference in adsorption speed [12]. The pore volume will decide the total adsorption amount for physical adsorption. The pore size and the pore size distribution, for short, PSD will influence the effective adsorption amount.

In the applications taking advantage of adsorption, there will always be a working relative pressure range depending on the working conditions, that is, the working window; and the adsorption amount within this range is called effective adsorption amount.

**Figure 1.15** gives an example how the PSD, namely, effective porosity influences effective adsorption amount. Real ACs composed of pores with various width, and usually having a wide pore size distribution (PSD). The wide PSD causes broad adsorption uptakes over a wide range of relative pressure, giving rise to a limited amount of effective adsorption amount. The pores with too small sizes or too large sizes can't make a contribution to the "effective adsorption amount" as the adsorption in these pores happen outside the working pressure range, these pores are "useless" for this application. By narrowing the PSD and centering it at the optimum pore size, the adsorption isotherm gives sharp adsorption uptake, and we can obtain higher effective adsorption amount.

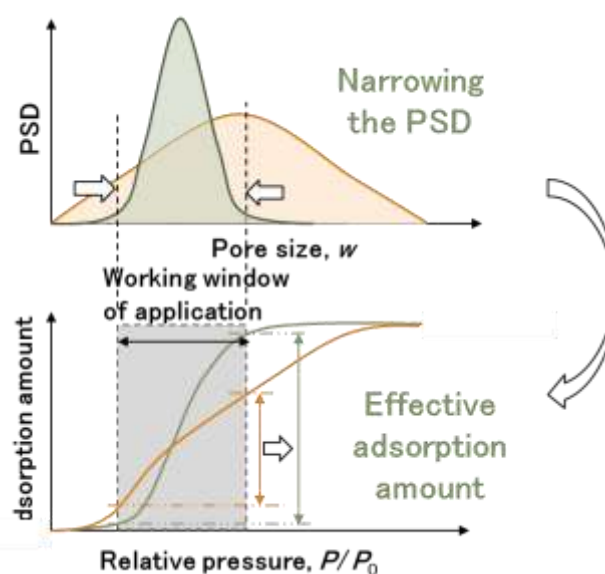


**Figure 1.15.** The influence of PSD on the adsorption performance.

Although the high pore volume and high surface area are certainly still important target to be pursued, As shown in **Table 1.2 (Section 1.2.2)**, different kind of pores (pore size) are corresponding to specific applications. Therefore, depending on the target purposes and applications the 1) fine tuning of pore size; 2) a narrow PSD, and 3) design of hierarchical porosity (ideal electric devices [20] are becoming vital to further improve the performance.

With a suitable porosity that the majority falls into the “efficient” window instead of an over-developed porosity with a part being effective for a certain application, the less dose, higher efficiency, as well as better mechanical properties can be realized in practical applications.

### 1.4.3 The porosity tuning methods

Based on the importance of porosity in applications and its tuning, the porosity tuning can be summarized as below.

1. High surface area and high pore volume (traditional)
2. Specified pore size depending on the application (traditional)
3. Designed hierarchical porosity (for electrochemical applications)
4. Uniform porosity, that is, narrow PSD

To achieve the goal to get as much “effective” porosity as possible, the porosity tuning, especially the PSD is a key topic.

**Table 1.6** gives the possible routines to tune the porosity for porous carbon materials.

As a kind of the bottom-up preparation, template method provides many alternative template agents and carbon-precursors. However, the complexity of the process and the cost are considerable deterrents to the use on a wide scale.

For traditional top-down preparation, usually the carbonization and/or activation of the bulk precursors, the methods to adjust the porosity can be divided according to the 3 stages: before, during, and after the production process by precursor choose/tuning, reaction conditions, and post-treatment, respectively.

In this study, by using spherical phenol resin as a precursor, various process conditions ( $N_2$  flow rate, heating rate, activation agents type & amount, mixing method, soaking time), also the mixing of physical and chemical activations, and chemical vapor deposition (CVD) post-treatment were trialed aiming at realizing the porosity tuning was investigated. As a result, the multi-step KOH activation using solution mixing method and lower heating rate was proved to be obviously effective in porosity tuning, which will be introduced in **Chapter 2**.

**Table 1.6.** Possible methods to control the porosity for graphitic carbon materials (Nano-pore size control technologies).[7]

Control method			Source (examples)	Control factor (examples)
Precursor		Proper chose (mainly for natural source)	Halogen-containing resin	The origin porosity of precursor, the reactivity in carbonization/activation, the content of metal or ash; composition; particle size,
		Production/Modification (mainly for artificial precursor)	Halogen-containing resin; Changing the type of either metal cation or ion exchangeable function group of resin	Composition of source, modification method & conditions (ex. heat treatment temperature, heat treatment time) additives (to artificial material)
		Mixing/Blend	Polymer blend method [21], Mixing of coal and organic additives Mixing of resins	Mixing ratio
		Molecular design [17] (for resins, and precursor of bottom-up)	C-containing organic materials (mainly for bottom-up composition)	
Control during pore formation	Top-down	Carbonization	Charcoal, resin, coal, biomass	Carbonization temperature, soaking time, gas flow rate
		Activation (Catalytic activation)	Natural/carbonized char	Activation method, agent, activation temperature, soaking time, heating rate, gas flow rate, binder (add proper catalyst and the impregnation condition)
	Bottom-up	Template method	Various template materials	Precursor choose/molecular modification/ design, template agent, process conditions
Post-treatment		Coating	Activated carbon, carbonized coal, carbonized biomass	Species and composition of impregnant, carbonization temperature
		Vaper deposition	Microporous activated carbon, coke, carbonized resin	Source of pyrolyzed carbon (aromatic hydrocarbon, aliphatic hydrocarbon, etc.), heat treatment temperature, heat treatment time
		Thermal shrinkage	Carbonized resin, carbonized coal	Heat treatment temperature, heat treatment time

	Oxidation (open windows for nanostructure porous materials; or further selectively remove carbon	Activated carbon, carbonized char, Nano-structure materials	Agent, reaction temperature, time
--	--	--	--------------------------------------

Note 1: Catalytic activation

## 1.5 The surface properties of porous carbons (representative: activated carbons)

### 1.5.1 The surface chemistry of ACs

The bonding nature of carbon atoms allows various possibilities for accepting foreign atoms, when it comes to the surface chemistry of carbon materials, the flexibility offered by porous carbons is rather unique because of the unique proton-, electron-, and oxygen-transfer characteristics.

The disordered “turbostratic” porous carbons (ACs) based on defective non-planar carbon layers, the defective layers have a large number of imperfections and defects (structural carbon vacancies, nonaromatic rings), contain heteroatoms or foreign species chemically bonded on both basal and edge carbon atoms.

Basal and edge carbon atoms are two different sites distinguishing in the reactivity with other molecules and in their susceptibility to undergoing chemical reactions. The imperfections and defects along the edges of graphene layers are the most active sites, owing to the high densities of unpaired electrons. On them, heteroatoms such as O, H, N, and S can be chemisorbed, leading to stable surface compounds.

These functionalities are not only responsible for the development of surface charge, but also for the “chemical activity” of carbons (especially at low temperatures) because of the  $sp^2$ -hybridized aromatic carbon atoms with a delocalized  $\pi$ -electron system. Together with the original active sites, the formed heteroatom-containing functional groups as the second-active sites can be further active sites of sorption and reaction, or as anchor sites for heteroatoms, chemical moieties, metals, and particles to realize more diversified functionalities.

The concentration and the distribution of active sites and surface functionalities depend to a large extent on the structure of the carbon material. Small and disordered crystallites/BSU can expose more edges; therefore, more surface groups can be formed.

The chemical complexity of the carbon surface and the fact that the heteroatoms are located in confined space means that the chemical reactivity/adsorption ability of the specific groups are affected by their local environment. The most direct example is that those in the basal plane (i.e., within graphene sheets) are much less (re)active.

### 1.5.2 The types of heteroatoms and surface functional groups

The common surface functional groups can be divided into oxygen-containing groups, nitrogen-groups, hydrogen groups, sulfur groups and halogenated groups.

Among them, oxygen-containing groups is the ubiquitous and most widely studied type in carbon materials. Although less famous than oxygen (at least they have been studied to a lesser extent), nitrogen and sulfur surface groups also play their role in many applications.

Figure 1.16 gives the common species of these three types.

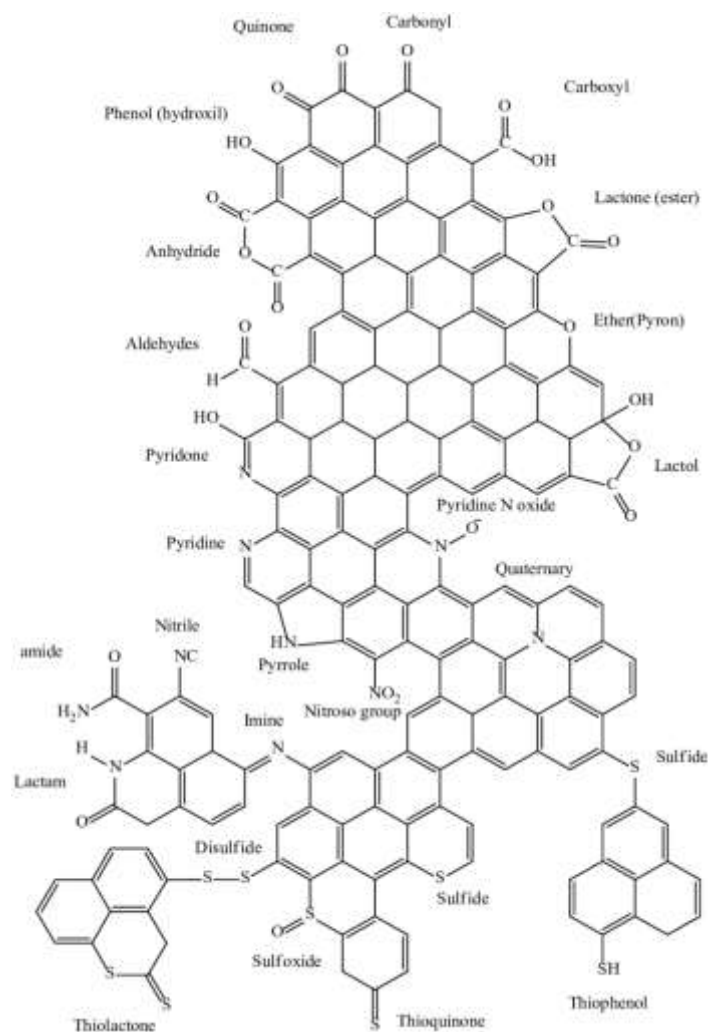


Figure 1.16. The main types of O, N and S containing surface functional groups [22].

### 1.5.3 The characterization of surface functionalities

The types and concentration of the relevant surface functional groups can be determined by temperature-programmed desorption (TPD), X-ray photoelectron spectroscopy (XPS), FT-IR (in-situ DRIFT), UV spectroscopy, Boehm titration, polar-molecular adsorption & desorption isotherms, and so on.

Among them, only the TPD seems to be the best method in the aspect to providing the information of overall material, while only the adsorption can directly provide the position of surface functionalities within the porosity system. For example, H<sub>2</sub>O adsorption isotherm measurement is the most powerful method to analyze the location of oxygen-containing functional groups especially for porous materials.

### 1.5.4 The importance of surface chemistry and its tuning

Nature, type, and distribution of surface functionalities all play a vital role in adsorptive properties, dispersion of supported catalysts, catalyst activity, electrochemical performance, biocompatibility, water repellency and etc. What's more, the introduced/existing surface functional groups can also serve to tether many different types of heteroatoms, chemical moieties, particles, biomolecules to opening a door to new functions and applications.

Surface properties are at the heart of almost all catalytic applications, chemisorption, and polar molecule adsorption. Taken the most commonly types, oxygen-containing functional groups as an example, here just listed 3 aspects where they may play a role:

- 1) They can influence the agglomeration and surface diffusion of catalyst particles across the graphene layers (not always beneficial);
- 2) Surface oxygen complexes also affect the electronic density of the graphene layers, so affecting the dispersion interactions between the carbon surface and adsorptive molecules. Carboxyl groups fixed at the edges of the graphene layers have the ability to withdraw electrons, whereas phenolic groups release electrons.
- 3) Surface oxygen complexes affect the surface hydrophobicity, which determines the hydrophobic interaction. In general, an increase in the oxygen content of carbon brings about a decrease in its hydrophobicity. As shown in **Figure 1.17**, when surface functionalities such as oxygen-containing surface functional groups are introduced, the onset of water adsorption shifts to a lower relative pressure; also, the adsorption capacity increases. This indicates that adsorption of polar molecules such as water is strongly influenced by oxygen containing surface functional groups. Therefore, the introduced polar surface groups will allow the pressure of the predominant adsorption uptake of polar molecules to be adjustable.

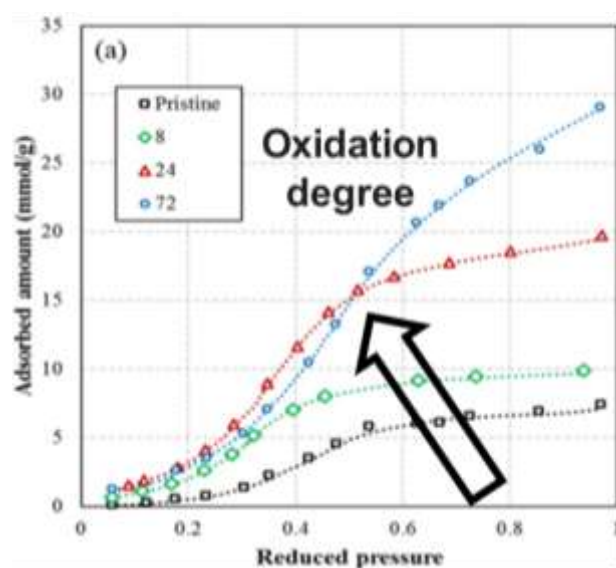


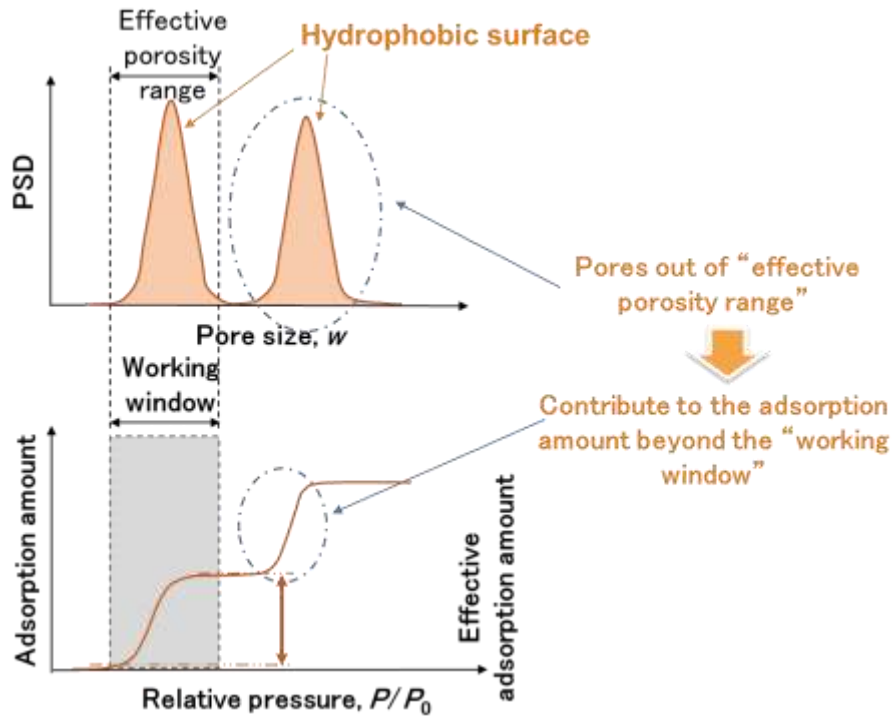
**Figure 1.17.** The influence oxygen-containing groups on the onset of water adsorption and the adsorption capacity [23].

**Figure 1.18** gave a detailed example of polar molecular physical adsorption to show how surface functional groups influence on the adsorption performance independently from porosity. The concept of “effective” porosity was introduced in **Section 1.4.2**. The example here shows that without tuning the porosity (sometime it is difficult), how the modification in surface chemistry turns the unusable pores into effective ones that are able to contribute the “effective adsorption amount”, therefore enable the performance improvement.

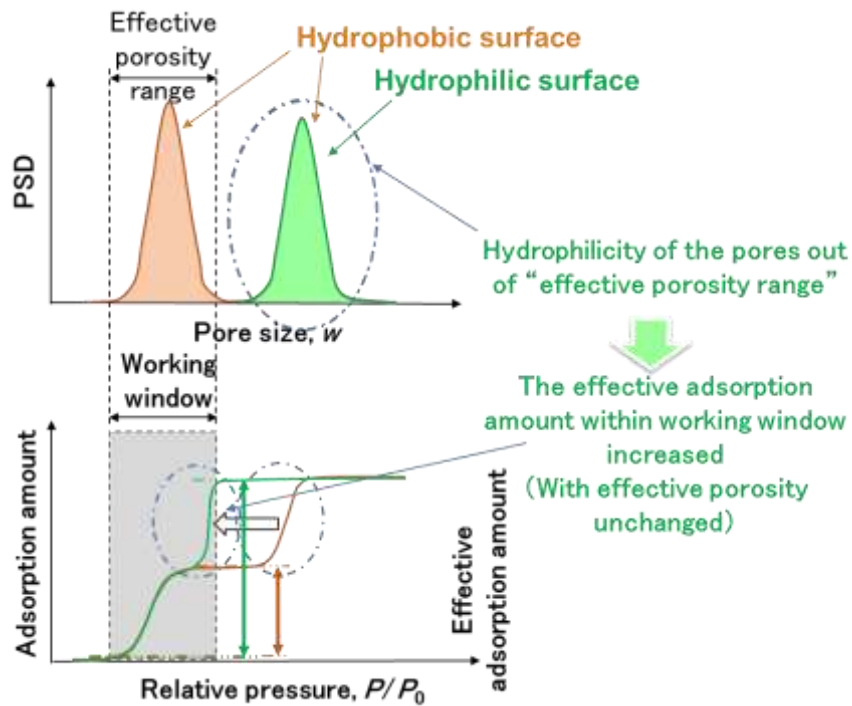
In **Figure 1.18(a)**, AC with a typical bimodal-peak PSD with a usually hydrophobic surface has a two-step adsorption isotherm of polar molecules covering a wide relative pressure range. Only the pores within proper pore-size-range give rise to adsorption uptake in the working pressure range, namely, contribute to the effective adsorption amount. As shown in **Figure 1.18(b)**, if we can change only surface of pores beyond the proper size range from hydrophobic to hydrophilic, the adsorption uptake of polar molecules of these pores will shift to lower relative pressure. Therefore, these pores can also contribute to an increase of the effective adsorption amount.

With the same pore size distribution, the selective change of surface properties (surface functional groups) can shift a part of isotherm curve, thus obviously increase the effective adsorption amount.

Such idea is the initial motivation of this study trying to realize pore-size-selective surface control.



(a)



(b)

**Figure 1.18.** The importance of surface property shown by an example of polar molecule adsorption. With the porosity unchanged, by selective modification the surface of un-effective pores, the adsorption amount contributed by these parts can also be shifted within the working window, namely, made the un-effective pores to be useful for a certain application (from (a) to (b)).



### 1.5.5 The importance of selective surface modifications

There are so many available methods to easily modify the all-surface chemistry by introducing/removing certain types of functional groups depending on the treatment conditions. Large amount of previous studies gave various choices and discussed their possible effect in improving the target performance.

However, similar to the concept of “effective porosity”, surface functionalities also has the effectiveness depending on where they are introduced: Firstly, their activity is largely influenced by the local “environment” where they are located, and secondly, when porous carbons working as catalyst support or adsorbents, the size of doped catalyst particles or adsorbates may depend on the pore size. As a result, only the functionalities or active sites on accessible pores can contact with these enthetic particles/molecules and play a role.

Since the performance of porous carbon is governed by both porosity and surface character, ideally, to exhibit the best performance by fully taking advantage of these two factors simultaneously, each pore should have its own custom surface property depending on its size. Besides the examples shown in **Figure 1.18**, the dispersion of a variety of supported catalysts as a function of pore size could be used to create versatile catalytic systems.

In spite of the obvious and exciting power of size-selective surface modification, rare research provides any strategy to make it into reality. Herein, in this thesis, a new strategy based on molecular pre-masking to realize the above-mentioned pore-size selective modification was proposed and verified.

## 1.6 Scope and objective of this thesis

Porous material (the representative member, activated carbon) is a versatile material as sorbents and storage media, catalyst/catalyst supports, electrodes, etc., was investigated here from the two main aspects, porosity and surface chemistry that largely condition its properties and performance. Both are tunable to make porous carbon an attractive and promising material.

Based on the understanding of its hierarchical structure that determined the porosity and surface chemistry, this thesis focused on pore size distribution (PSD) tuning and size-selective surface modification to improve the performance and exploiting new functionalities of porous carbons:

- (1) Pore size distribution (PSD) narrowing by multistep activation by physical and chemical activations (**Chapter 2**);
- (2) Pore-size-selective surface modification based on molecular pre-masking (**Chapter 3**);
- (3) Arbitrary controllability of the proposed size-selective surface modifications (**Chapter 4**).

## References

- [1] Inagaki M. Kang F. (Eds.) *Materials Science and Engineering of Carbon: Fundamentals*, Second Edition. Elsevier, 2014.
- [2] O'Malley B. Snook I. McCulloch D. Reverse Monte Carlo analysis of the structure of glassy carbon using electron-microscopy data. *Phys Rev B* 1998;57:14148.
- [3] Marsh H. Reinoso FR (Eds.). *Activated carbon*. Elsevier, 2006.
- [4] Shiratori N. Lee KJ. Miyawaki J. Hong SH. Mochida I. An B. Yokogawa K. Jang J. Yoon S-H. Pore structure analysis of activated carbon fiber by microdomain-based model. *Langmuir* 2009;25:7631–7.
- [5] Franklin RE. Gosling RG. G. Molecular configuration in sodium thymonucleate. *Nature* 1953;171:40–1.
- [6] Hao GP. Li WC. Qian D. Lu AH. Rapid synthesis of nitrogen-doped porous carbon monolith for CO<sub>2</sub> capture. *Adv Mater* 2010;22:853–7.
- [7] Kyotani T. Control of pore structure in carbon. *Carbon* 2000;38:269–86.
- [8] [http://www.toyotanso.co.jp/Products/new\\_developed\\_products/cnovel](http://www.toyotanso.co.jp/Products/new_developed_products/cnovel)
- [9] <https://www.pinterest.com.au/pin/573575702516348882/>
- [10] Seaton NA. Friedman SP. MacElroy JMD. Murphy BJ. The molecular sieving mechanism in carbon molecular sieves: a molecular dynamics and critical path analysis. *Langmuir* 1997;13:1199–1204.
- [11] Lee J. Kim J. Hyeon T. Recent progress in the synthesis of porous carbon materials. *Adv Mater* 2006;18:2073094.
- [12] Abe I. Hasegawa T. Preparation methods and pore-size control techniques of nanoporous carbon. *Tanso* 2005;218:197–201.
- [13] Marsh H. Mochida I. Catalytic gasification of metallurgical coke by carbon dioxide using potassium salts. *Fuel* 1981;60:231–9.
- [14] Abe I. Production methods of activated carbon. *Tanso* 2006;225:373–81.
- [15] Otowa T. Tanibata R. Itoh M. (1993). Production and adsorption characteristics of MAXSORB: high-surface-area active carbon. *Gas Separ Purif* 1993;7:241–5.
- [16] Romanos J. Beckner M. Rash T. Firlej L. Kuchta B. Yu P. Suppes G. Wexler C. Pfeifer P. Nanospace engineering of KOH activated carbon. *Nanotechnology* 2011;23:015401.
- [17] Borchardt L. Zhu Q-L. Casco ME. Berger R. Zhuang X. Kaskel S., Feng X. Xu Q. Toward a molecular design of porous carbon materials. *Mater Today* 2017;20:592–610.
- [18] Yang JB. Ling LC. Liu L. Kang FY Huang ZH Wu H. Preparation and properties of phenolic resin-based activated carbon spheres with controlled pore size distribution. *Carbon* 2002;40:911–6.
- [19] Inagaki M. Kang F. (Eds.) *Materials Science and Engineering of Carbon: Characterization*, Second Edition. Elsevier, 2016
- [20] Dutta S. Bhaumik A. Wu KCW. Hierarchically porous carbon derived from polymers and biomass: effect of interconnected pores on energy applications. *Energ Environ Sci* 2014;7:3574–3592.
- [21] Ozaki J. Endo N. Ohizumi W. Igarashi K. Nakahara M. Novel preparation method for the production of mesoporous carbon fiber from a polymer blend. *Carbon* 1997;35:1031–1033.

- [22] Jahromi FG, Ghahreman A. Effect of surface modification with different acids on the functional groups of AF 5 catalyst and its catalytic effect on the atmospheric leaching of enargite. *Colloids Interfaces* 2019;3(2):45.
- [23] Barton SS, Koresh JE. Adsorption interaction of water with microporous adsorbents. Part 1.— Water-vapour adsorption on activated carbon cloth. *J Chem Soc Faraday Trans* 1983;79:1147–55.

# Chapter 2 The porosity tuning of activated carbons by multistep activation [1]

## 2.1 Introduction

Together with specific surface area, pore size is an important pore structural parameter of adsorbents as it governs pressure or concentration at which adsorption of gases or ions takes place. Therefore, there will be a suitable pore size to maximize the adsorption performance depending on the application conditions of adsorbent. One significant index to assess the adsorption performance, the effective adsorption amount, which is the difference between the adsorption amounts at the applied and at the regeneration/recovery pressure or concentration of adsorbate, can be improved by tuning the pore size to optimized value.

Activated carbon (AC) is one of abundantly and often used adsorbents because of its low price, superior adsorption performance derived from the high specific surface area and well-developed pores, which are, more importantly, tunable. It thus indispensable in various applications, like gas storage/separation/purification, wastewater treatment, solvent recovery, catalyst support, energy-storage and conversion, and so on.

Typically, ACs are prepared by carbonization process of raw materials such as biomasses (*e.g.* wood and coconut shell), fossil resources (*e.g.* coal, petroleum, and their derivatives), and polymers (*e.g.* phenolic and acrylic plastics), followed by physical/chemical activation process using activating agents. In general, the chemical activation using agents such as zinc chloride, potassium hydroxide (KOH), and sodium hydroxide, provides ACs with larger specific surface area at higher activation yield than the physical activation using oxidation gases such as steam and CO<sub>2</sub> [2–5].

However, ACs often have relatively wide distribution in pore size. Neither too narrow nor too wide pores can contribute to increase effective adsorption amount. Therefore, narrowing the pore size distribution (PSD) is the key to upgrade the performance and to fulfil further demanding applications. Various studies have been carried out to obtain porous carbon materials with uniform pores and/or ideal PSD by different methods in addition to activation method [6, 7]. As summarized in **Figure 2.1**, the porosity tuning can be either during preparation process or by post-treatment. In the preparation process, the porosity tuning can be classified according to the two main production ways: activation and template methods. Template methods using silica and zeolites gave both mesoporous and microporous carbons with narrow PSD, but a requirement of costly exclusion processes of the templates is a problem [8, 9]. Polymer blend carbonization methods that two types of polymers (carbonizing and pyrolyzing polymers) are used can introduce mesopores, but an induction of narrow PSD (confined pore-size range, small variance and standard deviation values, etc.) is still challenging [10]. Carbon deposition method has been also proposed; this method is available to achieve the pore size control for microporous carbon, but not applicable to carbon materials with wide PSD ranging from micropore to mesopore [11, 12]. Although other interesting

and promising methods have been reported, they also not yet meet the demanding of scale-up production as a mature and cost-effective fabrication process [6, 7]. Thus, it is still a great challenge to produce porous carbon materials with tailored PSD by present-day productive method.

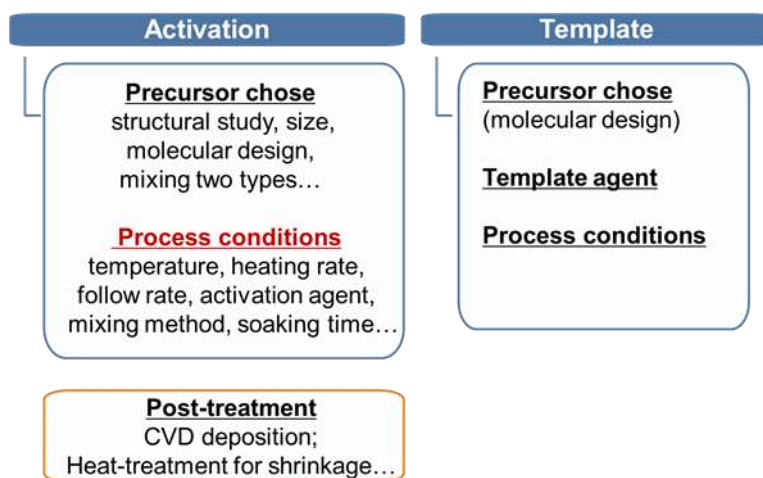


**Figure 2.1.** The candidate methods for porosity control of porous carbons.

A possible reason of wide PSD in ACs prepared by one-step activation process of carbonized species is the inhomogeneous reaction between carbon and activating agent. The activating agent would preferentially contact and react with only part of carbon particles, mainly at their external surface. Therefore, it would be crucial for the homogenous pore developments to induce the uniform reaction of activating agent with carbons not only at the external surface but also at the central parts of carbon particles.

In this study, stepwise activation process under various mixing/reaction conditions was attempted to obtain narrower PSD by trials of homogeneous activation. A once-activated carbon was chosen as the starting material. This sample possesses developed micropores in the microdomains, a basic structural unit (BSU) to constitute carbon particles [13]. By adopting proper conditions in the second activation step, better delivery of activating agent to central parts of microdomains within carbon particles *via* the developed micropores for more uniform reaction was expected.

## 2.2 Experimental

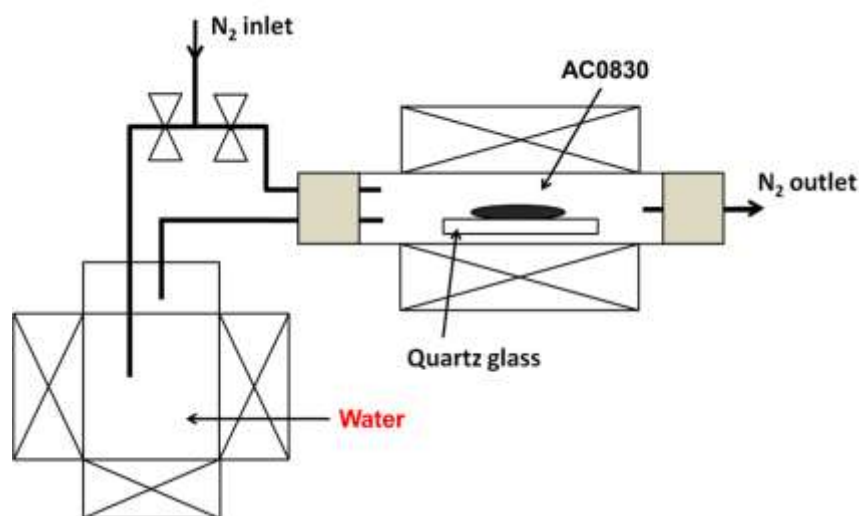
As a starting material, a commercial microporous AC (BEAPS-AC0830, ASAHI YUKIZAI CORPORATION, Japan) was used.

BEAPS-AC0830 was prepared by chemical activation using KOH of carbonized spherical phenol resin (BEAPS; ASAHI YUKIZAI CORPORATION, Japan), though the detailed preparation conditions were undocumented.

The second activation of BEAPS-AC0830 was carried out by physical or chemical activation method. For the physical activation, two kinds of typical activating agents, steam and CO<sub>2</sub>, were adopted. In case of steam activation, BEAPS-AC0830 was heated to 800, 850 or 900°C at a ramping rate of 5 °C/min in N<sub>2</sub> flow (100 mL/min), and then kept at the desired temperature for 1 h in a steam-containing N<sub>2</sub> gas flow (relative humidity ~90%), which was produced by bubbling N<sub>2</sub> through boiling distilled water. The prepared two-step activated samples using steam as the activating agent in the second activation was designated as AxS, where x indicates the activation temperature. **Figure 2.2(a)** gave the schematic of the apparatus for steam activation. For the CO<sub>2</sub> activation, as shown in **Figure 2.2(b)**, BEAPS-AC0830 was heated to 900, 950 or 1000°C at a ramping rate of 5 °C/min in CO<sub>2</sub> flow (100 mL/min), and then held at the desired temperature for 1 h. The prepared two-step activated samples using CO<sub>2</sub> was designated as AxC, where x indicates the activation temperature.

AC preparation by chemical activation was performed using KOH (purity > 85.0%; Wako Pure Chemical Industries, Ltd., Japan) as an activating agent. Two different mixing methods of BEAPS-AC0830 with KOH were applied; one was physical mixing of solid KOH particles with BEAPS-AC0830, the other was solution impregnation, where BEAPS-AC0830 was dispersed in KOH aqueous solution (100 mL) at room temperature for 6 h with a rotation speed of 400 rpm followed by the drying in a vacuum oven at 90°C for about 5 h. The weight ratio of KOH/BEAPS-AC0830 was set to be 4 or 6. The mixture of KOH and BEAPS-AC0830 was heat-treated at 700 or 900°C at a different heating rate of 2.5, 5 or 15 °C/min and then held at the desired temperature for 1 h under N<sub>2</sub> flow (100 mL/min). After the KOH activation, the remaining KOH and the derivatives formed during the activation were removed by washing with HCl aqueous solution and deionized water. The prepared two-step activated samples using KOH as the activating agent in the second activation were named as AxKy-z, where x, y, and z indicate the activation temperature, the KOH/BEAPS-AC0830 weight ratio, and the heating rate, respectively. For samples prepared by the solution impregnation method, a suffix “-(sol)” was given; for example, AxKy-z-(sol).

As a summary, the sample preparation conditions are summarized in **Table 2.1**.



(a)

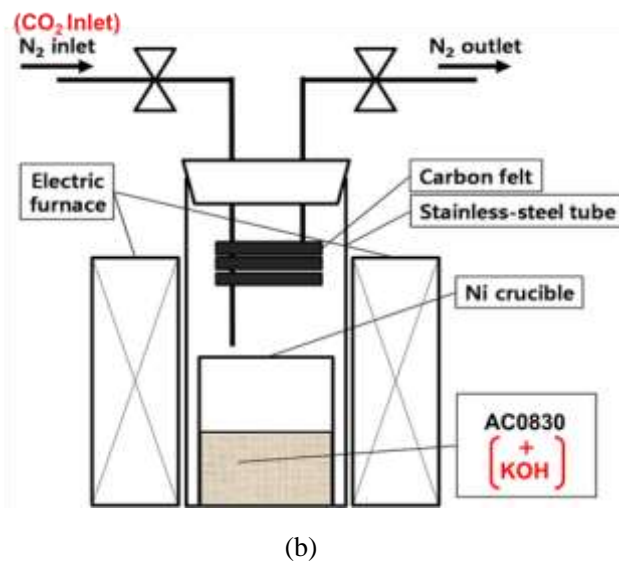


**Figure 2.2.** (a) Schematic of steam activation system; (b) Schematic of KOH/CO<sub>2</sub> activation system; for KOH activation, no flow of CO<sub>2</sub>; similarly, for CO<sub>2</sub> activation, no KOH in the Ni crucible.

**Table 2.1.** Preparation condition of ACs by multistep activation using BEAPS-AC0830 as a starting material.

Starting material: BEAPS AC0830* (Commercial AC with only micro pores)			
	Physical activation		Chemical activation
Agent	Steam	CO <sub>2</sub>	KOH
Agent amount	R.H. = 90%	100 mL/min	KOH : AC0830 (weight ratio) = 4, 6 or 8
Mixing method	—	—	Physical mixing** (solid-phase)   Solution mixing (within ethanol solution)
Activation temperature	750, 800, 850 or 900°C	900, 950 or 1000°C	700, 800 or 900°C
Soaking time	1, 2 or 4 h	20 min or 1 h	1 or 2 h
Heating rate	5 °C/min		2.5, 5 or 15 °C/min
Protection gas	N <sub>2</sub> (100 mL/min)		

\* Originated from the same phenol resin precursor as one-step activation.

\*\* 3-stages activation was also carried out.

N<sub>2</sub> adsorption and desorption isotherms at 77 K were measured using a volumetric adsorption apparatus (Belsorp-Max-S, BEL Japan Inc., Japan) to investigate porosity of the prepared multistep-activated carbons. The pore structural parameters and PSD were calculated using the N<sub>2</sub> adsorption and desorption isotherm data by applying the subtracting pore effect method of  $\alpha_s$  plots [14] and quenched solid density functional theory (QSDFT) method [15] with slit-shaped pore assumption, respectively. It has been reported that the QSDFT method, in which surface geometrical inhomogeneity (surface roughness) is taken into consideration, gives more reliable PSD profiles as compared with conventional non-local density functional theory method [16].

## 2.3 Results and discussion

### 2.3.1 Second activation using steam or CO<sub>2</sub> (physical activation)

Physical activation was firstly applied as the second activation due to its advantage as a low-cost process. **Figure 2.3(a)** shows N<sub>2</sub> adsorption and desorption isotherms at 77 K of the starting material, BEAPS-AC0830, and the two-step ACs activated from BEAPS-AC0830 using steam as the activating agent. The adsorption and desorption branches of BEAPS-AC0830 were well-overlapped with each other in the range of the whole relative pressure,  $P/P_0$ , indicating that BEAPS-AC0830 was microporous material without having mesopores. After the physical activation at 800°C as the second activation step, a small increase of saturated adsorption amount of N<sub>2</sub> was observed, whilst the adsorption amount in the low relative pressure region ( $P/P_0 < 0.2$ ) slightly decreased. These changes were reflected as a small increment of total pore volume,  $V_{\text{Total}}$ , and a decrease of total specific surface area,  $A_{\text{Total}}$ , giving rise to an increase of average pore width,  $w_{\text{Avg}}$ . (**Table 2.2**). PSD estimated by the QSDFT method shown in **Figure 2.3(b)** also suggested the formation of wide micropores at the expense of narrow micropores. However, the degree of these changes was quite limited. When the activation temperature increased, the N<sub>2</sub> adsorption amounts decreased for whole  $P/P_0$  region as compared with those of BEAPS-AC0830. Especially for A900S (second activated at 900°C with steam), both  $V_{\text{Total}}$  and  $A_{\text{Total}}$  decreased remarkably.

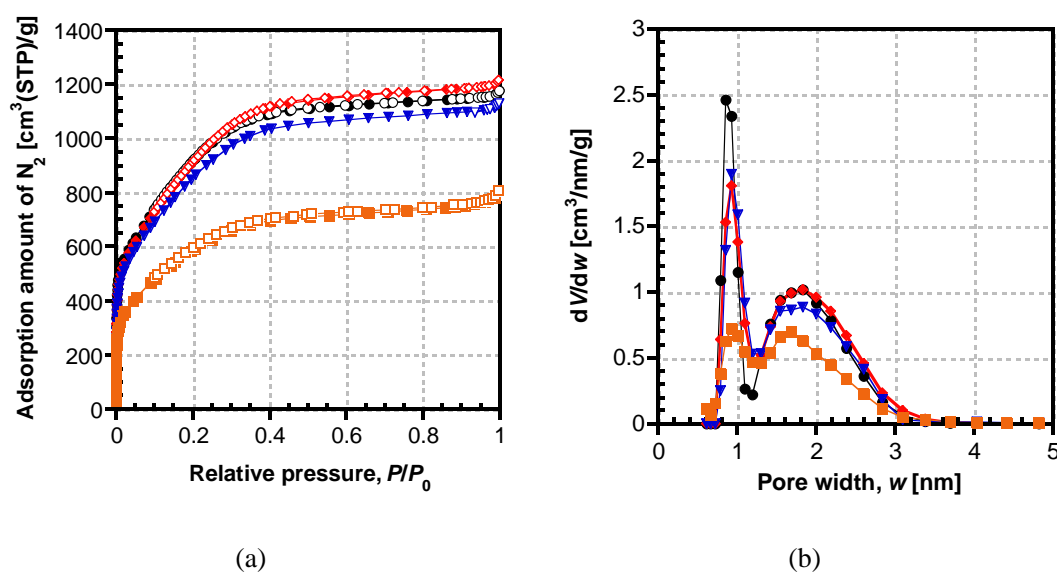


**Figure 2.3.** (a) N<sub>2</sub> adsorption and desorption isotherms at 77 K and (b) pore size distributions of BEAPS-AC0830 and its steam-activated samples at different temperatures. The solid and open symbols denote adsorption and desorption isotherms, respectively. (●, ○) BEAPS-AC0830; (◆, ◇) A800S; (▼, ▽) A850S; (■, □) A900S.



**Table 2.2.** Activation yield and pore structural parameters of BEAPS-AC0830 and its steam-activated samples at different temperatures.

Sample	Activation yield [wt.%]	Total specific surface area,	External surface area,	Total pore volume, $V_{Total}$	Average pore width, $w_{Avg.}$
		$A_{Total}$ [m <sup>2</sup> /g]	$A_{Ext.}$ [m <sup>2</sup> /g]	[cm <sup>3</sup> /g]	[nm]
BEAPS-AC0830	-	2851	10	1.76	1.24
A800S	69	2745	14	1.81	1.33
A850S	35	2606	16	1.68	1.30
A900S	1	1787	22	1.13	1.29

Similar results were obtained for the second activation using CO<sub>2</sub> as the activating agent. No noticeable changes of the N<sub>2</sub> adsorption and desorption isotherms were observed for A900C and A950C as shown in **Figure 2.4(a)**, while the CO<sub>2</sub> activation at 1000°C as the second activation (A1000C) caused a remarkable lowering of  $V_{Total}$  and  $A_{Total}$  (**Table 2.3**) accompanying noticeable decreases of the activation yield. Changes of the PSD also indicate that the second activation using CO<sub>2</sub> was ineffective to develop pores (**Figure 2.4(b)**).

Therefore, it is concluded that the second activation using steam or CO<sub>2</sub> was not suitable to induce effective pore development.

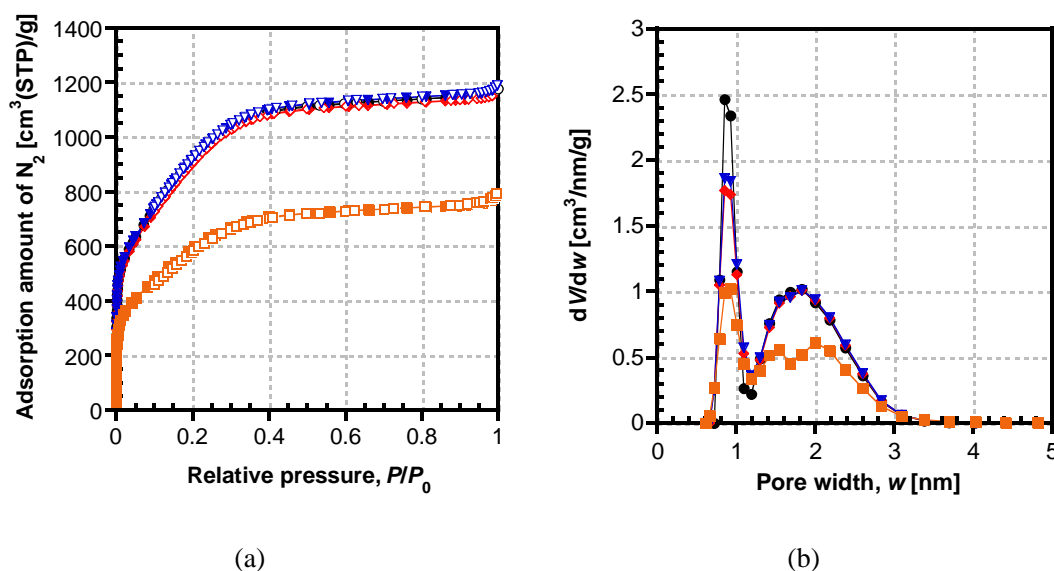


**Figure 2.4.** (a) N<sub>2</sub> adsorption and desorption isotherms at 77 K and (b) pore size distributions of BEAPS-AC0830 and its CO<sub>2</sub>-activated samples at different temperatures. The solid and open symbols denote adsorption and desorption isotherms, respectively. (●, ○) BEAPS-AC0830; (◆, ◇) A900C; (▼, ▽) A950C; (■, □) A1000C.

**Table 2.3.** Activation yield and pore structural parameters of BEAPS-AC0830 and its CO<sub>2</sub>-activated samples at different temperatures.

Sample	Activation yield [wt.%]	Total specific	External	Total pore	Average pore
		surface area, $A_{\text{Total}}$ [m <sup>2</sup> /g]	surface area, $A_{\text{Ext.}}$ [m <sup>2</sup> /g]	volume, $V_{\text{Total}}$ [cm <sup>3</sup> /g]	width, $w_{\text{Avg.}}$ [nm]
BEAPS-AC0830	-	2851	10	1.76	1.24
A900C	88	2790	14	1.74	1.25
A950C	40	2857	13	1.77	1.24
A1000C	22	1808	16	1.14	1.28

### 2.3.2 Second activation using KOH (chemical activation)

#### 2.3.2.1 Influence of second KOH activation temperature

Chemical activation can afford a superior degree of pore development with higher activation yield as compared with physical activation [2–5]. As for the second activation by means of the chemical activation method using KOH, it was found that pores were well developed when the activation temperature was high enough like 900°C (A900K4-5 in **Figure 2.5(a)**). Although the total specific surface area,  $A_{\text{Total}}$ , decreased to some extent, the total pore volume,  $V_{\text{Total}}$ , increased largely, causing an increase of average pore width,  $w_{\text{Avg.}}$ , as tabulated in **Table 2.4**. However, as can be expected from the appearance of adsorption hysteresis loop above  $P/P_0 = 0.4$ , mesopores were introduced into and PSD became wider after the second KOH activation at 900°C (**Figure 2.5(b)**). The similar mesopore development observed in both A900K4-5 and an AC prepared by one-step activation method using KOH at 900°C from a carbonized spherical phenol resin [5] suggests that KOH may inhomogeneously react with carbon atoms of BEAPS-AC0830 even by the two-step activation under milder preparation conditions. Most of KOH melted at around 360°C [16] during the heating-up process covered the external surface, but not the internal surface, of BEAPS-AC0830 particles. On the other hand, it has been reported that KOH starts to react with carbon from 400°C [17]. We assume that when the heating rate of the second KOH activation was too fast, KOH started to react only with carbons located nearby before the molten KOH and the derivatives diffused into deep part of pores already developed in BEAPS-AC0830, and the local reaction on external surface and on inner surface only near the pore entrance of BEAPS-AC0830 induced the wide PSD. Based on this hypothesis, the influence of heating rate of second activation using KOH on pore development was then examined in the following sections.

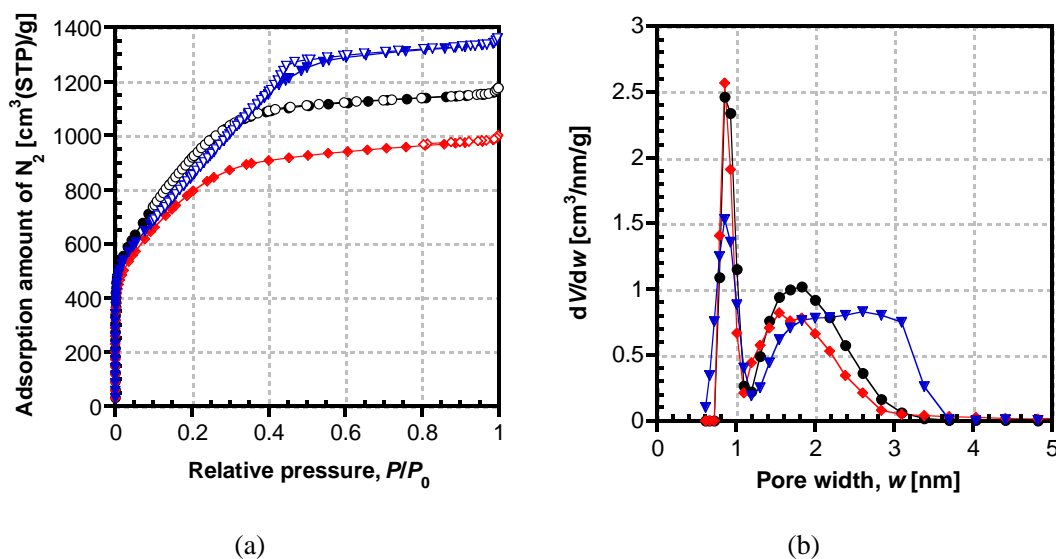


**Figure 2.5.** (a)  $N_2$  adsorption and desorption isotherms at 77 K and (b) pore size distributions of BEAPS-AC0830 and its KOH-activated samples at different temperatures. The solid and open symbols denote adsorption and desorption isotherms, respectively. (●, ○) BEAPS-AC0830; (◆, ◇) A700K4-5; (▼, ▽) A900K4-5.

**Table 2.4.** Activation yield and pore structural parameters of BEAPS-AC0830 and its KOH-activated samples at different temperatures.

Sample	Activation yield [wt.%]	Total specific surface area,	External surface area,	Total pore volume, $V_{Total}$	Average pore width, $w_{Avg.}$
		$A_{Total}$ [m <sup>2</sup> /g]	$A_{Ext.}$ [m <sup>2</sup> /g]	[cm <sup>3</sup> /g]	[nm]
BEAPS-AC0830	-	2851	10	1.76	1.24
A700K4-5	62	2534	12	1.49	1.18
A900K4-5	59	2757	13	2.04	1.48

### 2.3.2.2 Influence of heating rate of second KOH activation

**Figure 2.6** shows the  $N_2$  adsorption and desorption isotherms at 77 K and the corresponding PSDs of the second activated samples at 900°C of activation temperature and at 4 of KOH/BEAPS-AC0830 weight ratio with different heating rates. The activation yield and pore structural parameters are shown in **Table 2.5**. When the heating rate was slowed from 5 °C/min to 2.5 °C/min, the size of adsorption hysteresis loop apparently decreased, and from the PSD, the formation of wide pores was suppressed. At the high heating rate (15 °C/min), on the other hand, a remarkable hysteresis loop was observed and an obvious amount of mesopores above 3 nm appeared. The results showed that the heating rate of KOH activation indeed influenced on the pore development and PSD. The slow heating rate was considered to enable a better diffusion of molten KOH species into deep part of pores, giving rise to more uniform contact and reaction between active species and

carbon, and thus more uniformly developed porosity shown as a narrower PSD was successfully obtained.

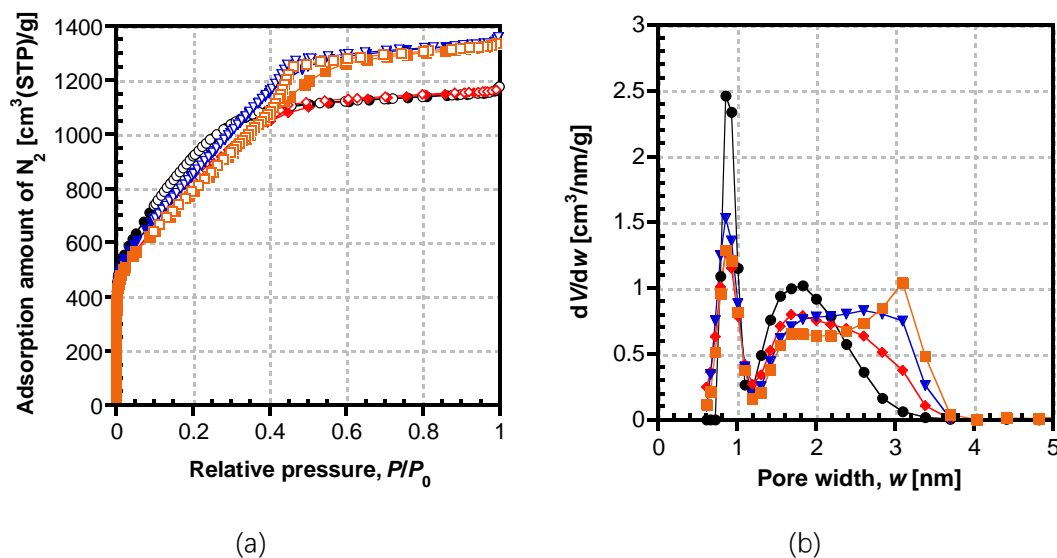


**Figure 2.6.** (a) N<sub>2</sub> adsorption and desorption isotherms at 77 K and (b) pore size distributions of BEAPS-AC0830 and its KOH-activated samples at 900°C with different heating rates. The solid and open symbols denote adsorption and desorption isotherms, respectively. (●, ○) BEAPS-AC0830; (◆, ◇) A900K4-2.5; (▼, ▽) A900K4-5; (■, □) A900-K4-15.

**Table 2.5.** Activation yield and pore structural parameters of BEAPS-AC0830 and its KOH-activated samples at 900°C with different heating rate.

Sample	Activation yield [wt.%]	Total specific surface area,	External surface area,	Total pore volume, $V_{\text{Total}}$ [cm <sup>3</sup> /g]	Average pore width, $w_{\text{Avg.}}$ [nm]
		$A_{\text{Total}}$ [m <sup>2</sup> /g]	$A_{\text{Ext.}}$ [m <sup>2</sup> /g]		
BEAPS-AC0830	-	2851	10	1.76	1.24
A900K4-2.5	58	2605	13	1.77	1.36
A900K4-5	59	2757	13	2.04	1.48
A900K4-15	64	2610	17	2.01	1.55

### 2.3.2.3 Influence of KOH amount of second KOH activation

When the weight ratio of KOH/BEAPS-AC0830 in the second activation increased from 4 to 6, a remarkable formation of mesopores was observed and the PSD curve leaned to the large-size-pore side, as shown in **Figure 2.7**. In addition, activation yields also decreased at higher KOH/BEAPS-AC0830 weight ratio (**Table 2.6**). Although the slow heating was found to be effective to alleviate a vigorous formation of mesopores even at the higher KOH/BEAPS-AC0830 weight ratio (cf. A900K6-2.5 and A900K6-5), a usage of excess amount of activating agent should be avoided to obtain ACs with narrow PSD. In fact, it was calculated that 3 g of KOH is enough to fill up all pores

developed in 1 g of BEAPS-AC0830 using the calculated density of 1.72 g/cm<sup>3</sup> of molten KOH [18].

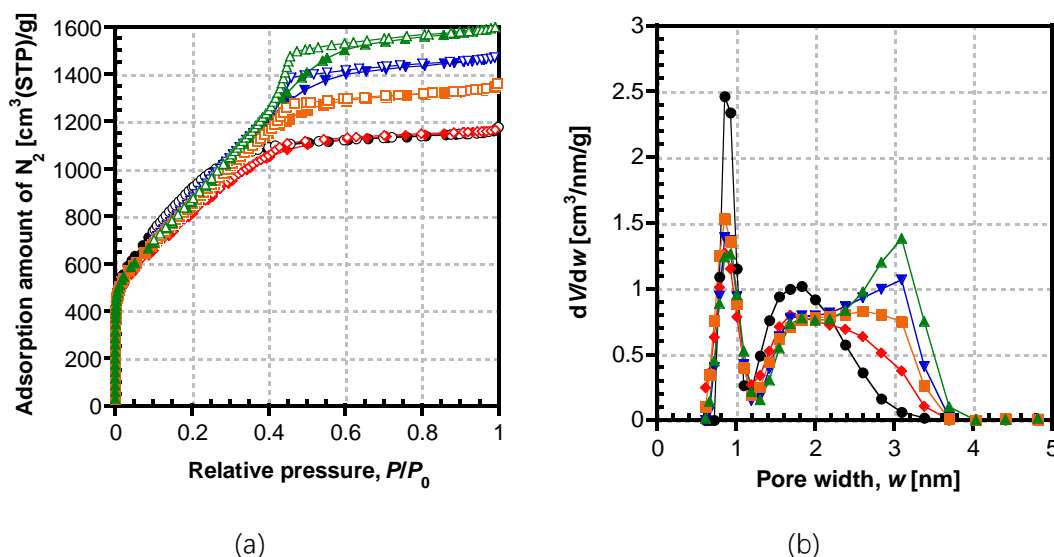


**Figure 2.7.** (a) N<sub>2</sub> adsorption and desorption isotherms at 77 K and (b) pore size distributions of BEAPS-AC0830 and its KOH-activated samples at 900°C with different KOH/BEAPS-AC0830 weight ratios. The solid and open symbols denote adsorption and desorption isotherms, respectively. (●, ○) BEAPS-AC0830; (◆, ◇) A900K4-2.5; (▼, ▽) A900K6-2.5; (■, □) A900K4-5; (▲, △) A900K6-5.

**Table 2.6.** Activation yield and pore structural parameters of BEAPS-AC0830 and its KOH-activated samples at 900°C with different KOH/BEAPS-AC0830 weight ratios.

Sample	Activation yield [wt.%]	Total specific surface area,	External surface area,	Total pore volume, $V_{\text{Total}}$ [cm <sup>3</sup> /g]	Average pore width, $w_{\text{Avg}}$ [nm]
		$A_{\text{Total}}$ [m <sup>2</sup> /g]	$A_{\text{Ext.}}$ [m <sup>2</sup> /g]		
BEAPS-AC0830	-	2851	10	1.76	1.24
A900K4-2.5	58	2605	13	1.77	1.36
A900K6-2.5	47	2783	14	2.23	1.61
A900K4-5	59	2757	13	2.04	1.48
A900K6-5	50	2787	17	2.42	1.74

### 2.3.2.4 Influence of mixing method of KOH with BEAPS-AC0830 in second KOH activation

As shown in the previous sections, the slow heating during the second KOH activation gave narrower PSD, most likely due to an improved contact between KOH and the internal surface at deep part of developed pores in BEAPS-AC0830. As another way to induce the improved contact, solution impregnation method was applied (as shown in **Figure 2.10**). The solution impregnation is

considered to allow a sufficient dispersion of KOH particles prior to activation into even deeper part of pores in BEAP-AC0830 prior to the activation. And thus, more uniform reaction (gasification) of carbons by KOH is expected to provide narrower PSD of resultant ACs as compared with the physical mixing method.

In **Figure 2.8** and **Table 2.7**, influence of mixing method on porosity is shown. At the same heating rate basis (2.5 °C/min), the AC prepared by the solution impregnation method (AC900K4-2.5-(sol)) showed higher pore development degree (higher  $A_{Total}$  and  $V_{Total}$  values) than that by the physical mixing (AC900K4-2.5). In addition, PSD of the former was reasonably narrower than the latter. Furthermore, even at higher heating rate of 5 °C/min, the effectiveness of the solution impregnation method was confirmed (A900K4-5-(sol)): although the PSD was wider to some extent as compared with the slow heating rate one (AC900K4-2.5-(sol)), the higher degree of pore development and narrower PSD were obtained than those of A900K4-2.5.

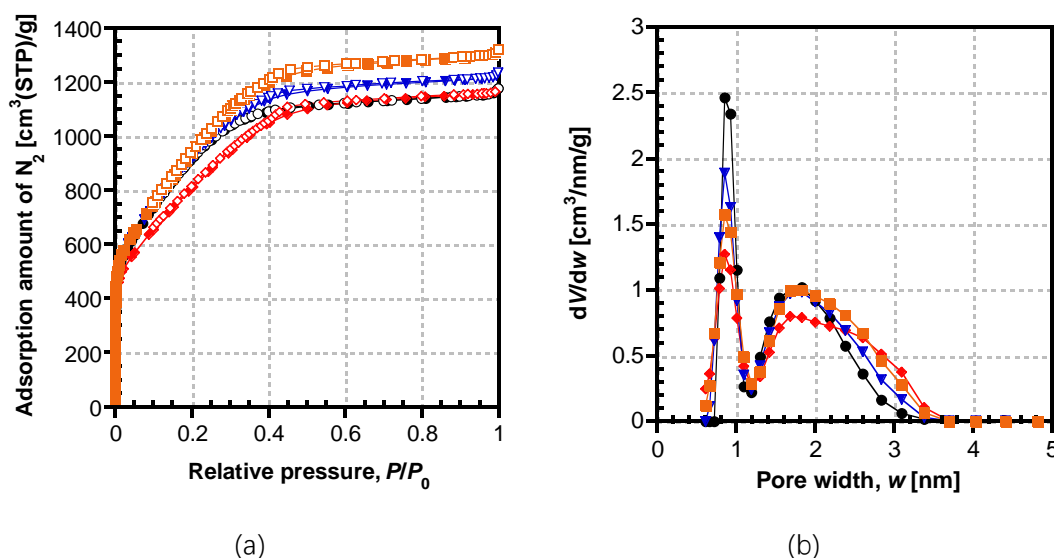


**Figure 2.8.** (a) N<sub>2</sub> adsorption and desorption isotherms at 77 K and (b) pore size distributions of BEAPS-AC0830 and its KOH-activated samples at 900°C prepared by different mixing methods. The solid and open symbols denote adsorption and desorption isotherms, respectively. (●, ○) BEAPS-AC0830; (◆, ◇) A900K4-2.5; (▼, ▽) A900K4-2.5-(sol); (■, □) A900K4-5-(sol).

**Table 2.7.** Activation yield and pore structural parameters of BEAPS-AC0830 and its KOH-activated samples at 900°C prepared by different mixing methods.

Sample	Activation yield [wt.%]	Total specific surface area,	External surface area,	Total pore volume, $V_{Total}$	Average pore width, $w_{Avg}$ .
		$A_{total}$ [m <sup>2</sup> /g]	$A_{Ext.}$ [m <sup>2</sup> /g]	[cm <sup>3</sup> /g]	[nm]
BEAPS-AC0830	-	2851	10	1.76	1.24
A900K4-2.5	58	2605	13	1.77	1.36
A900K4-2.5-(sol)	> 50*	2909	9	1.86	1.28
A900K4-5-(sol)	> 39*	2961	8	1.99	1.35

\* In the case of solution impregnation method, a loss of a small portion of mixture after the drying clung to inner wall of a container might cause an underestimation of the activation yields.

### **2.3.3 The general discussion for the phenomenon**

#### **2.3.3.1 The different effect of second-physical (steam & CO<sub>2</sub>) and chemical activation (KOH)**

By tuning the activation conditions such as temperature, soaking time, etc., the second-step physical (steam & CO<sub>2</sub>) activations showed a porosity loss; while the second-step chemical (KOH) activations showed a further porosity development. Such difference between physical and chemical second-activations can be explained considering the different reaction mechanisms.

For physical activations, when the activation temperature is high enough to a “critical” temperature, the yield and the porosity in A900S and A1000C have a sudden drop in the endothermic physical reactions. It was observed that all the temperatures in physical second-activation showed a loss in porosity more or less with a larger average pore width compared with AC, indicating that the second-step gas activation mainly widening and consuming the existing pores than creating new narrow pores in the endothermic selective gasification process explained in **Table 1.4**.

For chemical (KOH) activation, it was proposed that the intercalation mechanism that mainly helped to create new micropores and the catalyzed gasification mechanism resulted in a further development in porosity based on original one in AC0830.

Besides the above-mentioned molecular reaction mechanisms, the previous study about structural elucidation of the differences in physical and chemical activation mechanisms can also give an explanation using the concept of microdomain (introduced in Chapter1) as shown in **Figure 2.9**. The physical activations (steam) led to size decrease in both microdomains and particles; while the chemical (KOH) activations with both sizes kept unchanged [5]. It indicated that the physical activation happened more inhomogeneously on the surface of microdomains and particles.

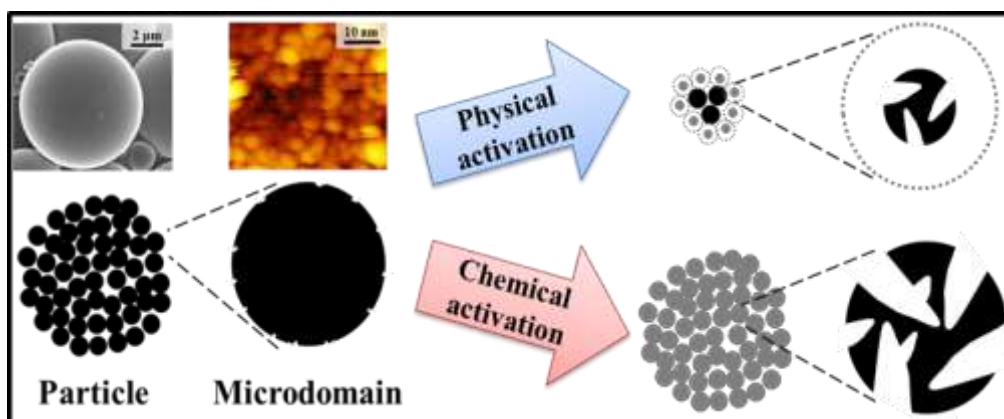


**Figure 2.9.** Structural elucidation of physical and chemical activation mechanisms based on the microdomain structure model [5].

### 2.3.3.2 Why the low heating rate and solution mixing in KOH second activation realized a narrower PSD during porosity development

As shown above, the second-step KOH activation under low heating rate and with solution mixing method enabled the porosity development with a narrow PSD. Such result can be attributed to the better contact between KOH and the starting sample with heating rate during activation or solution mixing method before activation. **Figure 2.10** gives the schematic diagrams.

During the activation process, KOH first melted with the increasing temperature. With a high heating speed, the molten KOH doesn't have enough time to sufficiently contact with the original pores of starting AC; while with a slow heating rate, molten KOH can penetrate deeply even into narrow pores. Similarly, the solution mixing method dissolved KOH in ethanol solutions, giving rise to the well dispersion of KOH into deep parts of pores before activation.

Therefore, a homogeneous reaction between KOH and carbon surface is available with a low heating rate and/or solution mixing method.



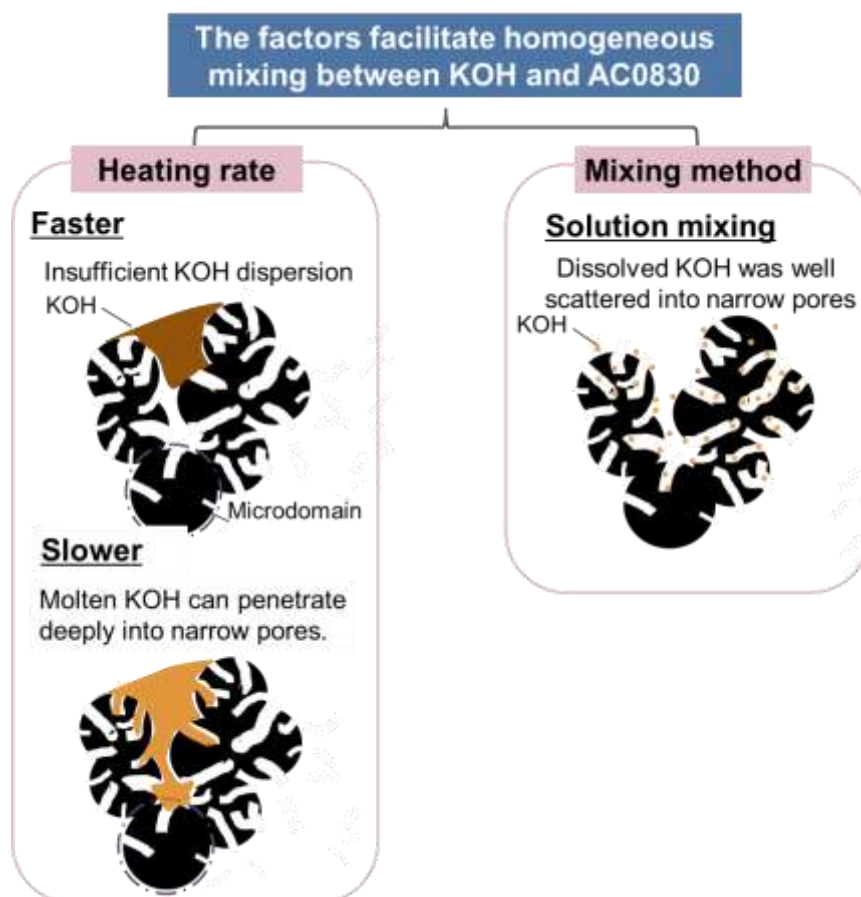


**Figure 2.10.** The explanation of the factors that facilitated the more homogeneously activation.

Together with the sufficient and homogeneous contact between KOH and AC0830, **Figure 2.11** gives another explanation from the aspect of reaction mechanism that how and why porosity development with a narrow PSD was possible with a low heating rate and solution mixing method.

With a low heating rate, a sufficient contact and longer reaction time at lower temperature resulted in more reaction chance between KOH and AC0830; that is, a low heating rate equals to a more thoroughly occurred activation process. The lower yield with a low heating rate is an evidence as shown in **Table 2.5**. Although the overall reaction occurred in a higher degree with a low heating rate, however, for local sites where the activation happened, the reaction process was mild and more homogeneous. What's more, a slow formation and fast removal of oxidative gas weakened the effect of catalyzed gasification, thus hindered the formation of mesopores; while the formation and dispersion of free K enforced the intercalation process, which was supposed to create only micropores.

For the solution mixing method, as a result of the better contact between KOH and starting AC, a more homogeneous carbon removal in both gasification and intercalation mechanisms facilitated to afford the narrow PSD.

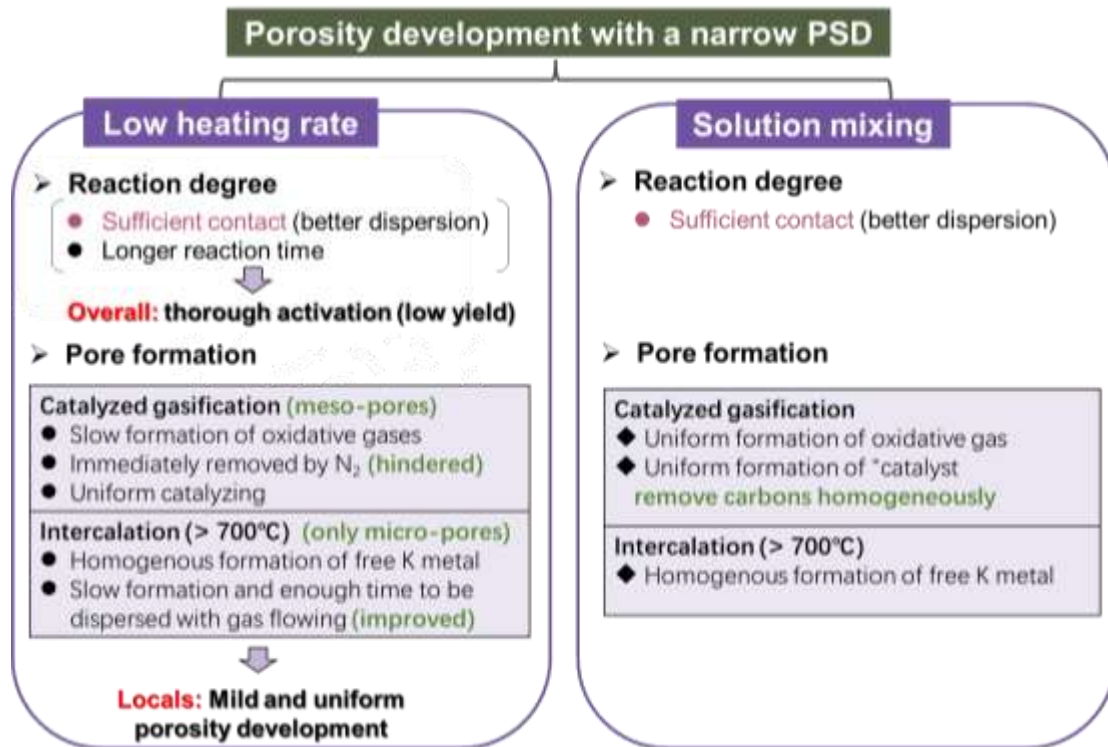


**Figure 2.11.** From the aspect of KOH activation mechanism, how the slow heating rate and solution mixing method led to porosity development with a narrow PSD.

## 2.4 Conclusion

Two kinds of approaches in the multistep activation were introduced to narrow the PSD of AC with its developed porosity almost untouched; one was to slow down the heating rate during KOH activation, the other was to mix the activating agent and starting carbon material by solution impregnation before the activation. Both approaches were applied to induce uniform distribution of activating agent on overall carbon surface in already introduced micropores of once-activated starting sample. Experimental results demonstrated that either single or combined usage of these two approaches was effective to narrow the PSD. By carefully adjusting the mixing and activation conditions in second activation, it is highly expected to develop ACs with narrow PSD centered at optimized average pore size, which exhibit maximized effective adsorption amount.

## 2.5 Future work

In this study, many precursors and factors during carbonization and activation process were examined. Many interesting points were found here and also the past 10 years' experience in our lab for AC preparation; however, all the trials are not all systematic and in a semi-experimental way.

By using the JMP, a strong statistical analysis and DOE (design of experiments) software, a multi-factor DOE is available. There, the experimental conditions, such as precursor types, activation

agents, heating rate, soaking temperature and time can be taken as the X values, while the characterization results, including the porosity (surface area, micropore volume, average pore size, PSD range), surface chemistry (like oxygen content), the stacking order ( $L_c$ ,  $L_a$ ,  $d_{002}$  values) can be taken as the Y values (**Figure 2.12**). By statistical analysis, one can know if and how a certain factor affects a target property, also how multi factors synthetically effect (interactions and their weight) on one property, as well as the trade-off relationships between properties

With such a “compass“ in scientific research, it’s possible to change costly and time-consuming trial-and-error searches to powerful, efficient experiments.

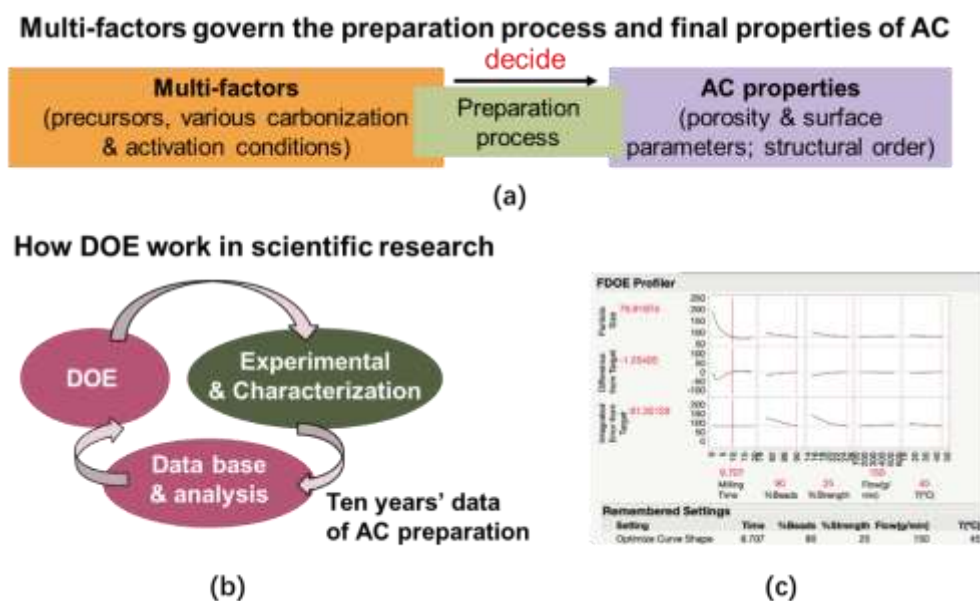


**Figure 2.12.** Future work by using the statistical analysis and design of experiment (DOE) with JMP.

## Acknowledgement

We gratefully acknowledge ASAHI YUKIZAI CORPORATION for providing BEAPS-AC0830.

## References

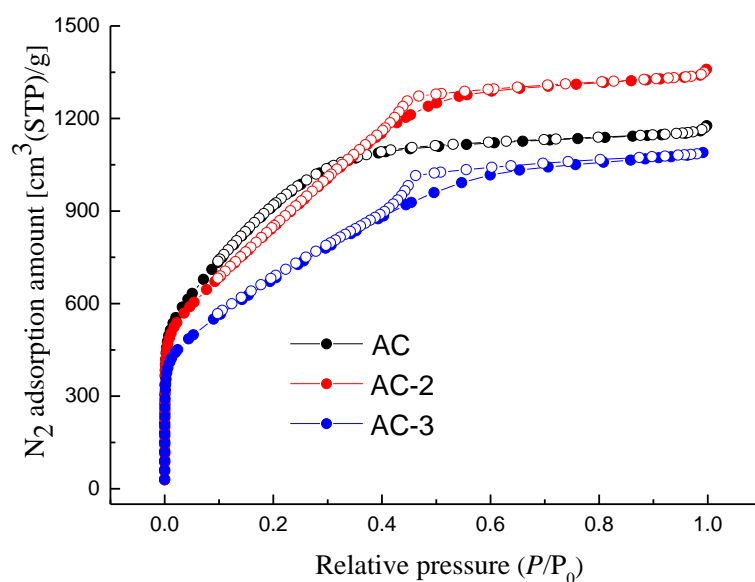
- [1] Yu Y. Kil H-S. Nakabayashi K. Yoon S-H. Miyawaki J. Toward development of activated carbons with enhanced effective adsorption amount by control of activation process. AIP Conference Proceedings 2019;2097:020002 (9 pages).
- [2] Ahmadpour A. Do DD. The preparation of active carbons from coal by chemical and physical activation. Carbon 1996;34:471–9.
- [3] Maciá-Agulló JA. Moore BC. Cazorla-Amorós D. Linares-Solano A. Activation of coal tar pitch carbon fibres: Physical activation vs. chemical activation. Carbon 2004;42:1367–70.
- [4] Wu FC. Tseng RL. Hu CC. Comparisons of pore properties and adsorption performance of KOH-activated and steam-activated carbons. Microporous Mesoporous Mater 2005;80:95–105.
- [5] Kim D-W., Kil H-S. Nakabayashi K. Yoon S-H. Miyawaki J. Structural elucidation of physical and chemical activation mechanisms based on the microdomain structure model. Carbon 2017;114:98–105.
- [6] Kyotani T. Control of pore structure in carbon. Carbon 2000;38:269–86.
- [7] Inagaki M. Pores in carbon materials-importance of their control. New Carbon Materials 2009;24:193–232.
- [8] Ryoo R. Joo SH. Kruk M. Jaroniec M. Adv Mater 2001;13:677–81.
- [9] Matsuoka K. Yamagishi Y. Yamazaki T. Setoyama N. Tomita A. Kyotani T. Extremely high microporosity and sharp pore size distribution of a large surface area carbon prepared in the nanochannels of zeolite Y. Carbon 2005;43:876–9.
- [10] Ozaki J. Endo N. Ohizumi W. Igarashi K. Nakahara M. Oya A. Yoshida S. Iizuka T. Novel preparation method for the production of mesoporous carbon fiber from a polymer blend. Carbon 1997;35:1031–3.
- [11] Kawabuchi Y. Kishino M. Kwano S. Whitehurst DD. Mochida I. Carbon deposition from benzene and cyclohexane onto active carbon fiber to control its pore size. Langmuir 1996;12:4281–5.
- [12] Kawabuchi Y. Oka H. Kawano S. Mochida I. Yoshizawa N. The modification of pore size in activated carbon fibers by chemical vapor deposition and its effects on molecular sieve selectivity. Carbon 1998;36:377–82.
- [13] Shiratori N. Lee KJ. Miyawaki J. Hong SH. Mochida I. An B. Yokogawa K. Jang J. Yoon S-H. Pore structure analysis of activated carbon fiber by microdomain-based model. Langmuir 2009;25:7631–7.
- [14] Kaneko K. Ishii C. Ruike M. Kuwabara H. Origin of superhigh surface area and microcrystalline graphitic structures of activated carbons. Carbon 1992;30:1075–88.
- [15] Neimark AV. Lin Y. Ravikovitch PI. Thommes M. Quenched solid density functional theory and pore size analysis of micro-mesoporous carbons. Carbon 2009;47:1617–28.
- [16] von Hevesy G. Über Alkalihydroxyde. L. Z Physik Chem 1910;73U:667–84 (in German).
- [17] Lillo-Ródenas MA. Cazorla-Amorós D. Linares-Solano A. Carbon 2003;41:263–75.
- [18] Janz GJ. Dampier FW. Lakshminarayanan GR. Lorenz PK. Tomkins RPT. “6. Numerical values of electrical conductance, density, and viscosity,” in National Standard Reference Data Series-National Bureau of Standards 15, Molten Salts: Volume 1, Electrical Conductance, Density, and Viscosity Data, (U.S. Department of Commerce, 1968), pp. 106.

## Appendix for Chapter 2

### A.1. Third activation using KOH (chemical activation)

The effect of third steps activation was also tried with a middle-severe activation condition as A900K4-5 (physical mixing). Three samples: BEAPS-AC0830, AC0830A900K4-5 and AC0830A900K4-5-A900K4-5, for short, AC, AC-2, AC-3, respectively, were compared in this section.

From the **Figure A1** and **Table A1**, third-activation was found not to give a further porosity development but a porosity loss in the chosen A900K4-5 condition.



(a)

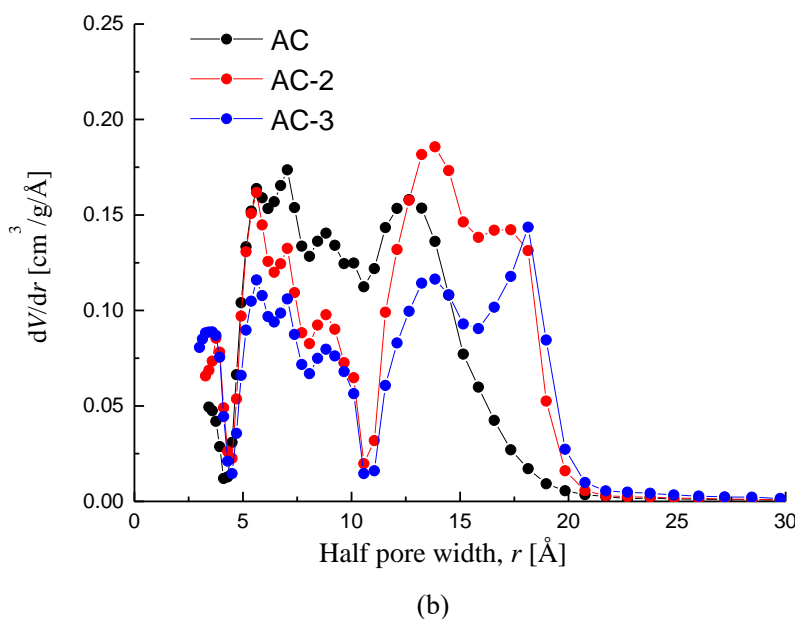


**Figure A1.** (a) N<sub>2</sub> adsorption and desorption isotherms at 77 K and (b) pore size distributions of BEAPS-AC0830 and its second and third activated samples prepared by the A900K4-5 conditions. The solid and open symbols in the isotherms denote adsorption and desorption, respectively.

**Table A1.** Activation yield and pore structural parameters of BEAPS-AC0830 and its second and third-activated samples prepared by the A900K4-5 conditions.

Sample	Activation yield [wt.%]	Total specific	External	Total pore	Average pore width, $w_{Avg}$ [nm]
		surface area, $A_{Total}$ [m <sup>2</sup> /g]	surface area, $A_{Ext.}$ [m <sup>2</sup> /g]	volume, $V_{Total}$ [cm <sup>3</sup> /g]	
AC	-	2851	10.5	1.76	1.24
AC-2	58.6	2757	13.2	2.04	1.48
AC-3	58.3	2300	16.5	1.64	1.43

## A.2 The influence of solution mixing time on KOH second activation

The champion sample in Chapter 2 was AC0830A900K6-2.5(sol.), which was prepared by a 6-h solution mixing and then activated with a heating rate of 2.5 °C/min to 900°C. To check the possible influence of solution mixing time, sample under exact same preparation conditions expect a longer mixing time of 18 h was prepared and characterized. **Figure A2** and **Table A2** give the comparison results.

Compared with the 6-h solution mixing time of champion conditions, 18-h-solution-mixing decreased the yield from 70.5% to 56.1% and a loss of porosity with wider average pore width. The longer mixing may result in a more sufficient contact between KOH and AC, as explained in **Section 2.3.3.2**, thus the activation occurred more thoroughly, larger amount of carbon removed during this process (lower yield) led to wider pores with a loss in porosity. Therefore, in this study, 6 h was determined as the standard for solution mixing method.

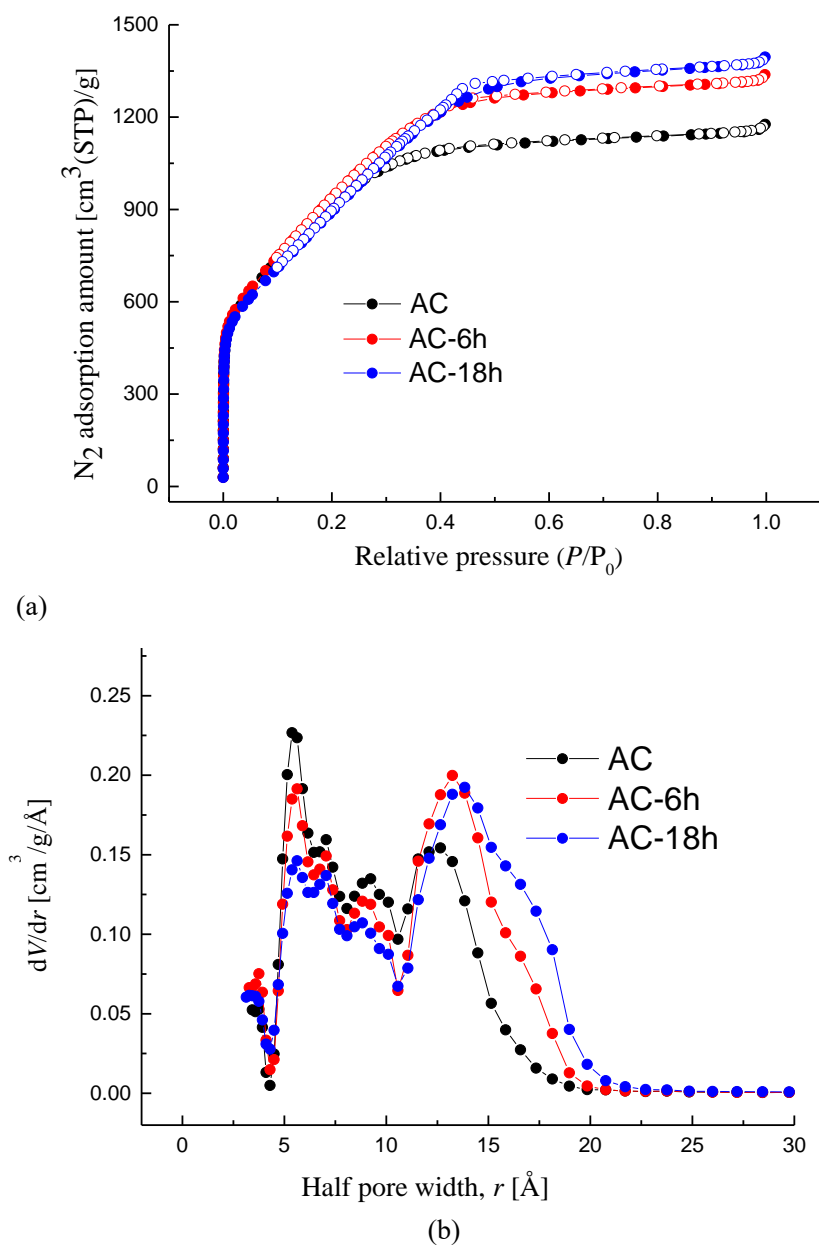


**Figure A2.** (a)  $N_2$  adsorption and desorption isotherms at 77 K and (b) pore size distributions of BEAPS-AC0830 and its second activated samples under AC0830A900K6-2.5-(sol) with mixing time of 6 or 18 h. The solid and open symbols in the isotherms denote adsorption and desorption, respectively.

**Table A2.** Activation yield and pore structural parameters of BEAPS-AC0830 and its second activated samples under AC0830A900K6-2.5-(sol) with mixing time of 6 or 18 h.

Sample	Activation yield [wt.%]	Total specific surface area, $A_{Total}$ [m <sup>2</sup> /g]	External surface area, $A_{Ext.}$ [m <sup>2</sup> /g]	Total pore volume, $V_{Total}$ [cm <sup>3</sup> /g]	Average pore width, $w_{Avg.}$ [nm]
AC	-	2851	10.5	1.76	1.24
AC-6h	70.5	2938	9.6	2.01	1.37
AC-18h	56.1	2826	11.8	2.10	1.49

### A.3 The comparison of KOH one-step and two-step activations with same surface area and pore width

This section will satisfy the curiosity that with the same total surface area or same average pore width, what are the difference between the other properties of the porosities resulted from one-step activation and two-step activation.

The first-step activations were applied to the 600°C-1h (heating rate: 5 °C/min) carbonized sphere phenol resins (BEAPS 8 μm; ASAHI YUKIZAI CORPORATION, Japan), a same precursor as BEAPS-AC0830) under various activation conditions. The second-step activations were applied to BEAPS-AC0830 also with different activation conditions. All the samples shown in this section are KOH activated with a physical mixing method.

From all these first-step activated and two-step KOH activated samples, two groups, A and B, were chosen. The two samples in each group have a similar surface area that resulted from one-step and two-step activation, respectively. The sample names and their meanings in this section are:

AC: BEAPS-AC0830

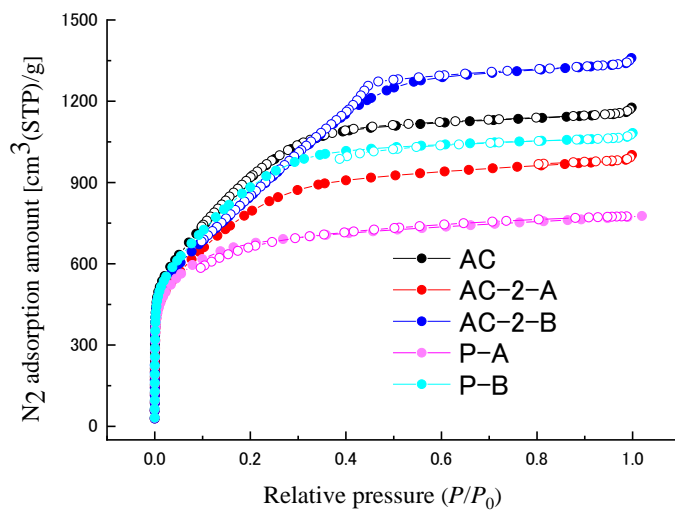
AC-2-A/B: second-step KOH activated BEAPS-AC0830, group A/B

P-A/B: one-step KOH activated phenol resins, group A/B

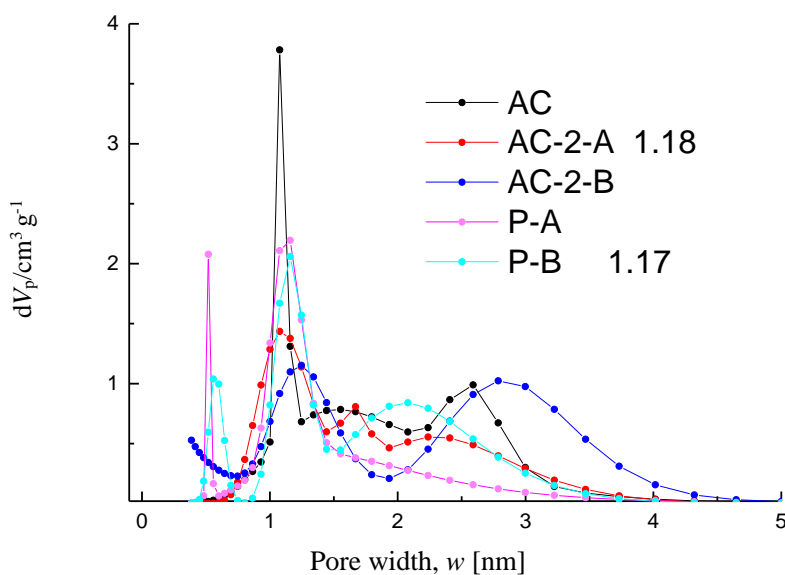
**Figure A3** and **Table A3** give the porosity information of these samples. In both groups A and B, although the two samples from one-step or two-step KOH activation have a similar specific surface area, the two-step activated ones have a larger the average pore width, total pore volume, and external surface area compared to the corresponding one-step activated sample.



For AC-2-A and P-B, they have similar average pore width of 1.18 nm and 1.17 nm respectively. However, the P-B has a bit larger total surface area.



(a)



(b)

**Figure A3.** (a) N<sub>2</sub> adsorption and desorption isotherms at 77 K and (b) pore size distributions of 1) BEAPS-AC0830 and its second activated samples under various conditions, 2) one-step activated samples under different conditions. The solid and open symbols in the isotherms denote adsorption and desorption, respectively.

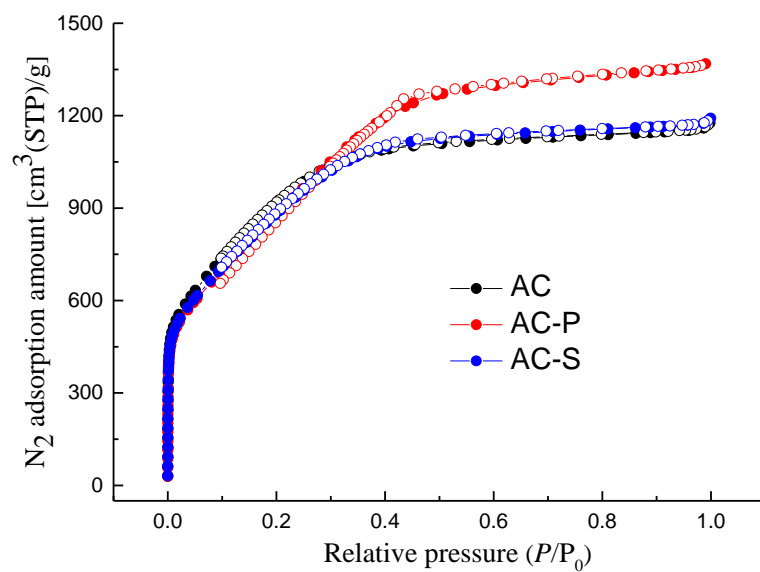
**Table A3.** Activation yield and pore structural parameters of 1) BEAPS-AC0830 and its second activated samples under various conditions, 2) one-step activated samples under different conditions.

Sample	Activation yield [wt.%]	Total specific surface area, $A_{Total}$ [m <sup>2</sup> /g]	External surface area, $A_{Ext.}$ [m <sup>2</sup> /g]	Total pore volume, $V_{Total}$ [cm <sup>3</sup> /g]	Average pore width, $w_{Avg.}$ [nm]
AC	-	2851	10.5	1.76	1.24
AC-2-A	62.3	2534	9.5	1.49	<b>1.18</b>
P-A	84.2	2497	5.2	1.18	0.95
AC-2-B	58.6	2757	13.2	2.04	1.48
P-B	58.4	2790	7.3	1.63	<b>1.17</b>

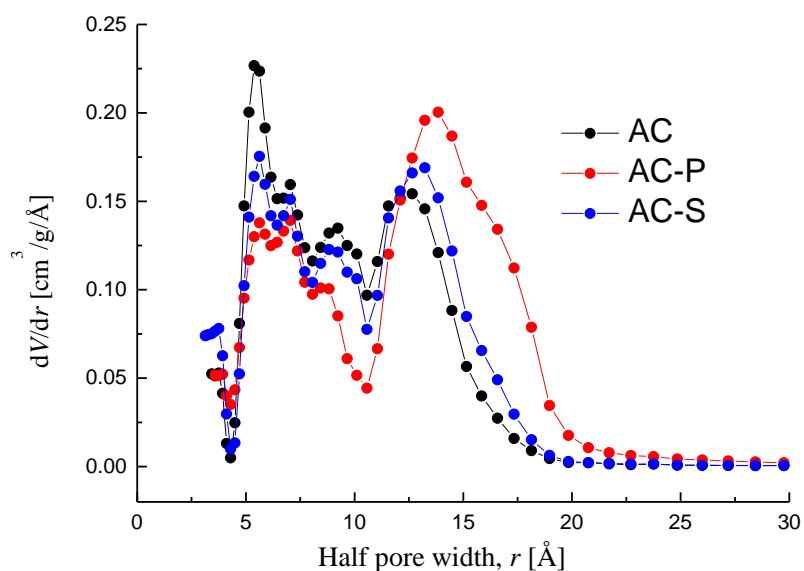
#### A.4 The influence of mixing method on KOH second activation under AC0830A800K6-5

Except the champion conditions in Chapter 2: AC0830A900K6-2.5(sol), the effect of solution mixing method was also checked on other conditions. This section shows a comparison between AC0830A800K6-5 with physical and solution mixing methods, as shown in **Figure A4.** and **Table A4.**

In this activation condition, both samples didn't show a further developed porosity. The solution mixing one has a narrower average pore width with similar porosity compared with physical mixed sample. Therefore, the solution mixing method should be applied to a proper second-activation condition to play a role.



(a)



(b)

**Figure A4.** (a)  $N_2$  adsorption and desorption isotherms at 77 K and (b) pore size distributions of BEAPS-AC0830 and its second KOH activated samples AC0830A800K6-5 with physical and solution mixing methods. The solid and open symbols in the isotherms denote adsorption and desorption, respectively.

**Table A4.** Activation yield and pore structural parameters of BEAPS-AC0830 and its second KOH activated samples AC0830A800K6-5 with physical and solution mixing methods.

Sample	Activation yield [wt.%]	Total specific surface area, $A_{\text{Total}}$ [m <sup>2</sup> /g]	External surface area, $A_{\text{Ext.}}$ [m <sup>2</sup> /g]	Total pore volume, $V_{\text{Total}}$ [cm <sup>3</sup> /g]	Average pore width, $w_{\text{Avg.}}$ [nm]
AC	-	2851	10.5	1.76	1.24
AC-P	46.7	2709	14.9	2.07	1.53
AC-S	75.2	2756	9.4	1.79	1.30

## A.5 Apply the different mixing methods in one-step activation

This section partly answered a question that what will happen if we directly use the solution mixing method in one-step activation. Here, KOH activation under A800K6-5 conditions were applied to 600°C-1h (heating rate: 5 °C/min) carbonized sphere phenol resins (BEAPS 8 μm; ASAHI YUKIZAI CORPORATION, Japan) with both physical and solution mixing method, and denoted as P-P and P-S, respectively. P represents carbonized phenol resins.

**Figure A5** and **Table A5** give the porosity information of these samples. The solution mixing method under this activation condition produced a highly developed porosity with a large total specific surface area of 2535 m<sup>2</sup>/g, however, with a narrow PSD close to that of carbonized precursors. Such a porous carbon with high-developed micropores with a narrow PSD may be a good candidate as molecular sieve carbons for gas separation.

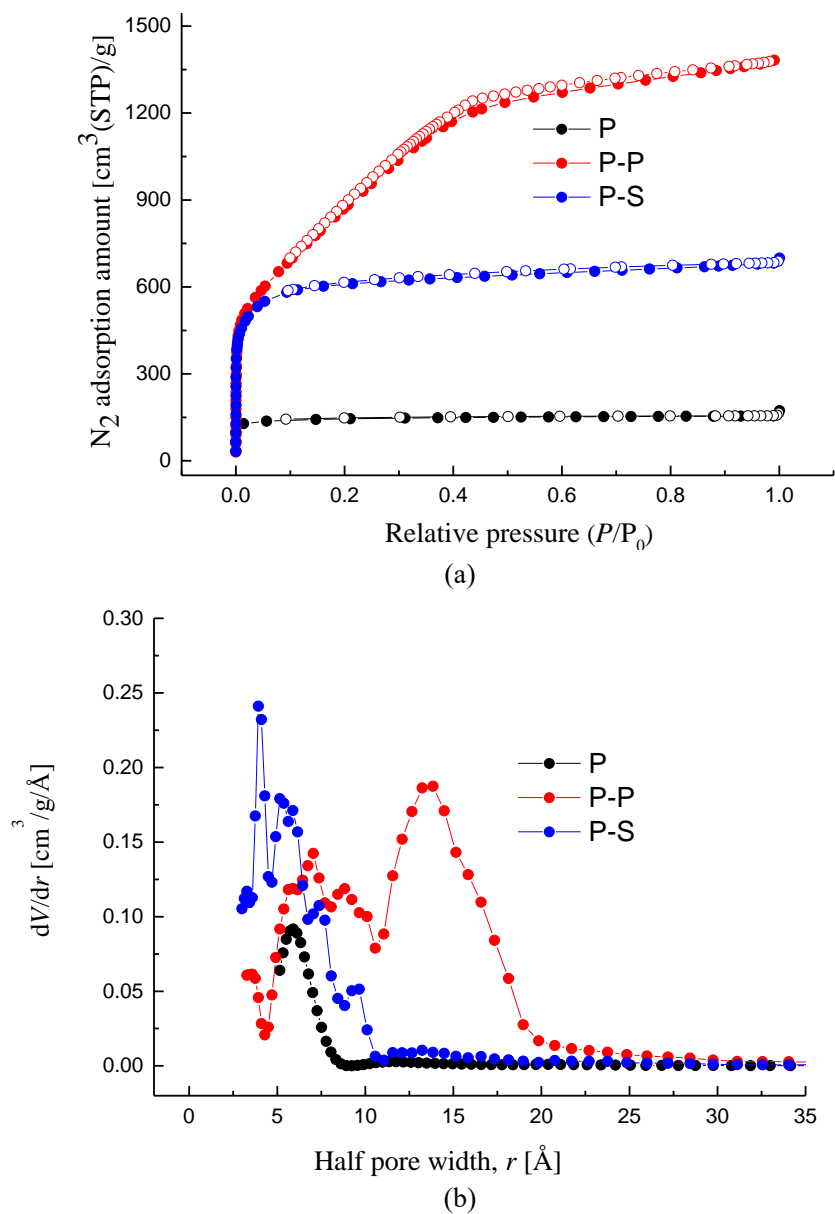


**Figure A5.** (a)  $N_2$  adsorption and desorption isotherms at 77 K and (b) pore size distributions of phenol resins (P) and its KOH activated samples PA800K6-5 with physical and solution mixing methods. The solid and open symbols in the isotherms denote adsorption and desorption, respectively.

**Table A5.** Activation yield and pore structural parameters of phenol resins (P) and its KOH activated samples PA800K6-5 with physical and solution mixing methods.

<b>Sample</b>	<b>Activation yield [wt.%]</b>	<b>Total specific surface area, <math>A_{Total}</math> [m<sup>2</sup>/g]</b>	<b>External surface area, <math>A_{Ext.}</math> [m<sup>2</sup>/g]</b>	<b>Total pore volume, <math>V_{Total}</math> [cm<sup>3</sup>/g]</b>	<b>Average pore width, <math>w_{Avg.}</math> [nm]</b>
P	-	682	2.0	0.24	0.69
P-P	31.8	2679	20.3	2.07	1.56
P-S	58.7	2535	6.4	1.04	0.82

# Chapter 3 Pore-size-selective control of surface properties of porous carbons by molecular masking [1]

## 3.1 Introduction

Porous carbon is an indispensable material for today's environmental, energy-related, chemical, and electronics technologies. The performance of porous carbon is governed by both porosity and surface character. Ideally, to exhibit the best performance, each pore should have its own custom surface property depending on its size. The surface property is governed by surface species, which can serve as active sites of sorption and reaction, or as anchor sites for heteroatoms, chemical moieties, and particles. Therefore, selectively introducing specific surface-bound species into pores within a desired pore size range could result in new functional porous carbon materials. For example, polar surface groups selectively introduced into certain pores will allow the pressure of the predominant adsorption uptake of polar molecules to be adjustable. Also, the dispersion of a variety of supported catalysts as a function of pore size could be used to create versatile catalytic systems. In contrast to the extensive body of literature describing entire-surface modifications, to the best of our knowledge, only one report has exploited the molecular sieving effect of porous materials to selectively modify the surface of certain pores [2]. Herein, we propose a strategy based on molecular masking to afford flexible pore-size-dependent surface-property control. **Figure 3.1** shows a schematic of the demonstrative preparation of porous carbon with hydrophobic narrow pores and hydrophilic wide pores by the proposed three-step sequential treatments—selective molecular pre-masking, surface modification, and unmasking.

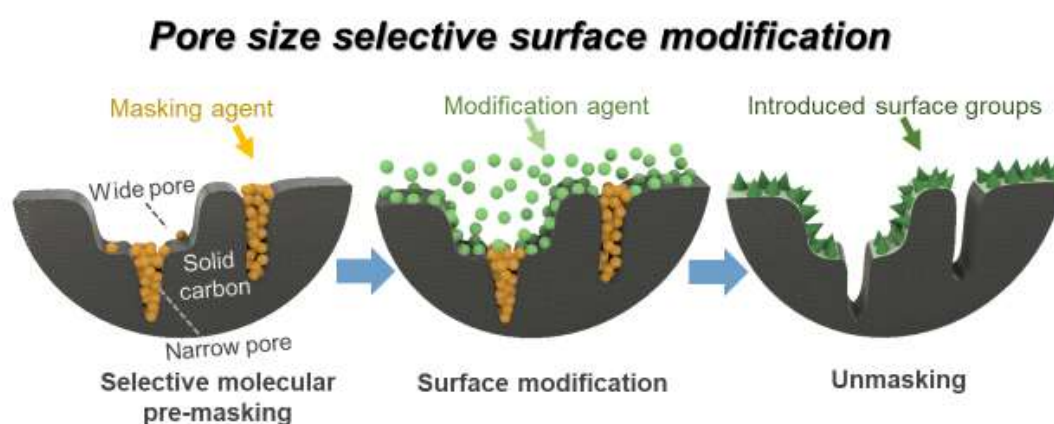


**Figure 3.1.** The three-step strategy of pore-size-selective surface modification of porous carbons.

### 3.2 The proposed strategy for pore-size selective surface modification

The proposed three-step sequential treatment is illustrated in **Figure 3.2**, which shows how a single porous carbon material containing narrow pores with a specific surface property (denoted as A) and wide pores with a different surface characteristic (B) can be obtained. The first step is selective molecular pre-masking. In this step, pores that we did not wish to alter their surface properties (in this case, narrow pores) were covered with a protective molecular masking agent. In the second step, the surface properties of the unprotected pores (in this case, wide pores) were altered, leaving the masked pores unaffected. In the third step, the protective masking agent was removed to obtain a porous carbon material with different surface properties depending on the pore size.

To realize such pore-size-selective control, the following three criteria must be met:

- 1) high selectivity of pre-masking (Step 1);
- 2) stable masking, i.e., the mask does not detach during subsequent surface modification (Step 2);
- 3) simple and thorough unmasking without affecting the modified surface properties (Step 3).

In addition to these requirements, satisfying a fourth criterion is desirable:

- 4) none of the treatments should impact on the porosity of the material.

These criteria dictate the most suitable combinations of molecular pre-masking agents and surface-modification methods. As reversible and easily controllable processes, physical adsorption and desorption are intrinsically well-suited for pre-masking and satisfy criteria 1), 3), and 4).

The adsorbate, *n*-nonane, which stably adsorbs to fill narrow pores at room temperature [3], fulfils criterion 2). Furthermore, the amount adsorbed, *i.e.*, the masking degree, can be controlled by adjusting the temperature during vacuum heating to partially desorb the pre-adsorbed *n*-nonane [4]. On the other hand, the most appropriate surface modification protocol can be determined based on the target surface properties and the conditions required for stable masking. As a demonstration in this study, we prepared a sample in which surface properties A and B in **Figure 3.2** were hydrophobic and hydrophilic, respectively. Since the hydrophilicity can be enhanced by introducing oxygen-containing surface functional groups, here we adopted room-temperature ozonation to mainly generate carboxylic groups [5] for wide-pore-selective hydrophilization.



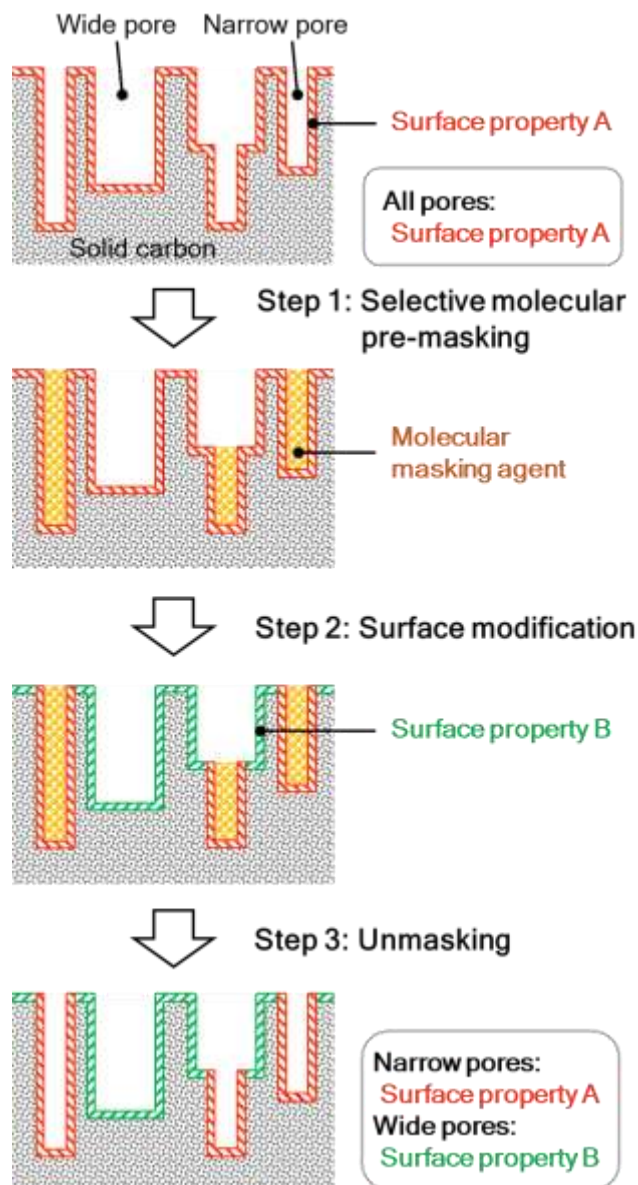


**Figure 3.2.** The concept of using three sequential treatments to realize pore-size-selective control of surface properties in porous carbon materials. This illustration shows an example of wide pore-selective surface modification, whereby a change in the characteristics of wide pores from property A to property B leaves the narrow pores unchanged.

### 3.3 Experimental

The starting sample was prepared as an all-surface hydrophobic activated carbon with a wide pore size distribution (denoted as H<sub>2</sub>-AC). Under a flow of nitrogen, a spherical phenol resin (BEAPS; ASAHI YUKIZAI CORPORATION, Japan) was carbonized at 873 K for 1 h, and then activated (KOH:the ground carbonized resin = 6:1 (w/w)) at 1273 K for 1 h. The reason why phenol resin was adopted as the precursor is because of its stable composition without containing ash, and

thus the stable properties between different batches of same samples is available. In addition, the possible influence of the ash on the performance of samples can be excluded.

The activated sample was heat-treated under a reducing atmosphere ( $\text{H}_2:\text{Ar} = 1:4$  (v/v), total flow rate =  $250 \text{ cm}^3/\text{min}$ ) at 873 K for 24 h to remove hydrophilic surface groups introduced during activation (**Figure 3.3**). In Step 1 (selective molecular pre-masking), the method of Gregg and Langford was applied [6]. With the apparatus shown in **Figure 3.4**,  $\text{H}_2\text{-AC}$  was exposed to a saturated vapor of degassed liquid *n*-nonane, first at 303 K (water bath) for 19 h and then at 77 K) for 40 min. Excess adsorbed *n*-nonane was removed under vacuum at 298 K (water bath) for 90 min. This resulted in occupation of 62 vol.% of the total pore volume. Here, the value of 62 vol.% was calculated from the total pore volume ( $V_{\text{total}}$ ), weight increase after Step 1 per sample weight ( $\Delta w$ ), and the liquid density of *n*-nonane ( $\rho$ ) according to the following equation.

$$\text{Pore filling ratio} = \frac{(\Delta w / \rho)}{V_{\text{total}}}$$

Based on the pore size distribution (*cf.* **Section 3.4.2**), the threshold of pore size dividing masked (protected) pores and unmasked ones was calculated to be ca. 3.6 nm.



**Figure 3.3.** High temperature vacuum furnace for  $\text{H}_2$  treatment.

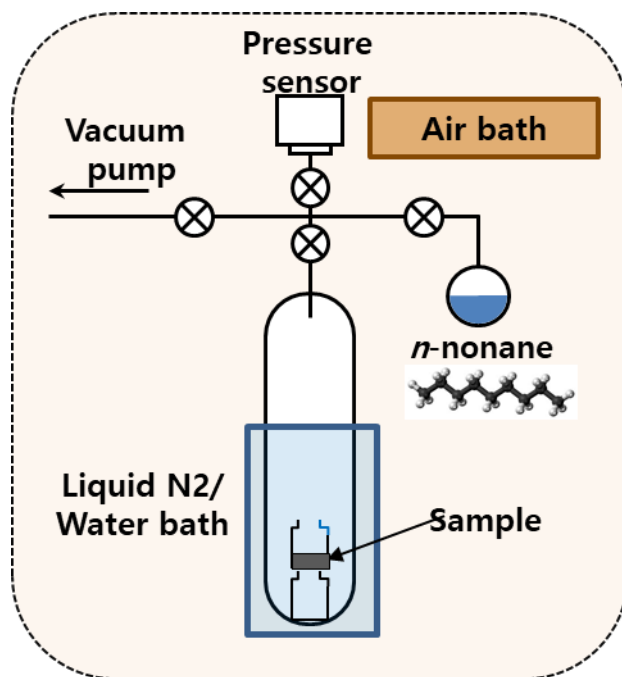


**Figure 3.4.** Schematic diagram of the adsorption apparatus for pre-masking (Step 1).

In Step 2 (surface modification), both the pre-masked and non-masked H<sub>2</sub>-AC were ozonated at around 298 K for 1 h with O<sub>3</sub> concentration of 73 g/m<sup>3</sup>(STP) using a commercial O<sub>3</sub> generator (NZR-06MF; ROKI TECHNO CO., LTD., Japan) (**Figure 3.5(a)**). The ozonated non-masked H<sub>2</sub>-AC was designated O<sub>3</sub>-H<sub>2</sub>-AC and should be all-surface hydrophilic. At 423–523 K, *n*-nonane desorbs even from narrow micropores with a pore size close to the minimum dimension of an *n*-nonane molecule [4, 7]. Thus, Step 3 (unmasking) was performed under vacuum at 463 K for 12 h with the apparatus in **Figure 3.5(b)**, retaining the introduced surface groups during the removal of residual *n*-nonane from pre-masked sample, to obtain the final sample of O<sub>3</sub>-nonane-H<sub>2</sub>-AC. A reference sample (ref.-AC) that underwent only *n*-nonane masking and unmasking was also prepared.



**Figure 3.5.** (a) The O<sub>3</sub> generator for room-temperature surface modification (Step 2); (b) The vacuuming furnace for unmasking (Step 3).

For a straightforward understanding, **Figure 3.6** gives the preparation process of the above 4 introduced samples in this chapter.

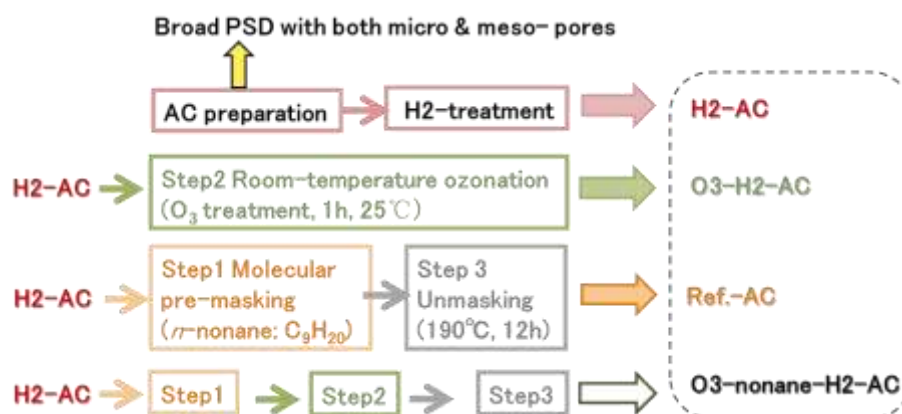


**Figure 3.6.** The preparation process of 4 samples.

To evaluate the influence of these two steps on porosity and surface properties, the amount of oxygen-containing surface functional groups of the four prepared samples was examined using a CHN analyzer (MT-5; ANATEC YANACO CORPORATION, Japan). The pore-size-dependent distribution of these groups was evaluated by H<sub>2</sub>O adsorption and desorption isotherms measured at 298 K using a volumetric adsorption apparatus (Belsorp-Max-S; Microtrac BEL Corp., Japan). Porosity was assessed by N<sub>2</sub> adsorption and desorption isotherms at 77 K using the same apparatus.

Among various analytical methods for surface functional groups, such as FT-IR, XPS, TPD, Boehm titration, etc., H<sub>2</sub>O adsorption isotherm measurement is the most powerful method to analyze the location of oxygen containing functional groups especially for porous materials. Other methods cannot provide such information. In this study, based on a confirmation of similar porosity (pore size distribution) by N<sub>2</sub> adsorption isotherm analyses, we'd like to confirm the difference of surface properties depending on the pore size, and thus, we adopted the H<sub>2</sub>O adsorption isotherm measurements.

## 3.4 Results and discussion

### 3.4.1 Elemental composition (CHN result)

**Table 3.1** shows the changes in oxygen content ( $O_{\text{diff}}$ ) induced by the different surface treatments. Without *n*-nonane pre-masking,  $O_{\text{diff}}$  increased from 3.9 to 8.6 wt.% by ozonation (H<sub>2</sub>-AC vs. O<sub>3</sub>-H<sub>2</sub>-AC), while with pre-masking the  $O_{\text{diff}}$  value of only 5.0 wt.% was obtained under the same conditions (O<sub>3</sub>-nonane-H<sub>2</sub>-AC). The increase in  $O_{\text{diff}}$  indicates that oxygen-containing surface functional groups were efficiently introduced by room-temperature ozonation, regardless of pre-masking. In addition, the smaller  $O_{\text{diff}}$  value of O<sub>3</sub>-nonane-H<sub>2</sub>-AC than that of O<sub>3</sub>-H<sub>2</sub>-AC implies that a proportion of pores became inaccessible to O<sub>3</sub> due to pre-adsorbed *n*-nonane.

**Table 3.1.** Changes in elemental composition and pore structural parameters resulting from different treatments.

Sample	Elemental composition [wt.%]				Pore structural parameter**			
	C	H	N	O <sub>diff.</sub> *	Total specific surface area [m <sup>2</sup> /g]	External specific surface area [m <sup>2</sup> /g]	Total pore volume [cm <sup>3</sup> /g]	Average pore width [nm]
H <sub>2</sub> -AC	95.7	0.3	0.1	3.9	2460	70	2.44	2.0
O <sub>3</sub> -H <sub>2</sub> -AC	91.3	0.0	0.1	8.6	2450	60	2.42	2.0
O <sub>3</sub> -nonane-H <sub>2</sub> -AC	94.1	0.8	0.1	5.0	2270	70	2.31	2.1
ref.-AC	96.2	0.7	0.0	3.2	2350	70	2.42	2.1

\*O<sub>diff.</sub> = 100 – (H + C + N)

\*\*Pore structural parameters were calculated by the  $\alpha_S$ -plot analysis of N<sub>2</sub> adsorption isotherms at 77 K.

### 3.4.2 Porosity information

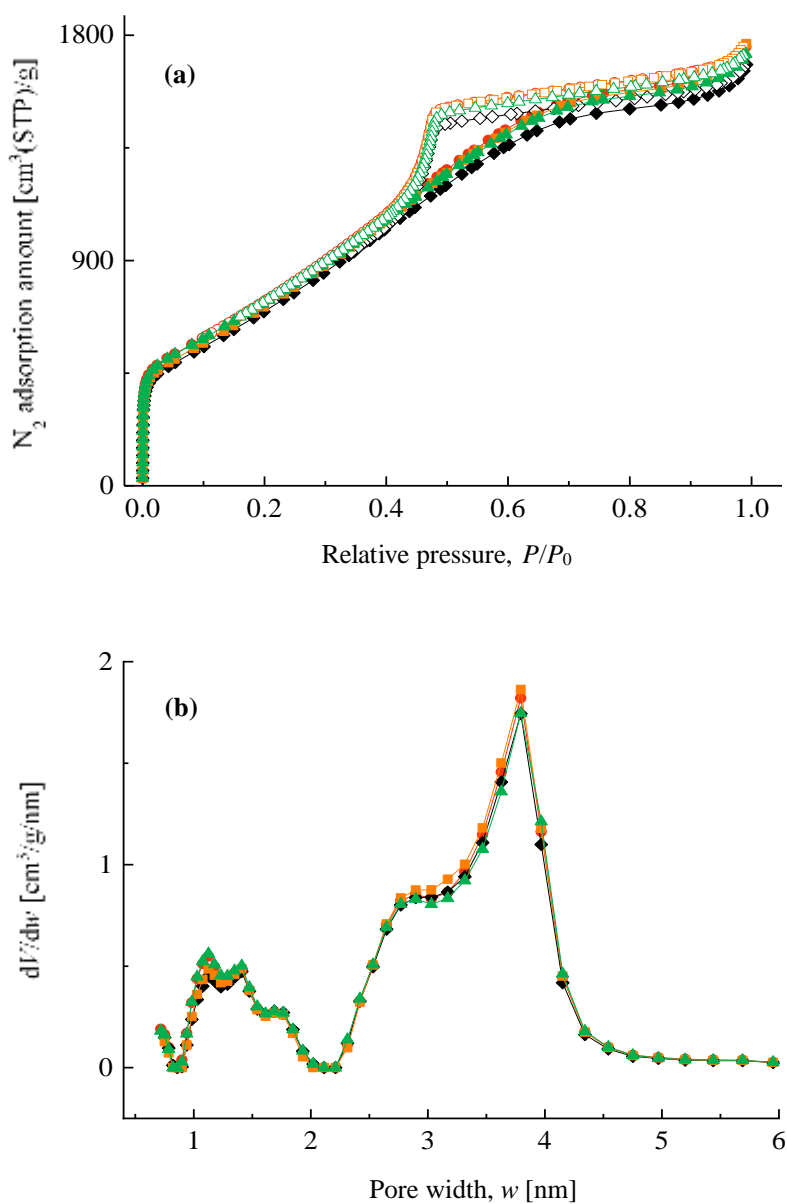
In contrast to the obvious variations in O<sub>diff.</sub>, no noticeable change in porosity was induced by any of the three treatments. This was confirmed by the similarity of the pore structural parameters (**Table 3.1**) and the overlapped pore size distributions (**Figure 3.7(b)**), derived by  $\alpha_S$ -plot analysis and the quenched solid density functional theory method, respectively, from N<sub>2</sub> adsorption and desorption isotherms at 77 K (**Figure 3.7 (a)**).

There were decreases in both specific surface area and pore volume of O<sub>3</sub>-nonane-H<sub>2</sub>-AC compared with ref.-AC and O<sub>3</sub>-H<sub>2</sub>-AC. Firstly, there is a possibility that tiny amount of adsorbed *n*-nonane still remained in narrow pores even after the unmasking process. In fact, ref.-AC showed small decreases in both specific surface area and pore volume as compared with H<sub>2</sub>-AC (**Table 3.1**). However, the degree of porosity loss in ref.-AC was obviously less than that in O<sub>3</sub>-nonane-H<sub>2</sub>-AC. In addition, N<sub>2</sub> adsorption isotherms at 77 K of these samples almost overlapped with each other even in low relative pressure range (**Figure 3.7(c)**). This indicated that the porosity loss resulted from remained *n*-nonane was negligible in these samples. Therefore, it is considered that the smaller specific surface area and pore volume of O<sub>3</sub>-nonane-H<sub>2</sub>-AC than O<sub>3</sub>-H<sub>2</sub>-AC were mainly caused by the ozonation.

If the loss of porosity was mainly due to the ozonation, we tentatively hypothesize the unexpected differences in porosity loss as a result of different resistance of pores against O<sub>3</sub> oxidation depending on their pore size. It has been reported that the O<sub>3</sub> preferentially reacted with mesopores than micropores [8]. With the same dose, for O<sub>3</sub>-nonane-H<sub>2</sub>-AC, all O<sub>3</sub> molecules reacted with mesopores

whose walls are supposed to be more fragile than those of micropores, causing a corruption of mesopores. On the other hand, for O<sub>3</sub>-H<sub>2</sub>-AC, we think that a part of O<sub>3</sub> molecules were “assigned” to react with micropores which have higher resistance, thus less amount of O<sub>3</sub> molecules reacted with mesopores compared with the masked sample, giving rise to a lower level of the oxidative corruption of mesopores.

Because the N<sub>2</sub> adsorption isotherms (**Figures 3.7(a)** and **(c)**) and the pore size distributions (**Figure 3.7(b)**) agreed well each other, respectively, the porosity of these 4 samples can be taken as practically same.



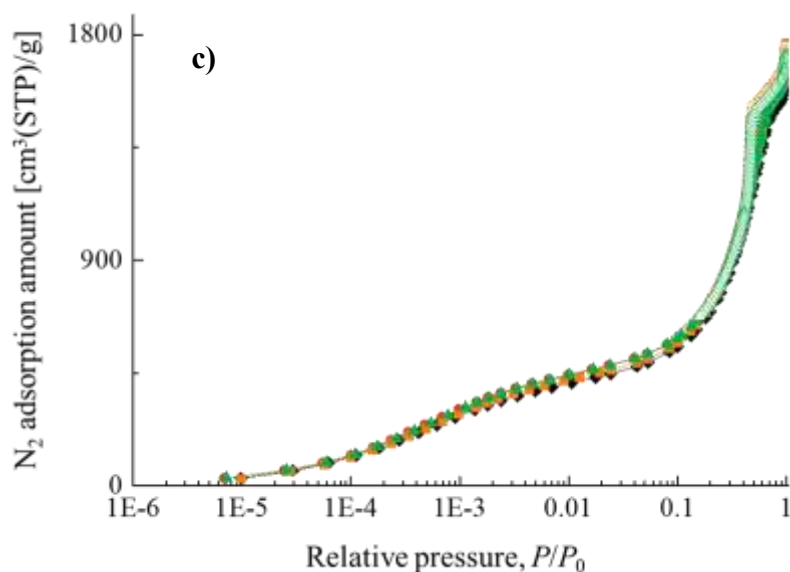


**Figure 3.7.** The influence of *n*-nonane masking/unmasking and ozone treatments on porosity are shown based on (a) N<sub>2</sub> adsorption and desorption isotherms at 77 K, (b) pore size distributions, and (c) N<sub>2</sub> adsorption and desorption isotherms at 77 K in logarithmic scales of relative pressure,  $P/P_0$ . The solid and open symbols in the isotherms denote adsorption and desorption, respectively. (●) H<sub>2</sub>-AC, (▲) O<sub>3</sub>-H<sub>2</sub>-AC, (◆) O<sub>3</sub>-nonane-H<sub>2</sub>-AC, (■) ref.-AC.

### 3.4.3 The distribution of oxygen-containing groups probed by H<sub>2</sub>O adsorption isotherms

Given the same porosity, the adsorption characteristics of polar molecules are governed only by the surface properties of the material. Therefore, the apparent differences in H<sub>2</sub>O adsorption at 298 K (**Figure 3.8**) can be attributed to a diverse distribution of the introduced hydrophilic functional groups. During adsorption, there was obvious variation in the relative pressure ( $P/P_0$ ) whereby a noticeable increment in the adsorption amount appeared. The starting sample (H<sub>2</sub>-AC) started to adsorb remarkable amounts of H<sub>2</sub>O at above  $P/P_0 = 0.8$ , which is typical of a hydrophobic surface. In contrast, the O<sub>3</sub>-treated sample without pre-masking (O<sub>3</sub>-H<sub>2</sub>-AC) showed a significant shift in adsorption uptake to around  $P/P_0 = 0.4$ . Of note, the pre-masked sample (O<sub>3</sub>-nonane-H<sub>2</sub>-AC) started to adsorb at about  $P/P_0 = 0.7$ , falling between the values of the former two samples. These results indicate that O<sub>3</sub>-nonane-H<sub>2</sub>-AC possessed hydrophilized wide pores that resulted in H<sub>2</sub>O adsorption starting at  $P/P_0 = 0.7$ , while the narrow pores remained hydrophobic without adsorption from  $P/P_0 = 0.4$ .

The desorption isotherms further revealed the effects of molecular pre-masking on selective surface modification. The pre-masked sample (O<sub>3</sub>-nonane-H<sub>2</sub>-AC) showed a single desorption step at around  $P/P_0 = 0.7$ . The non-masked sample (O<sub>3</sub>-H<sub>2</sub>-AC) showed two desorption steps, at around  $P/P_0 = 0.7$  and 0.4. There is a possibility of the existence of bottle-neck-type pores. In that case, however, similar stepwise adsorption phenomena of O<sub>3</sub>-H<sub>2</sub>-AC would also be observed in the parent

sample, H<sub>2</sub>-AC, considering the ozonation did not induce noticeable changes in porosity as confirmed by N<sub>2</sub> adsorption isotherm analyses. In addition, usually the stepwise desorption isotherm will not be observed in the case of bottle-neck-type pores, since the desorption is considered to occur at once at the pressure where the adsorbed state of H<sub>2</sub>O molecules at narrow “neck” part becomes unstable. Thus, we think that at least for our samples used in this study we can almost rule out the possibility of bottle-neck type pores. Therefore, the additional desorption step of O<sub>3</sub>-H<sub>2</sub>-AC at low  $P/P_0$  was due to the desorption of H<sub>2</sub>O molecules that had been adsorbed onto the hydrophilic surfaces of the narrow pores. This confirmed that hydrophilic groups were not introduced into the pre-masked narrow pores.

In addition, although the possible reaction between the adsorbed *n*-nonane and O<sub>3</sub> cannot be ruled out, its influence on the effect of *n*-nonane masking was negligible here. Furthermore, the similarity in H<sub>2</sub>O adsorption characteristics between ref.-AC and H<sub>2</sub>-AC confirmed that the pre-masking and unmasking steps did not significantly affect the surface properties. Thus, wide-pore-selective hydrophilization was achieved, with no loss in porosity, by applying the aforementioned three-step surface-treatment protocol.

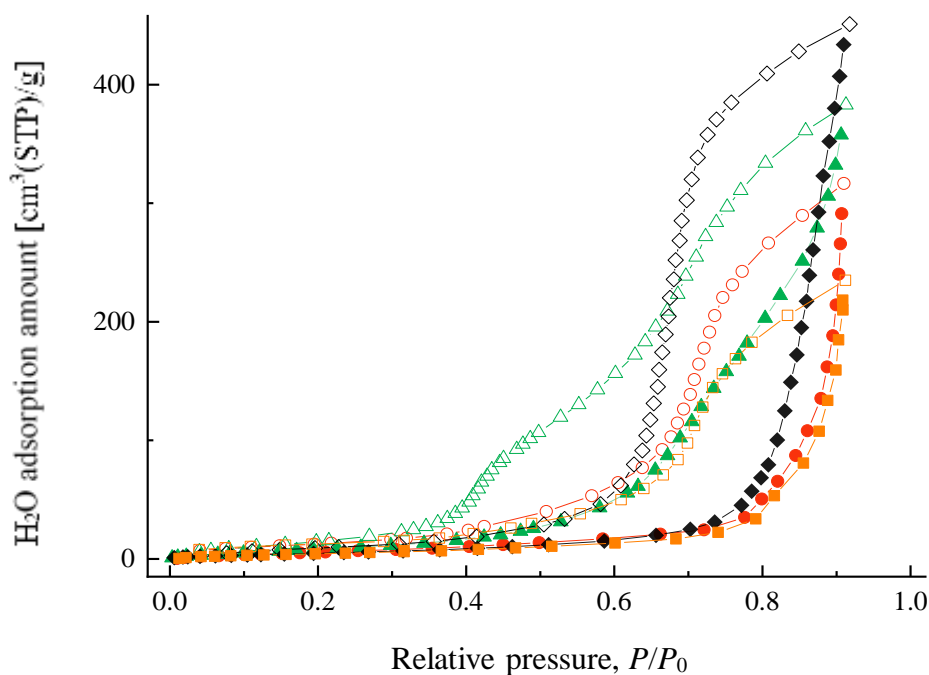


**Figure 3.8.** H<sub>2</sub>O adsorption and desorption isotherms at 298 K show different distributions of hydrophilic surface functional groups. The solid and open symbols denote adsorption and desorption, respectively. (●) H<sub>2</sub>-AC, (▲) O<sub>3</sub>-H<sub>2</sub>-AC, (◆) O<sub>3</sub>-nonane-H<sub>2</sub>-AC, (■) ref.-AC.



### 3.4.4 The adsorption phenomenon (total adsorption amount of H<sub>2</sub>O)

It has been reported that a higher oxidation content led to larger amount of oxygen functionalities, thus more adsorption amount of H<sub>2</sub>O (e.g. [9]). Our results did not follow the trend; such a phenomenon includes interesting themes of adsorption science.

One of the reasons would be the measurement pressure range ( $P/P_0 = 0-0.9$ ) of H<sub>2</sub>O adsorption isotherms: The H<sub>2</sub>O adsorption isotherms were not measured up to a very high relative pressure under which all pores reach the saturation. That is, the values of adsorption amount in **Figure 3.8** were not the saturated ones. In fact, the calculated adsorption amount of H<sub>2</sub>O for a sample with 2.4 cm<sup>3</sup>/g of pore volume is about 3000 cm<sup>3</sup>(STP)/g ( $\approx \frac{2.4 [\frac{\text{cm}^3}{\text{g}}] \times 1 [\frac{\text{g}}{\text{cm}^3}]}{18 [\frac{\text{g}}{\text{mol}}]} \times 22400 [\frac{\text{cm}^3(\text{STP})}{\text{mol}}]$ ), if we assumed the density of adsorbed H<sub>2</sub>O is 1 g/cm<sup>3</sup>.

To further explain why the sample with less oxygen groups showed more adsorption amount halfway of adsorption, the discussion about different strength (concentration) of introduced hydrophilic oxygen functional groups into different pore size is given in **Appendix A.7**.

## 3.5 Conclusion

This study describes a new three-step strategy for pore-size-dependent surface modification of porous carbon materials. To demonstrate this strategy, *n*-nonane was physically adsorbed as a molecular pre-masking agent; subsequent room-temperature ozonation was applied for surface modification to realize wide-pore-selective hydrophilization. This strategy can be employed using a variety of molecular masking agents and/or surface-modification methods, based on the proposed set of criteria, thereby allowing design of specific surface properties in pores within a specified size range. This in turn allows for performance optimization and multi-functionalization of porous carbon materials.

Here gives some examples of possible applications of our method. As mentioned in **Chapter 1**, instead of pursuing a high surface area and large pore volume, by selectively introducing the proper surface property to the pores within target pore size range that actually plays a role in certain application, we can improve the mechanical strength and packing density of the material because of less porosity with similar performance. On the other hand, with the same porosity, the selectivity/catalytic efficiency will be also improved by optimizing the surface properties of target pore size range in size-dependent separation process/surface catalysis. Another important application is the multi-functional porous carbons. For example, in wastewater treatment, we may wish to remove a small-molecular-size contaminant A and a larger-molecular size contaminant B at the same time. The simultaneously high-efficient removal would be possible by using a customized porous carbon with narrow pore of surface property A' that has high affinity to the contaminant A and wide pores with the corresponding surface property B' for the contaminant B.

In this Chapter, we focused on introducing an idea and demonstrating its feasibility and effectiveness. The simplification and standardization of the preparation process will be introduced in **Chapter 4**. Furthermore, the controllability and applicability of this 3-step strategy will be discussed in **Chapter 4**.

## **Acknowledgments**

We gratefully acknowledge ASAHI YUKIZAI CORPORATION for providing spherical phenol resins.

## References

- [1] Yu Y, Miyawaki J. Pore-size-selective control of surface properties of porous carbons by molecular masking. *Carbon* 2020, *in press*. (<https://doi.org/10.1016/j.carbon.2020.07.050>)
- [2] Frechet JMJ, Svec F. Pore-size selective modification of porous materials. U.S. Patent No. 5593729 (Jan. 14, 1997).
- [3] Stoeckli F, Huguenin D, Rebstein P. Characterization of active carbons by combined preadsorption and immersion techniques. *J Chem Soc Faraday Trans* 1991;87:1233–6.
- [4] Carrott PJM, Drummond FC, Kenny MB, Roberts RA, Sing KSW. Desorption of n-nonane from microporous carbons. *Colloids Surf* 1989;37:1–13.
- [5] Valdés H, Sánchez-Polo M, Rivera-Utrilla J, Zaror CA. Effect of ozone treatment on surface properties of activated carbon. *Langmuir* 2002;18:2111–6.
- [6] Gregg SJ, Langford JF. Evaluation of microporosity, with special reference to a carbon black. *Trans Faraday Soc* 1969;65:1394–1400.
- [7] Carrott PJM, Conceição FL, Carrott MR. Use of n-nonane pre-adsorption for the determination of micropore volume of activated carbon aerogels. *Carbon* 2007;45:1310–3.
- [8] Rivera-Utrilla J, Sánchez-Polo M, Gómez-Serrano V, Álvarez PM, Alvim-Ferraz MCM. Activated carbon modifications to enhance its water treatment applications. An overview. *J Hazard Mater* 2011;187:1–23.
- [9] Barton SS, Koresh JE. Adsorption interaction of water with microporous adsorbents. Part 1.— Water-vapour adsorption on activated carbon cloth. *J Chem Soc Faraday Trans* 1983;79:1147–55.

# Chapter 4 The controllability of size-selective-modifications by various pre-masking agent and heating temperature

## 4.1 Introduction

In **Chapter 3**, a newly proposed 3-step size-selective surface modification was explained (**Figure 3.1**) and proved to be effective by using a demonstration of pore-size-dependent hydrophilization [1]. Based on **Chapter 3**, this chapter focused on the flexibility and controllability of this proposed method; then, the applicability to other porous carbon materials with high controllability was proved.

### 1. Potential of the flexibility of the proposed method

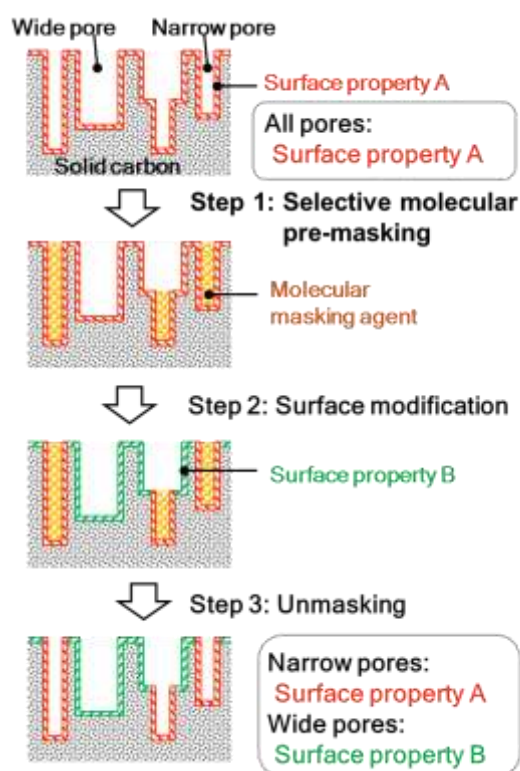


**Figure 4.1.** The concept of using three sequential treatments to realize pore-size-selective control of surface properties in porous carbon materials. This illustration shows an example of wide pore-selective surface modification, whereby a change in the characteristics of wide pores from property A to property B leaves the narrow pores unchanged.

As shown in **Figure 4.1**, the surface property A and B are not necessarily to be hydrophobic and hydrophilic, respectively, as demonstrated in **Chapter 3**. Similarly, the pre-masking method and the surface medication method can be other methods instead of the examples shown in **Chapter 3**. The flexible combinations of various pre-masking methods (conditions) and modification methods

are available to selectively modify the surface of the target part of pores to desired properties., since the three criteria proposed in **Chapter 3** are satisfied:

- 1) High selectivity of pre-masking (Step 1);
- 2) Stable masking, *i.e.*, the mask does not detach during subsequent surface modification (Step 2);
- 3) Simple and thorough unmasking without affecting the modified surface properties (Step 3)

## **2. Potential of the controllability of the proposed method**

The key point, the selectivity of the 3-step treatment strategy, is originated from the selective molecular pre-masking (step 1). And, the stable pre-masked status during surface modification (step 2) helps to guarantee such selectivity.

So, it's vital to find a proper pre-masking method and the conditions to realize the high selectivity (criterion 1)) and the stable masking state (criterion 2)).

To realize the good selectivity depending on pore size, the physical adsorption is an ideal choice in Step 1. Usually, the adsorption usually starts from narrow pores to wide pores because of the deeper adsorption potential well, while the desorption occurs from the wide pores to narrow pores. Taking advantage of these pore-size orders in adsorption phenomenon, in Step 1, we carried out the molecular pre-masking in following two sub-steps:

- ① Saturated adsorption: Complete filling of all pores;
- ② Controlled desorption: Partial removal of adsorbed masking agent by vacuum heating.

The desorption degree is easily controllable in physical adsorption and desorption process. By controlling the desorption degree, that is, the amount of adsorbed masking to be removed, one can adjust the pre-masking degree [2, 3].

It is expected that by adjusting the degree of pre-masking, the pore size range within which the pores are selectively modified is tunable. As shown in **Figure 4.2**, low pre-masking degree will further expose the narrow pores that should be pre-masked under high pre-masking degree, therefore the pore size range of pre-masked pores is adjustable. Therefore, the pore-size-range of unmasked pores whose surface properties will be selectively modified is also tunable.

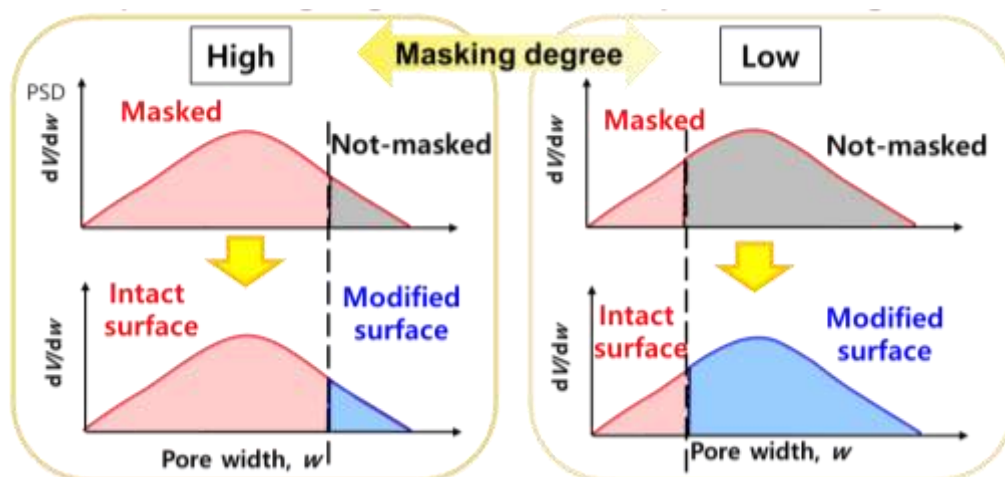


**Figure 4.2.** Proposals for arbitrary control: How pre-masking degree influences on the pore size range of selective surface modification.

To quantify pre-masking degree, the percentage of pore volume occupied by pre-masking agent (vol.%) is calculated as an indicator. For convenience, it is named as pore filling ratio. With such an indicator, the comparison and discussion about pre-masking degree of samples becomes convenient. A larger value of vol.% means a higher pre-masking degree. It was calculated from the total pore volume ( $V_{total}$ ), weight increase after Step 1 per sample weight ( $\Delta w$ ), and the liquid density of  $n$ -nonane ( $\rho$ ) according to the following equation.

$$\text{Pore filling ratio} = \frac{(\Delta w / \rho)}{V_{total}}$$

Since the pre-masking degree is adjustable by controlling the desorption degree, the factors that influence on the desorption process need to be considered. Two characters governing the physical desorption process provide us the ideas to make a control.

- i) Higher desorption temperature will facilitate the physical desorption.
- ii) Depending on the properties (boiling point, molecular structures) of adsorbates, the levels of the difficulty to desorb them from the porous adsorbents are different.
- iii) The longer the desorption time, the more the desorption amount.

Therefore, after reaching the saturated/near-saturated adsorption in Step 1, there are two possible ways to control the desorption degree according to the above i) and ii), respectively:

- i) Changing the temperature of vacuum heating ( $T_{VH}$ ) to remove excess adsorbed  $n$ -nonane;
- ii) Changing the molecular masking agent from  $n$ -nonane to other molecules;
- iii) Changing the desorption time.

In this study, vacuum heating was used to fast remove the excess pre-masked agent (fasten the desorption). Since it's difficult to guarantee the exactly same working status of the pumping system, especially the rotary pump we use (the longer working time, more hydrocarbons dissolved into the oil, thus less pumping efficiency), so the desorption time control is not proper to give a reliable

comparison between samples with different desorption time. So here, above i) and ii) were adopted to control the desorption degree.

For i), the higher  $T_{VH}$ , more pre-adsorbed amount of masking agent to be removed, thus a lower masking degree. In this study, besides the 30°C in **Chapter 3**, 70°C and 110°C were also tried.

For ii), easier for the masking agent to be removed, with under conditions same, lower the masking degree. In this study, other than *n*-nonane (C<sub>9</sub>H<sub>20</sub>) used in **Chapter 3**, other linear alkanes with higher boiling points and longer molecular chains that are more difficult to be desorbed were used [3]. Boiling points of used linear alkanes are listed in **Table 4.1**.

**Table 4.1.** Boiling points of C<sub>9</sub>H<sub>20</sub>, C<sub>12</sub>H<sub>26</sub> and C<sub>14</sub>H<sub>30</sub>.

	Boiling point [°C]
<i>n</i> -nonane (C <sub>9</sub> H <sub>20</sub> )	151
<i>n</i> -dodecane (C <sub>12</sub> H <sub>26</sub> )	215
<i>n</i> -tetradecane (C <sub>14</sub> H <sub>30</sub> )	254

In summary, higher vacuuming heating temperature or pre-masking agent with lower boiling point (weaker inter-molecule interaction) will lead to a lower pre-masking degree. By adjusting the pre-masking degree, the pore-size-selective surface modification is expected to be controllable.

A controllable pore size range for selective modification in pre-masking step, together with aforementioned flexibility of random combinations of various pre-masking methods (conditions) and surface modification methods, enable diversified surface properties to simultaneously appear on the surfaces of pores within arbitrary pore size ranges, respectively. As shown in **Figure 4.3**, flexible combinations of a random pore-size-range and a corresponding target surface property of the pores within this range are possible; two or three groups of such combination can simultaneously appear within one porous carbon material.

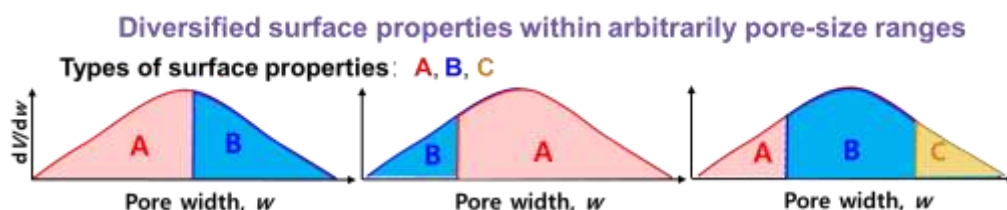


**Figure 4.3.** Various porous materials having different surface properties depending on pore size.

### **3. The applicability of this strategy**

In **Chapter 3**, an “home-made” activated carbon having a wide pore size distribution with both micro- and meso- pores were used to demonstrate the effectiveness of the proposed method. To confirm if the 3-step strategy is also applicable to other porous carbon materials, in this chapter, this 3-step strategy was also applied to a commercial microporous activated carbon, Maxsorb III [4], to prove the universality of our method.

## 4.2 Experimental

### 4.2.1 Sample preparation

Based on the proposed method in **Chapter 3**, the operation process for selective surface modification was simplified to it more operable, also standardized to enable the comparison between different treatment conditions. **Figure 4.4** displays the schematic with the italic part showing the differences compared with **Chapter 3**.

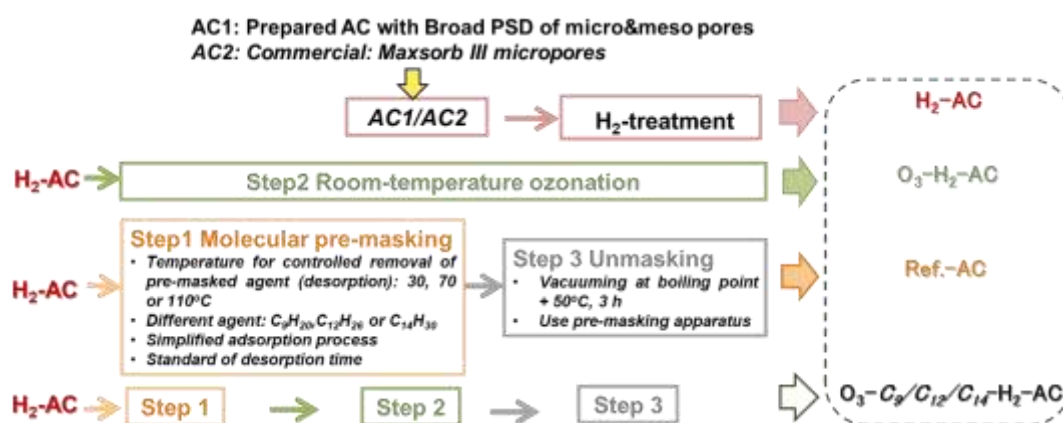


**Figure 4.4.** The simplified and standardized sample preparation process based on **Chapter 3**, using one more starting material and under various conditions. The *italic* part are the differences compared with **Chapter 3**.

The fixed experimental routines are introduced as below. The differences in experimental aspect and added samples compared with **Chapter 3** are emphasized with *italic* words in sub-titles in time order of sample preparation:

#### **1) Starting samples: *One more porous carbon to check the applicability this 3-step method***

Two starting samples were prepared as all-surface hydrophobic activated carbons, self-prepared micro- and mesoporous AC wide PSD: B17C600A1000K6 (denoted as H<sub>2</sub>- B17) and commercial micropores-only Maxsorb III (denoted as H<sub>2</sub>-Maxs) (KANSAI COKE AND CHEMICALS COMPANY, LIMITED, Japan). They were heat-treated under a reducing atmosphere (H<sub>2</sub>:Ar = 1:4 (v/v), total flow rate = 250 cm<sup>3</sup>/min) at 873 K for 24 h to remove hydrophilic surface groups introduced during activation.

#### **2) Standardized pre-treatment before Step 1**

Directly before the Step 1, the H<sub>2</sub>-treated sample will be further underwent pre-treatment within the system shown in **Figure 4.5**, 150°C vacuuming heating for 2 h to guarantee that no newly adsorption of air nor other gases in the atmosphere within the system.



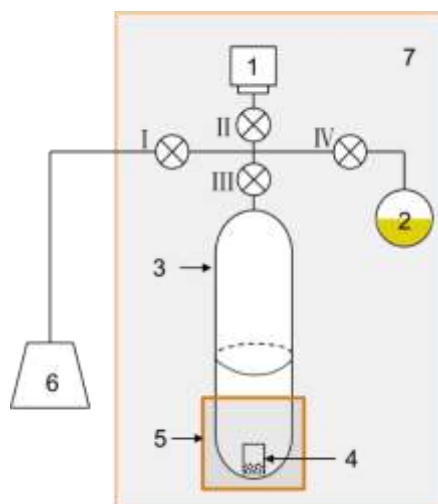


**Figure 4.5.** Schematic diagram of the adsorption & desorption apparatus for pre-treatment, pre-masking and unmasking, and unmasking in **Chapter 4**.

1. Pressure gauge, 2. Liquid pre-masking agent vessel, 3. Adsorption chamber, 4. Sample basket, 5. Isothermal heating by water bath (< 70°C) or electrical furnace (> 70°C), 6. Diffusion and rotary pumps, 7. Isothermal air bath (35°C); I-IV: valves.

As shown in **Figure 4.4**, here, the pre-masking agent was not limited to *n*-nonane (C<sub>9</sub>H<sub>20</sub>), longer chains with higher boiling point (C<sub>12</sub>H<sub>26</sub> and C<sub>14</sub>H<sub>30</sub>) were also adopted.

**3) Step 1 (selective molecular pre-masking): simplified adsorption process without 77 K step; a new standard to decide the desorption time (degree); various pre-masking agent & vacuuming heating temperatures.**

In Step 1 (selective molecular pre-masking), the pre-treated H<sub>2</sub>-B17 or H<sub>2</sub>-Maxs was exposed to a saturated vapor of degassed liquid pre-masking agent (C<sub>9</sub>H<sub>12</sub>/C<sub>12</sub>H<sub>26</sub>/C<sub>14</sub>H<sub>30</sub>), first at 30°C for more than 19 h and then the excess adsorbed masking agent was removed under vacuum at 30, 70 or 110°C of *T*<sub>VH</sub>. As mentioned before, the desorption time itself is not a trustworthy standard because of the pumping system we use. Here, we use the speed of pressure drop as a standard that when to stop the vacuuming heating (desorption process). When the speed of pressure drops shown by the pressure gauge (**Figure 4.5**, 1) was less than 1.0 Pa/5 min, the desorption process was finished. The resulted occupation of remained masking agent was calculated from the total pore volume (*V*<sub>total</sub>), weight increase after Step 1 per sample weight ( $\Delta w$ ), and the liquid density of pre-masking agent ( $\rho$ ) according to the following equation.

$$\text{Pore filling ratio} = (\Delta w / \rho) / V_{\text{total}}$$

**4) Step 2 (surface modification)**

In Step 2 (surface modification), both the pre-masked and non-masked H<sub>2</sub>-B17/H<sub>2</sub>-Maxs were ozonated at around 298 K for 1 h with O<sub>3</sub> concentration of 73 g/m<sup>3</sup>(STP) using a commercial O<sub>3</sub> generator (NZR-06MF; ROKI TECHNO CO., LTD., Japan) as shown in **Figure 3.5(a)**. The ozonated non-masked H<sub>2</sub>-B17 and H<sub>2</sub>-Maxs were designated O<sub>3</sub>-C<sub>9</sub>(C<sub>12</sub>/C<sub>14</sub>)-30(70/110)-H<sub>2</sub>-B17(Maxs) depending on the exact conditions.

### **5) Step 3 (unmasking): using the apparatus of Figure 4.5 with various unmasking conditions**

In Step 3 (unmasking) was performed again in the system of **Figure 4.5**, under vacuum at a temperature 50°C higher than the boiling point of the pre-masking agent for 3 h to obtain the final samples. The main reason to change the unmasking apparatus is the vacuuming furnace in **Figure 3.5(b)** can only work below 200°C. By using the same apparatus in Step 1, the vacuuming temperature required to remove C<sub>12</sub>H<sub>26</sub> and C<sub>14</sub>H<sub>30</sub> is reachable; with a more powerful pumping system and higher vacuum degree of the system, 3 h is supposed to be enough instead of previous 12 h.

Reference samples that underwent only *n*-nonane masking and unmasking was also prepared.

For a straightforward understanding, **Table 4.2** lists the prepared samples in this Chapter.

**Table 4.2.** List of representative samples prepared in **Chapter 4**.

<b>H<sub>2</sub>-B17C600A1000K6 series</b>		<b>Sample List</b>
original and O <sub>3</sub> -treated		H <sub>2</sub> -B17
		O <sub>3</sub> -1h-H <sub>2</sub> -B17
C <sub>9</sub> H <sub>20</sub>	30°C	O <sub>3</sub> -C <sub>9</sub> -30-H <sub>2</sub> -B17
	70°C	O <sub>3</sub> -C <sub>9</sub> -70-H <sub>2</sub> -B17
	110°C	O <sub>3</sub> -C <sub>9</sub> -110-H <sub>2</sub> -B17
C <sub>12</sub> H <sub>26</sub>	70°C	O <sub>3</sub> -C <sub>12</sub> -70-H <sub>2</sub> -B17
C <sub>14</sub> H <sub>30</sub>	70°C	O <sub>3</sub> -C <sub>14</sub> -70-H <sub>2</sub> -B17
<b>Maxsorb III series</b>		
original and O <sub>3</sub> -treated		H <sub>2</sub> -Maxs
		O <sub>3</sub> -1h-H <sub>2</sub> -Maxs
C <sub>9</sub> H <sub>20</sub>	30°C	O <sub>3</sub> -C <sub>9</sub> -30-H <sub>2</sub> -Maxs
	70°C	O <sub>3</sub> -C <sub>9</sub> -70-H <sub>2</sub> -Maxs
	110°C	O <sub>3</sub> -C <sub>9</sub> -110-H <sub>2</sub> -Maxs
C <sub>12</sub> H <sub>26</sub>	30°C	O <sub>3</sub> -C <sub>12</sub> -30-H <sub>2</sub> -Maxs

### **4.2.2 Sample evaluations**

To evaluate the influence of the treatments on porosity and surface properties, the amount of oxygen-containing surface functional groups of the four prepared samples was examined using a CHN analyzer (MT-5; ANATEC YANACO CORPORATION, Japan). The pore-size-dependent distribution of these groups was evaluated by H<sub>2</sub>O adsorption and desorption isotherms measured at 298 K using a volumetric adsorption apparatus (Belsorp-Max-S; Microtrac BEL Corp., Japan). Porosity was assessed by N<sub>2</sub> adsorption and desorption isotherms at 77 K using the same apparatus.

## 4.3 Results and discussion

### 4.3.1 Different heating temperature in pre-masking step to control the pre-masking degree

By adjusting the masking degree in Step 1, it would be possible to control the threshold of pore size—the pores whose sizes are smaller than this threshold size was masked (protected), while larger ones were unmasked. The ways to control the masking degree were, for example, by changing the temperature of vacuum heating ( $T_{\text{VH}}$ ) to remove excess adsorbed *n*-nonane, or by changing the molecular masking agent from *n*-nonane to other molecules.

#### **1. B17C600A1000K6, $T_{\text{VH}} = 30, 70$ or $110^\circ\text{C}$ , Masking agent: $\text{C}_9\text{H}_{20}$**

Firstly, we tried to control the masking degree and the threshold of pore size dividing the hydrophobic and hydrophilic surfaces by changing  $T_{\text{VH}}$  using  $\text{H}_2\text{-B17}$  as starting AC and *n*-nonane ( $\text{C}_9$ ) as the masking agent.

In **Table 4.3**, the pore structural parameters obtained from the  $\alpha_s$  analysis of  $\text{N}_2$  adsorption isotherms at 77 K (**Figure 4.6**) and oxygen content are given.

As for the porosity, the reference sample and the ozonated samples with a pre-masking showed similar porosities with each other, making the comparison between their  $\text{H}_2\text{O}$  adsorption and desorption isotherms more reliable to show the distribution status of introduced oxygen-containing functional groups under different  $T_{\text{VH}}$ . The slight porosity loss in these samples compared with the starting  $\text{H}_2\text{-B17}$  sample and  $\text{O}_3(1\text{h})\text{-H}_2\text{-B17}$ , may be mainly attributed to the oxidative corruption of wide pores due to the higher dose/concentration of  $\text{O}_3$  that reacted with unmasked wide pores; as discussed in **Chapter 3 (Section 3.4.2)**.

The oxygen contents and pore filling ratios in **Table 4.3** indicated that with the decrease of pre-masking degree (lower filling ratio), more oxygen was introduced into the pore surface. It is because that lower pre-masking degree, more exposed surface onto which oxygen-containing surface groups may be anchored with the same dose of  $\text{O}_3$ . From the  $\text{H}_2\text{O}$  adsorption isotherms in **Figure 4.7**, a decrease of pre-masking degree (from pre-masked  $\text{O}_3(1\text{h})\text{-C}_9\text{-30-30-H}_2\text{-B17}$  with a 37 vol.% pore filling ratio, to less pre-masked samples and then non-masked samples) resulted in an obvious trend that the relative pressure ( $P/P_0$ ), where the remarkable adsorption uptake started, shifted to lower values (corresponding to narrower pores). It means that when we reduced the pre-masking degree, the hydrophilic functional groups were able to be introduced to these further exposed surfaces of narrower pores. All these data proved that by adjusting the pre-masking degree, the pore selective modification is controllable. These data, again, confirmed the verification of our proposed three-step strategy for pore-size-dependent surface modification of porous carbons.

**Table 4.3.** Pore structural parameters and oxygen content of B17C600A1000K6-derived samples prepared with various desorption temperature.

Sample	Total specific surface area [m <sup>2</sup> /g]	External specific surface area [m <sup>2</sup> /g]	Total pore volume [cm <sup>3</sup> /g]	Average pore width [nm]	Oxygen content, O <sub>diff.</sub> [wt.%]	Pore filling ratio after C <sub>9</sub> pre-masking [vol.%]
H <sub>2</sub> -B17	2320	14	2.47	2.1	2.8	-
O <sub>3</sub> (1h)-H <sub>2</sub> -B17	2330	15	2.45	2.1	7.3	-
Ref.-B17	2100	18	2.25	2.2	-	-
O <sub>3</sub> (1h)-C <sub>9</sub> -30-30-H <sub>2</sub> -B17	2080	7	2.25	2.2	7.1	37
O <sub>3</sub> (1h)-C <sub>9</sub> -30-70-H <sub>2</sub> -B17	2080	7	2.26	2.2	8.3	18
O <sub>3</sub> (1h)-C <sub>9</sub> -30-110-H <sub>2</sub> -B17	2100	7	2.25	2.1	8.9	7

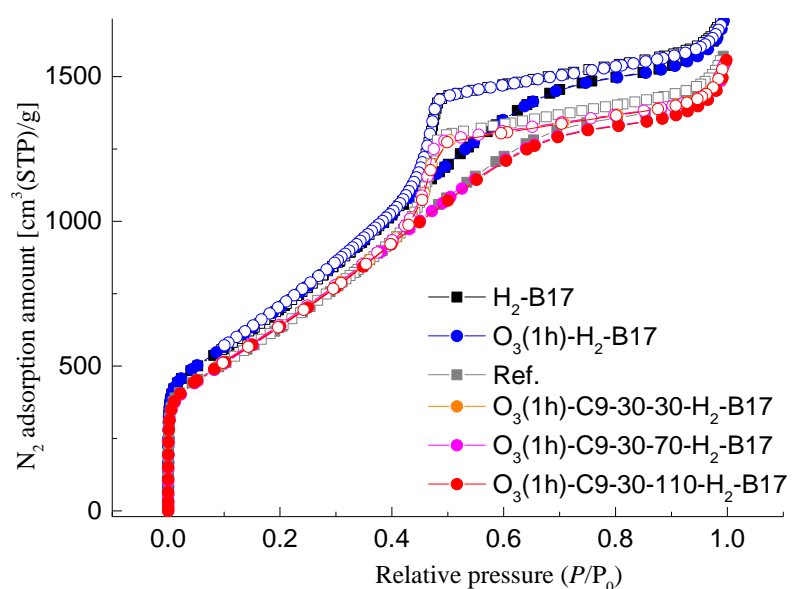


**Figure 4.6.** N<sub>2</sub> adsorption and desorption isotherms at 77 K of B17C600A1000K6-derived samples underwent different vacuum heating temperatures.

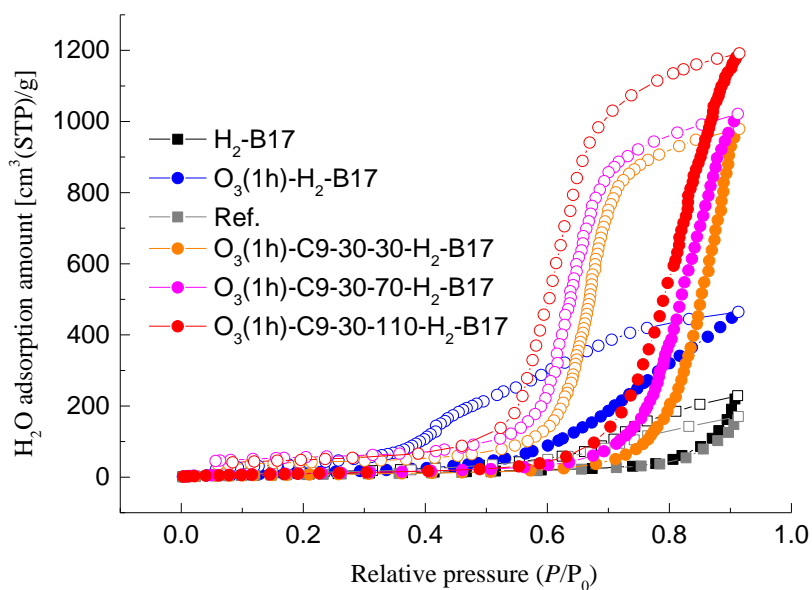


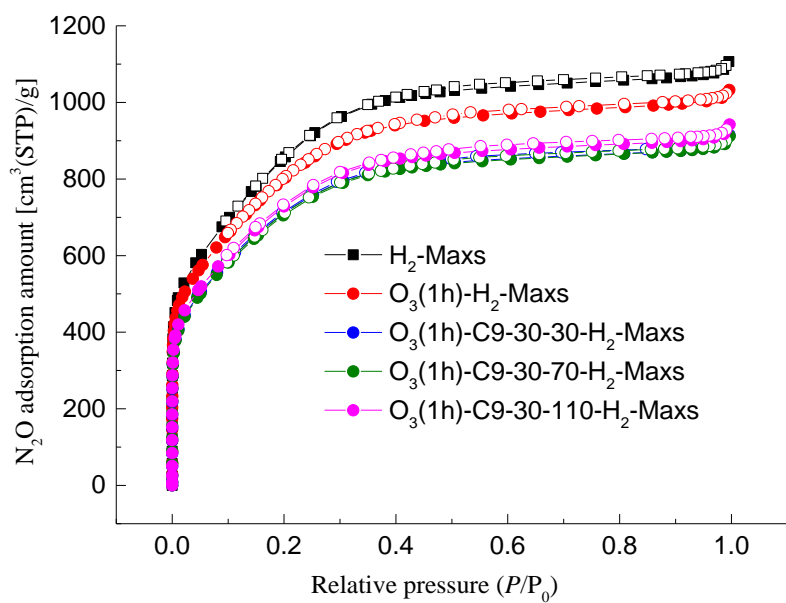
**Figure 4.7.** H<sub>2</sub>O adsorption and desorption isotherms at 298 K of B17C600A1000K6-derived samples underwent different vacuum heating temperatures.

## **2. Maxsorb III, $T_{VH} = 30, 70$ or $110^{\circ}\text{C}$ , Masking agent: $\text{C}_9\text{H}_{20}$**

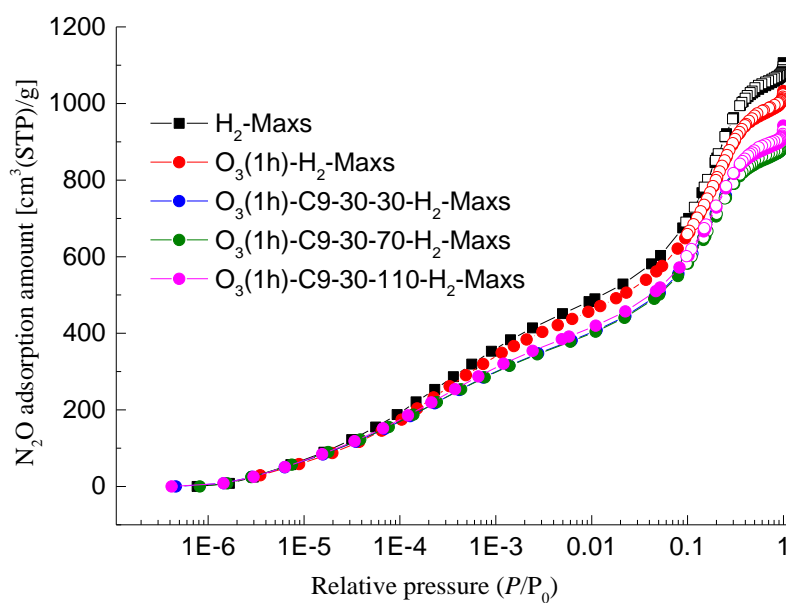
Similar to the B17C600A1000K6, Maxsorb III samples were also prepared under different desorption temperatures (30, 70 or  $110^{\circ}\text{C}$ ) in pre-masking step. As shown in **Table 4.4**, with an increase of  $T_{VH}$ , the pore filling ratio decreased. The similar porosity of the pre-masked samples was confirmed from **Figure 4.8** and **Table 4.4**. Therefore, the difference in H<sub>2</sub>O adsorption characteristics in **Figure 4.9** indicates that the tuning by controlling  $T_{VH}$  was also applicable to Maxsorb III.

**Table 4.4.** Pore structural parameters and oxygen content of Maxsorb III-derived samples prepared with various desorption temperature.

Sample	Total specific surface area [m <sup>2</sup> /g]	External specific surface area [m <sup>2</sup> /g]	Total pore volume [cm <sup>3</sup> /g]	Average pore width [nm]	Oxygen content, O <sub>diff.</sub> [wt.%]	Pore filling ratio after C <sub>9</sub> pre-masking [vol.%]
H <sub>2</sub> -Maxs	2810	2	1.68	1.2	1.5	-
O <sub>3</sub> (1h)-Maxs	2660	1	1.57	1.2	11.5	-
O <sub>3</sub> (1h)-C <sub>9</sub> -30-30-H <sub>2</sub> -Maxs	2370	2	1.37	1.2	8.8	69
O <sub>3</sub> (1h)-C <sub>9</sub> -30-70-H <sub>2</sub> -Maxs	2350	2	1.37	1.2	8.9	44
O <sub>3</sub> (1h)-C <sub>9</sub> -30-110-H <sub>2</sub> -Maxs	2420	2	1.41	1.2	9.3	15



(a) Normal X axis



(b) Log X axis

**Figure 4.8.**  $N_2O$  adsorption and desorption isotherms at 77 K of Maxsorb III-derived samples prepared with various desorption temperature.

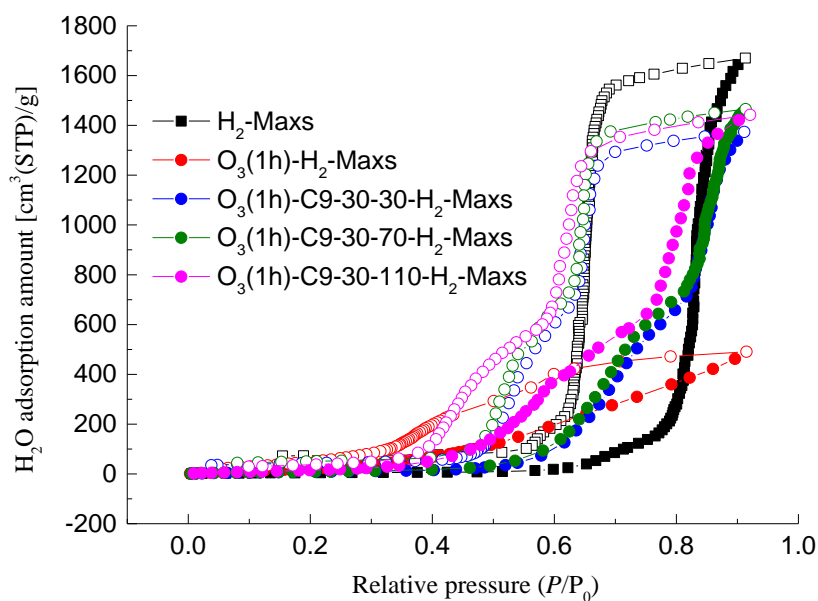


**Figure 4.9.** H<sub>2</sub>O adsorption and desorption isotherms at 298 K of Maxsorb III-derived samples prepared with various desorption temperature.

### 4.3.3 Different pre-masking agent for pre-masking degree

#### 1. B17C600A1000K7, $T_{VH} = 70^{\circ}\text{C}$ , Masking agent: C<sub>9</sub>H<sub>20</sub>, C<sub>12</sub>H<sub>26</sub> or C<sub>14</sub>H<sub>30</sub>

Other molecules, *n*-dodecane (C<sub>12</sub>H<sub>26</sub>) and *n*-tetradecane (C<sub>14</sub>H<sub>30</sub>), as the molecular masking agents were also applied to the H<sub>2</sub>-B17 sample. As the boiling points ( $T_b$ ) of those molecules are different from that of *n*-nonane ( $T_{b, \text{nonane}} = 151^{\circ}\text{C}$ ,  $T_{b, \text{dodecane}} = 215^{\circ}\text{C}$ ,  $T_{b, \text{tetradecane}} = 254^{\circ}\text{C}$ ), the different masking levels (pore filling ratios) were achieved even at the same vacuum-heating temperature ( $T_{VH}$ ) as shown in **Table 4.5**. With increasing the boiling point (longer chain), a clear increasing trend was observed in the pre-masking degree, and thus less oxygen-containing groups introduced. The take-up point of the H<sub>2</sub>O adsorption isotherms also shows that shorter chain (C<sub>9</sub>H<sub>20</sub>) gave the lowest relative pressure for adsorption amount uptake, indicating that it can only cover the small pores compared with C<sub>12</sub>H<sub>26</sub> and C<sub>14</sub>H<sub>30</sub> (**Figure 4.10**)

In **Table 4.5**, the pore structural parameters obtained from the  $\alpha_s$  analysis of N<sub>2</sub> adsorption isotherms at 77 K (**Figure 4.11**) and oxygen content are also given for B17C600A1000K6-derived samples pre-masked by C<sub>9</sub>H<sub>20</sub>, C<sub>12</sub>H<sub>26</sub> or C<sub>14</sub>H<sub>30</sub> under same vacuum heating temperature at 70°C.

These data re-confirmed the validity of pore-size-selective surface modification and proved the controllability and versatility of the proposed three-step method.

**Table 4.5.** Pore structural parameters and oxygen contents of B17C600A1000K6-derived samples pre-masked by C<sub>9</sub>H<sub>20</sub>, C<sub>12</sub>H<sub>26</sub> or C<sub>14</sub>H<sub>30</sub> under same vacuum heating temperature at 70°C.

Sample	Total specific surface area [m <sup>2</sup> /g]	External specific surface area [m <sup>2</sup> /g]	Total pore volume [cm <sup>3</sup> /g]	Average pore width [nm]	Oxygen content, O <sub>diff.</sub> [wt.%]	Pore filling ratio after pre-masking [vol.%]
H <sub>2</sub> -B17	2320	14	2.47	2.1	2.8	-
O <sub>3</sub> (1h)-H <sub>2</sub> -B17	2330	15	2.45	2.1	7.3	-
O <sub>3</sub> (1h)-C <sub>9</sub> -30-70-H <sub>2</sub> -B17	2080	7	2.26	2.2	8.3	18
O <sub>3</sub> (1h)-C <sub>12</sub> -30-70-H <sub>2</sub> -B17	1910	8	2.16	2.3	5.6	36
O <sub>3</sub> (1h)-C <sub>14</sub> -30-110-H <sub>2</sub> -B17	2160	6	2.37	2.2	4.5	49

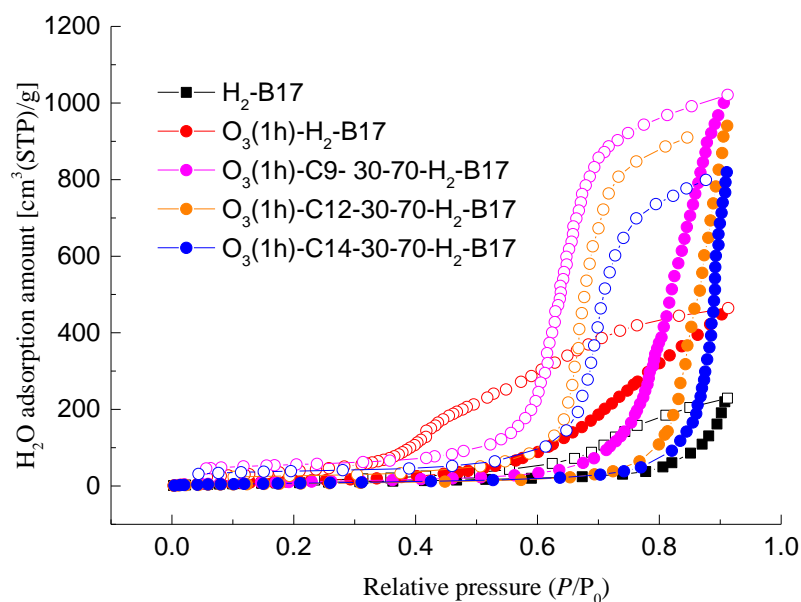
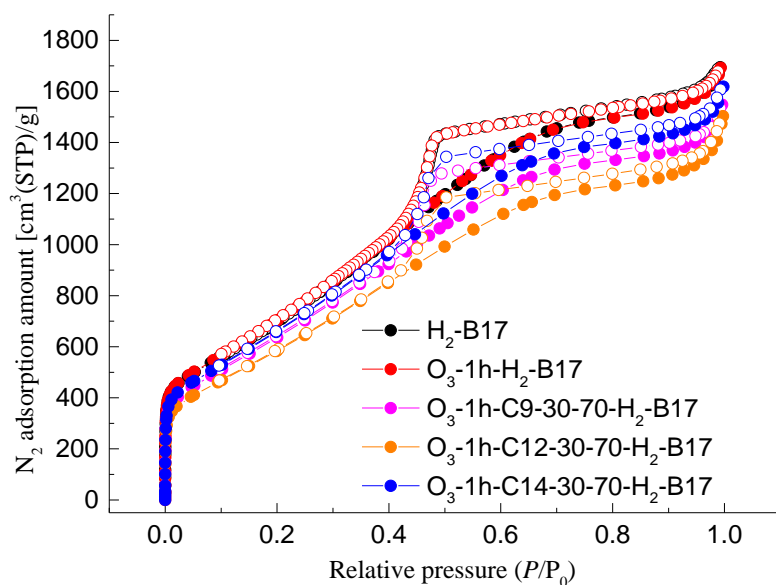
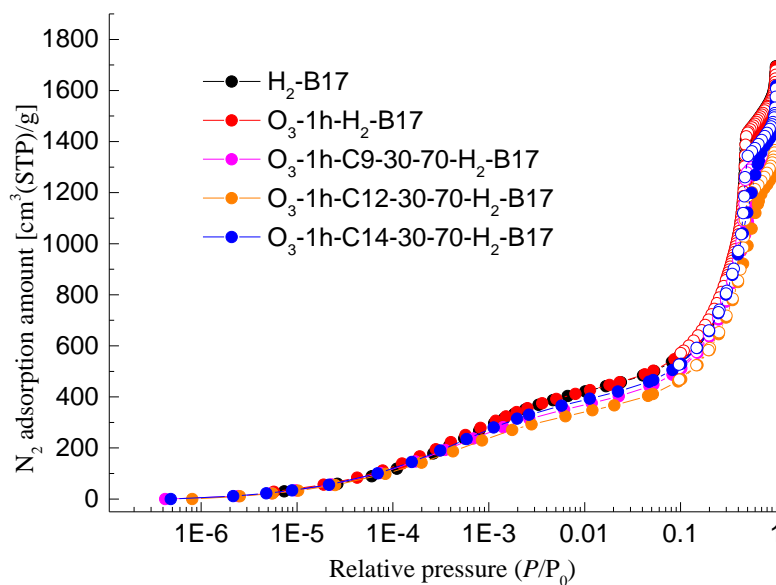


**Figure 4.10.** H<sub>2</sub>O adsorption and desorption isotherms at 298 K of B17C600A1000K6-derived samples pre-masked by C<sub>9</sub>H<sub>20</sub>, C<sub>12</sub>H<sub>26</sub> or C<sub>14</sub>H<sub>30</sub> under same vacuum heating temperature at 70°C.





(a) Normal X axis



(b) Log X axis

**Figure 4.11.**  $N_2$  adsorption and desorption isotherms at 77 K of B17C600A1000K6-derived samples pre-masked by  $C_9H_{20}$ ,  $C_{12}H_{26}$  or  $C_{14}H_{30}$  under same vacuum heating temperature at  $70^\circ\text{C}$ .

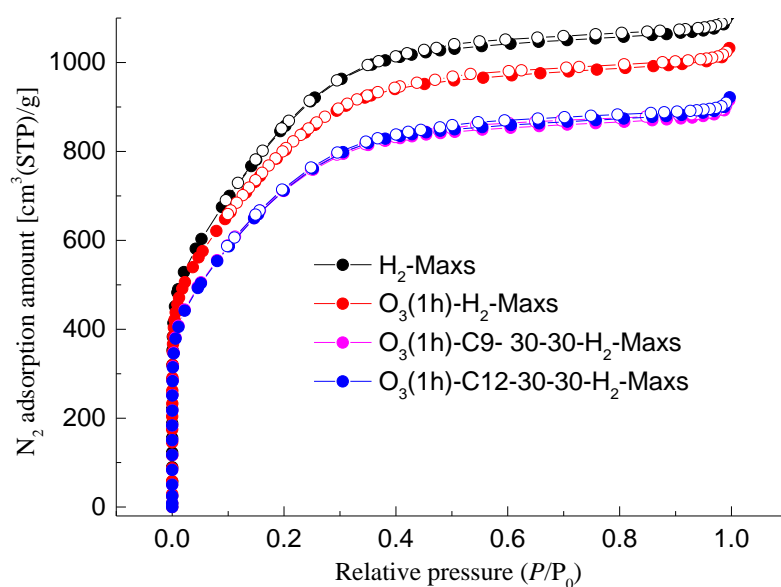
**2. Maxsorb III,  $T_{VH} = 30^\circ\text{C}$ , Masking agent:  $C_9H_{20}$ ,  $C_{12}H_{26}$  or  $C_{14}H_{30}$**

Similar to B17C600A1000K6, two other molecular masking agents,  $C_9H_{20}$  and  $C_{12}H_{26}$ , were also applied to Maxsorb III. As found in **Table 4.6**, by changing the pre-masking agent, the pre-masking

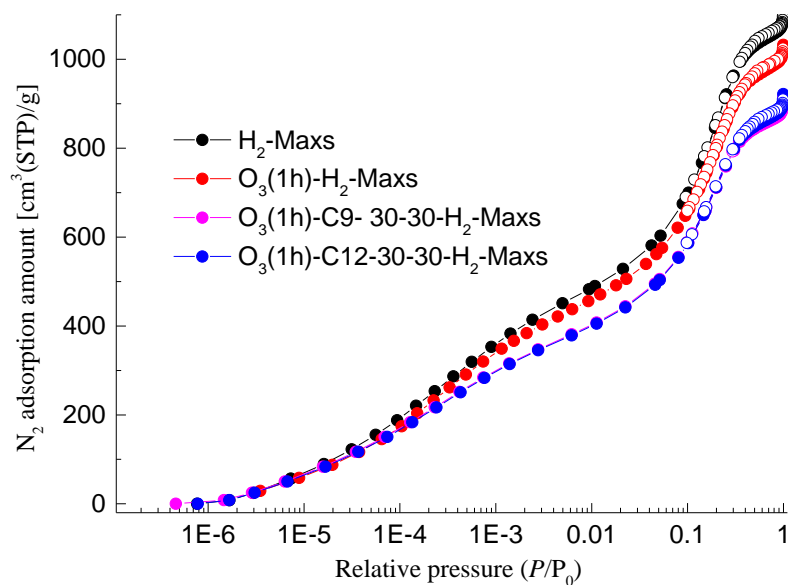
degree was also controllable for Maxsorb III. And, **Figures 4.12** and **4.13**, similar conclusions were obtained for commercial microporous activated carbon, Maxsorb III.

**Table 4.6.** Pore structural parameters and oxygen contents of Maxsorb III-derived samples pre-masked by  $C_9H_{20}$  or  $C_{12}H_{26}$  under same vacuum heating temperature at  $30^\circ C$ .

Sample	Total specific surface area [ $m^2/g$ ]	External specific surface area [ $m^2/g$ ]	Total pore volume [ $cm^3/g$ ]	Average pore width [nm]	Oxygen content, $O_{diff}$ [wt.%]	Pore filling ratio after pre-masking [vol.%]
H <sub>2</sub> -Maxs	2810	2.	1.68	1.2	1.5	-
O <sub>3</sub> (1h)-Maxs	2660	1.	1.57	1.2	11.5	-
O <sub>3</sub> (1h)-C <sub>9</sub> -30-30-H <sub>2</sub> -Maxs	2370	2	1.37	1.2	8.8	69
O <sub>3</sub> (1h)-C <sub>12</sub> -30-30-H <sub>2</sub> -Maxs	2350	2	1.38	1.2	6.8	95



(a) Normal X axis



(b) Log X axis

**Figure 4.11.** N<sub>2</sub> adsorption and desorption isotherms at 77 K of Maxsorb III-derived samples pre-masked by C<sub>9</sub>H<sub>20</sub> or C<sub>12</sub>H<sub>26</sub> under same vacuum heating temperature at 30°C.

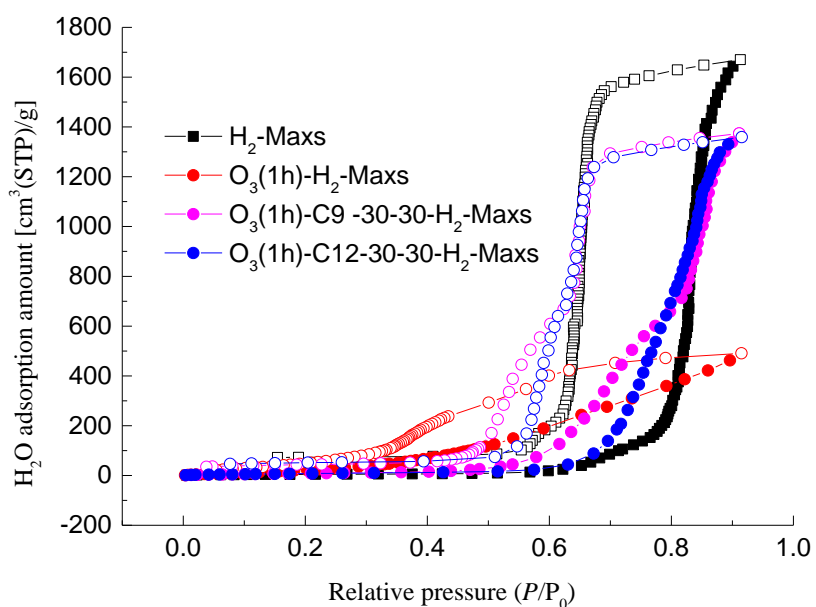


**Figure 4.12.** H<sub>2</sub>O adsorption and desorption isotherms at 298 K of Maxsorb III-derived samples pre-masked by C<sub>9</sub>H<sub>20</sub> or C<sub>12</sub>H<sub>26</sub> under same vacuum heating temperature at 30°C.

## 4.4 Conclusion

Based on the 3-step pore-size-selective surface modification methods detailedly explained and demonstrated in **Chapter 3**, this chapter further checked the controllability of this strategy by adopting 1) different vacuuming heating temperature ( $T_{VH}$ ) in pre-masking step for removal of excess adsorbed *n*-nonane, and 2) other pre-masking agents with different boiling point. The results showed that higher vacuuming heating temperature or pre-masking agent with lower boiling point (weaker inter-molecule reaction) led to lower pre-masking degree. By adjusting the pre-masking degree, the pore-size-selective surface modification proved to be controllable. An arbitrary pore-size-range within which the pores fall into were selectively surface modified is available by adjusting the pre-masking degree.

This 3-step strategy was also applied to commercial microporous activated carbon, and similar effectiveness and the controllability were demonstrated in these samples. The effectiveness and similar controllability of this molecular pre-masking-based size-selective surface modification method were well demonstrated. Therefore, the proposed 3-step method is also applicable to other porous carbons.

## 4.5 Future work

To realize the more arbitrary control of surface property depending on the pore size, the precise pre-masking of the desired pore-size range can be tried by adjusting the pre-masking degree through fine-tuning the conditions in each step, and more diversified masking agents, which not has to be limited to the chain-molecular masking agents applied in this thesis.

In order to get the optimum condition for desired target, it is also indispensable to experimentally confirm the desorption phenomena of pre-masked *n*-nonane. Similarly, more thoroughly understandings of adsorption and desorption phenomena of H<sub>2</sub>O and other working agent/target in specified applications are necessary.

Meanwhile, various combinations of molecular masking agents and surface modification methods as for as the aforementioned requirements are selectable; creating more possibilities of porous carbon materials. For example, the reversed “narrow pores hydrophilic-wide pores hydrophobic” samples. What’s more, flexible assembles of the 3-step treatments with these selectable agents and methods enable diversified (3 types or more) surface properties to simultaneously appear within the different pore-size ranges, respectively (depending on the pore size) of the same porous carbon material to satisfy a demanding application.

All these arbitrary pore-size selective controls should broaden the future of porous carbon materials.

## References

- [1] Yu Y, Miyawaki J. Pore-size-selective control of surface properties of porous carbons by molecular masking. *Carbon* 2020, *in press*. (<https://doi.org/10.1016/j.carbon.2020.07.050>)
- [2] Carrott PJM, Drummond FC, Kenny MB, Roberts RA, Sing KSW. Desorption of n-nonane from microporous carbons. *Colloids Surf* 1989;37:1–13.
- [3] Stoeckli F, Huguenin D, Rebstein P. Characterization of active carbons by combined preadsorption and immersion techniques. *J Chem Soc Faraday Trans* 1991;87:1233–6.
- [4] Otowa T, Tanibata R, Itoh M. (1993). Production and adsorption characteristics of MAXSORB: high-surface-area active carbon. *Gas Separ Purif* 1993;7:241–5.

## Appendix for Chapter 3 and Chapter 4

### A.6 Ozonation conditions

#### **B17C600A1000K6 (wide PSD activated carbon)**

As a prior trial, two group of samples starting from H<sub>2</sub>-B17C600A1000K6 with different pre-masking degree and ozonation time were prepared: O<sub>3</sub>-1h-C<sub>9</sub>-60vol%-H<sub>2</sub>-B17 and O<sub>3</sub>-3h-C<sub>9</sub>-30vol%-H<sub>2</sub>-B17. Although being the trial samples, they still provide us some valuable information as helps to fix the better experimental conditions, explain some phenomenon, and indicating the potential of flexible controllability of our method.

#### 1. The influence of ozonation time

Usually the ozonation could cause a decrease of specific surface area of carbon materials. In fact, with the same O<sub>3</sub> concentration, we also found that the longer ozonation period (1 h → 3 h) gave rise to the lower specific surface area and pore volume (**Table A6**). It has been reported that the impact of O<sub>3</sub> on the texture of porous carbon materials appears to be highly dependent on the dose: some researches showed no obvious change, and for the underdeveloped porosity system, small dose of O<sub>3</sub> resulted in an increased surface area due to carbon gasification [1]. Here, we chose the 1-h treatment as a moderate condition for its tolerable influence on the porosity.

**Table A6.** Pore structural parameters and oxygen content.

Sample	Total specific surface area [m <sup>2</sup> /g]	External specific surface area [m <sup>2</sup> /g]	Total pore volume [cm <sup>3</sup> /g]	Average pore width [nm]	Oxygen content, O <sub>diff.</sub> [wt.%]
H <sub>2</sub> -B17	2460	70	2.44	2.0	3.9
O <sub>3</sub> -H <sub>2</sub> -B17 (1 h)	2450	60	2.42	2.0	8.6
O <sub>3</sub> -H <sub>2</sub> -B17 (3 h)	2310	60	2.27	2.0	11.0
O <sub>3</sub> -H <sub>2</sub> -B17 (12 h)	50	20	0.19	12	41.9
O <sub>3</sub> -C <sub>9</sub> -H <sub>2</sub> -B17 (1 h)	2270	70	2.31	2.1	5.0
O <sub>3</sub> -C <sub>9</sub> -H <sub>2</sub> -B17 (3 h)	1900	60	1.95	2.1	9.2
Ref.-B17	2350	70	2.42	2.1	3.2

When we further increase the ozonation time to 12 h for 0.3 g sample, much less sample was remained after the treatment. The total specific surface area reduced to 50 m<sup>2</sup>/g with average pore width of 12 nm. **Figure A6** gives the H<sub>2</sub>O adsorption and desorption isotherms at 298 K of O<sub>3</sub>-treated non-masked samples (O<sub>3</sub>-H<sub>2</sub>-B17) under different ozonation times with the same O<sub>3</sub> concentration used in **Chapter 3**. With the longer ozonation time, the introduced oxygen amount increased from 3.9 wt.% to 41.9 wt.% (**Table A6**), and the adsorption amount at  $P/P_0 = 0.9$  increased.

In addition, the take-up point of adsorption amount shifted to the left side, indicating a more hydrophilic surface. These results also indicate that the amount of hydrophilic oxygen-containing functional groups introduced into smaller pores may also increase with the longer ozonation time. What has to be emphasized here is that the pore structure was not same with each other as shown in **Table A6**.

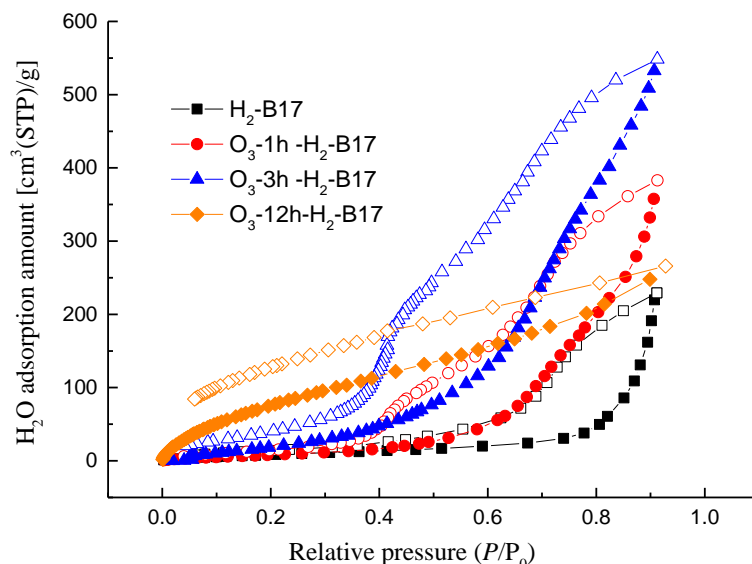


**Figure A6.** H<sub>2</sub>O adsorption and desorption isotherms at 298 K of B17C600A1000K6-derived samples prepared under different ozonation time.

## 2. The influence ozonation concentration under same total doze

After checking the influence of ozonation time, we concluded that 1-h treatment was proper for the O<sub>3</sub> treatment as no obvious change in porosity. Next, the influence of the O<sub>3</sub> concentration was also checked.

With keeping the ozonation time to be 1 h, we reduced the O<sub>3</sub> concentration by increasing the O<sub>2</sub> flow rate from 1 L/min to 2 L/min. According to the output properties of the O<sub>3</sub> generator, to keep the same total amount of O<sub>3</sub> that react with samples by extending the treatment time to 105 min for 2 L/min of flow rate.

**Table A7** summarizes the pore structural parameters and **Figure A7** shows H<sub>2</sub>O adsorption and desorption isotherms at 298 K, respectively. No obvious difference among the two samples under the chosen conditions with same total O<sub>3</sub> amount.

**Table A7.** Pore structural parameters and oxygen content.

Sample	Total specific surface area [m <sup>2</sup> /g]	External specific surface area [m <sup>2</sup> /g]	Total pore volume [cm <sup>3</sup> /g]	Average pore width [nm]	Oxygen content, O <sub>diff.</sub> [wt.%]
H <sub>2</sub> -AC	2460	70	2.44	2.0	3.9

O <sub>3</sub> -H <sub>2</sub> -AC (1 h, 1 L/min)	2330	15	2.45	2.1	8.2
O <sub>3</sub> -H <sub>2</sub> -AC (105 min, 2 L/min)	2335	15	2.44	2.1	8.4

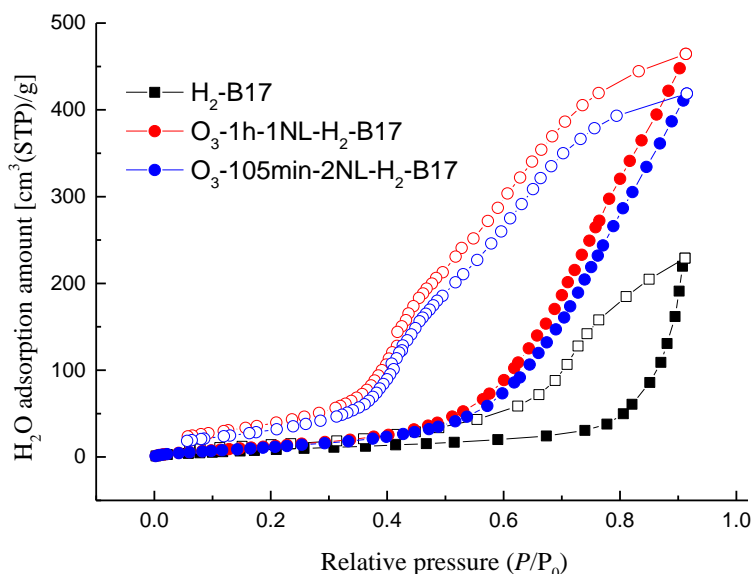


**Figure A7.** H<sub>2</sub>O adsorption and desorption isotherms at 298 K for B17C600A1000K6-derived samples prepared under different O<sub>3</sub> concentration (same total O<sub>3</sub> amount).

### 3. The influence of sample amount on the ozonation treatment

The sample amount influenced on the effect of ozonation treatment. The samples of different AC amount but same ozonation conditions showed a bit different shapes of H<sub>2</sub>O adsorption isotherm curves; however, the take-up point of adsorption amount didn't see large difference. (Detailed data not shown here)

Therefore, to be prudent, the sample amount was fixed in our study as 100 mg in **Chapter 4**.

### Maxsorb III (Narrow PSD, microporous activated carbon)

#### The influence of O<sub>3</sub> concentration under same treating time

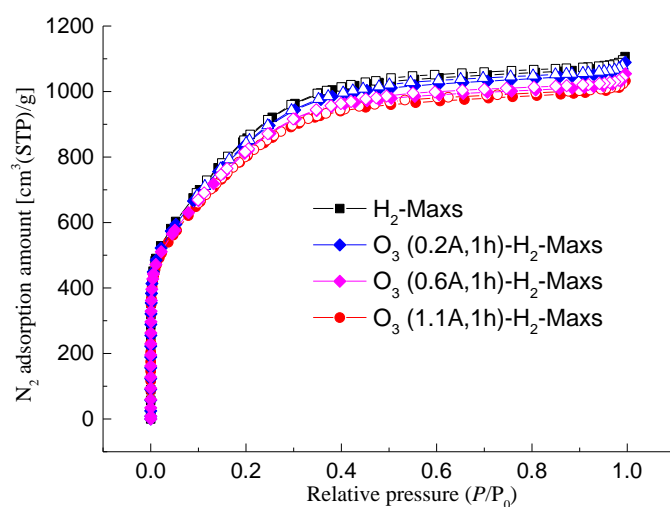
For Maxsorb III, based on the experience on B17C600A1000K6, we adopted the 1-h ozonation time with 1 A of the applied current of the O<sub>3</sub> generator (**Figure 3.5(a)**), denoted as 1A-1h under 1 L/min flow rate, which is the "standard condition" for ozonation in this thesis. To find the proper ozonation condition for this sample with narrower PSD and mainly composed of micropores, different from the "standard condition", the concentration of O<sub>3</sub> for 1 h treatment was reduced by changing the applied current, and denoted as 0.6A-1h and 0.2A-1h, respectively.



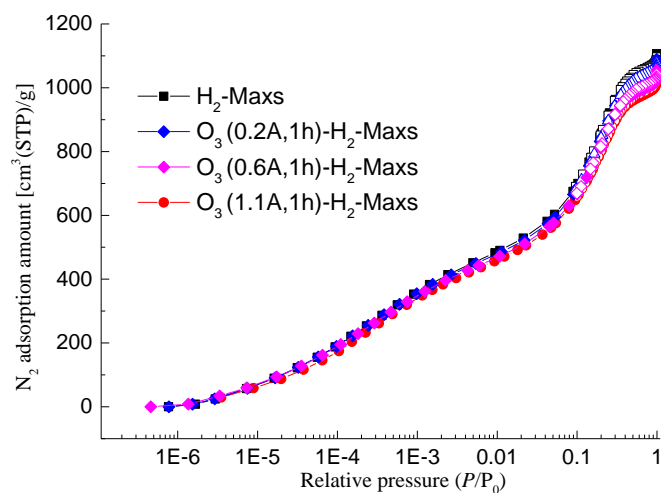
In **Table A8**, the pore structural parameters obtained from the  $\alpha_s$  analysis of  $N_2$  adsorption isotherms at 77 K (**Figure A8**) and oxygen content are given. With the similar porosity, the 1.1A-1h treatment afforded to introduce the largest amount of oxygen functional groups with oxygen content of 11.4 wt.%. Therefore, in **Chapter 4**, the ozonation condition for Maxsorb III was chosen as 1.1A for 1h.

**Table A8.** Pore structural parameters and oxygen content for different  $O_3$  concentration for Maxsorb III.

Sample	Total specific surface area [m <sup>2</sup> /g]	External specific surface area [m <sup>2</sup> /g]	Total pore volume [cm <sup>3</sup> /g]	Average pore width [nm]	Oxygen content, $O_{diff}$ [wt.%]
H <sub>2</sub> -Maxs	2810	2	1.68	1.2	1.5
O <sub>3</sub> (1 h, 0.2 A)-H <sub>2</sub> -Maxs	2760	2	1.65	1.2	3.9
O <sub>3</sub> (1 h, 0.6 A)-H <sub>2</sub> -Maxs	2700	2	1.59	1.2	5.9
O <sub>3</sub> (1 h, 1.1 A)-H <sub>2</sub> -Maxs	2660	1	1.57	1.2	11.4



(a) Normal X axis



(b) Log X axis

**Figure A8.** N<sub>2</sub> adsorption and desorption isotherms at 77 K of Maxsorb III-derived samples prepared under different O<sub>3</sub> concentration.

**Figure A9** shows H<sub>2</sub>O adsorption and desorption isotherms at 298 K.

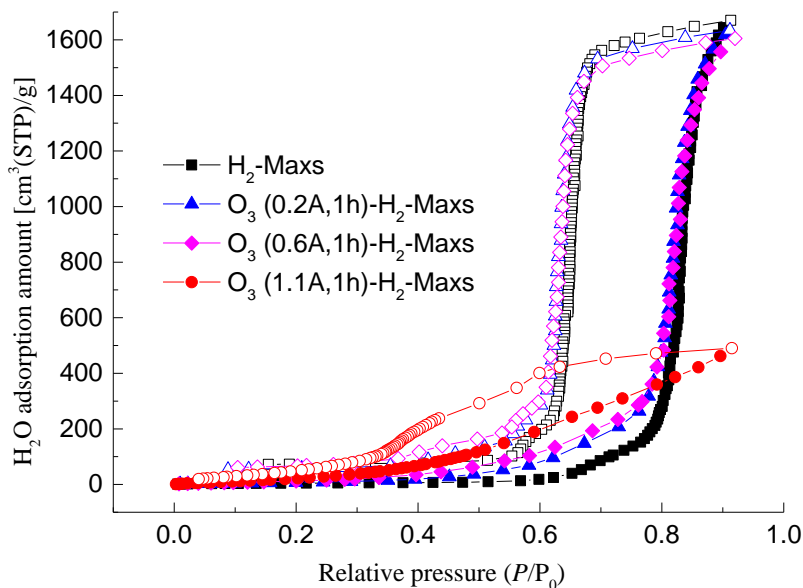


**Figure A9.** H<sub>2</sub>O adsorption and desorption isotherms at 298 K of Maxsorb III-derived samples prepared under different O<sub>3</sub> concentration.

## **A.7 Information to explain the experimental phenomenon**

### **1. Information about the reaction between gaseous O<sub>3</sub> & activated carbon and the degree of *n*-nonane unmasking**

For our samples, more or less, the decreases of specific surface area and pore volume were more remarkable for the pre-masked samples under the same ozonation period (both 1-h and 3-h groups) as shown in **Table A6**. It was contrary to the expectation that the O<sub>3</sub>-H<sub>2</sub>-B17 samples should have a smaller specific surface area than the corresponding O<sub>3</sub>-nonane-H<sub>2</sub>-B17 ones.

Firstly, there is a possibility that a tiny part of adsorbed *n*-nonane still remained in narrow pores even after the unmasking process. In fact, ref.-B17 showed small decreases in both specific surface area and pore volume as compared with H<sub>2</sub>-B17. However, the degree of porosity loss in ref.-B17 was obviously less than that in O<sub>3</sub>-nonane-H<sub>2</sub>-B17. In addition, the N<sub>2</sub> adsorption isotherms at 77 K of these samples almost overlapped with each other even in the range of very low relative pressure (which can be clearly observed in **Figure 3.7**). It indicated that the porosity loss resulted from remained *n*-nonane was negligible in our samples. Therefore, we consider that the smaller specific surface area and pore volume of O<sub>3</sub>-nonane-H<sub>2</sub>-B17 than those of O<sub>3</sub>-H<sub>2</sub>-B17 were mainly caused by the ozonation.

Secondly, if the loss of porosity was mainly due to the ozonation, we tentatively hypothesize the unexpected differences in porosity loss as a result of the different resistance of pores against O<sub>3</sub> oxidation depending on their pore size. It has been reported that O<sub>3</sub> preferentially reacted with mesopores than micropores [1]. With the same dose, for O<sub>3</sub>-nonane-H<sub>2</sub>-B17, all O<sub>3</sub> molecules reacted with mesopores whose walls are supposed to be more fragile than those of micropores, causing a corruption of mesopores. On the other hand, for O<sub>3</sub>-H<sub>2</sub>-B17, we think that a part of O<sub>3</sub> molecules were “assigned” to react with micropores which have higher resistance, giving rise to lower level of the oxidative corruption of mesopores.

As the influence of pore size on surface modification degree of O<sub>3</sub> treatment is an interesting research topic, we believe that in the future it should be studied in detail as a discussion for surface modification method.

### **2. The information helpful to explain of H<sub>2</sub>O adsorption phenomenon (adsorption amount): Strength (concentration) of introduced oxygen-containing surface functionalities on H<sub>2</sub>O adsorption phenomena**

As shown in **Figure A10**, the higher the oxygen content (more hydrophilic surface functionalities), the more the adsorption amount of H<sub>2</sub>O at high relative pressure (for example, at about  $P/P_0 = 0.9$ ), if we compare two non-masked samples (O<sub>3</sub>-H<sub>2</sub>-B17) and two pre-masked ones (O<sub>3</sub>-nonane-H<sub>2</sub>-B17), respectively. The phenomenon, was also observed in the 3-h O<sub>3</sub> treated sample pairs: pre-masked O<sub>3</sub>-nonane-H<sub>2</sub>-B17 with lower oxygen content showed larger adsorption amount of H<sub>2</sub>O, as compared with O<sub>3</sub>-H<sub>2</sub>-B17 at about  $P/P_0 = 0.9$ . From the aspect of “strength” of the introduced oxygen-containing groups, we tentatively hypothesize the possible reason as follows.

We used the same ozonation conditions, that is, the same dose of O<sub>3</sub>. In the case of O<sub>3</sub>-H<sub>2</sub>-B17, the O<sub>3</sub> molecules hydrophilized the surfaces of both narrow pores and wide pores. On the other hand, all O<sub>3</sub> molecules focused their “attack” only on wide pores because the pre-masked narrow pores were inaccessible, giving rise to the higher hydrophilization degree of wide pores in O<sub>3</sub>-nonane-H<sub>2</sub>-B17 than that in O<sub>3</sub>-H<sub>2</sub>-B17. As the total pore volume of samples in this study was more attributed from wide pores than narrow ones, the well-hydrophilized wide pores of O<sub>3</sub>-nonane-H<sub>2</sub>-B17 might give the larger adsorption amount of H<sub>2</sub>O as compared with O<sub>3</sub>-H<sub>2</sub>-B17. **Figure A11** gives the schematic diagram of such phenomenon.

It is a very interesting topic of adsorption science and worth to be carefully investigated as an independent research topic using various porous carbon materials in the future.

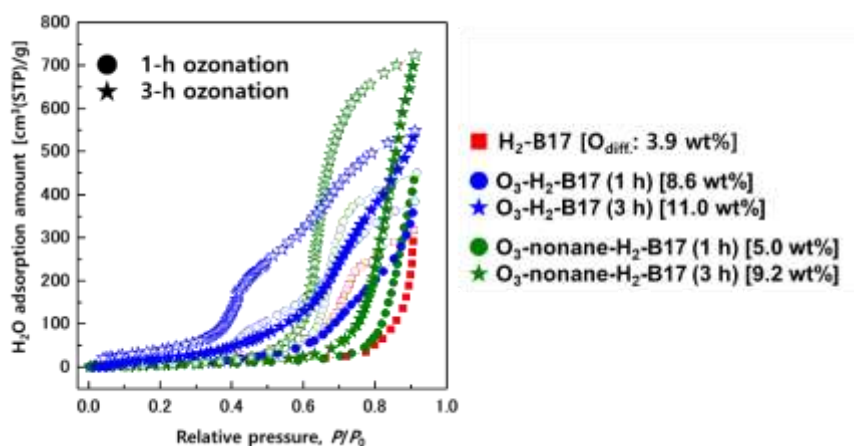


**Figure A10.** H<sub>2</sub>O adsorption and desorption isotherms of B17C600A1000K6-derived samples at 298 K.

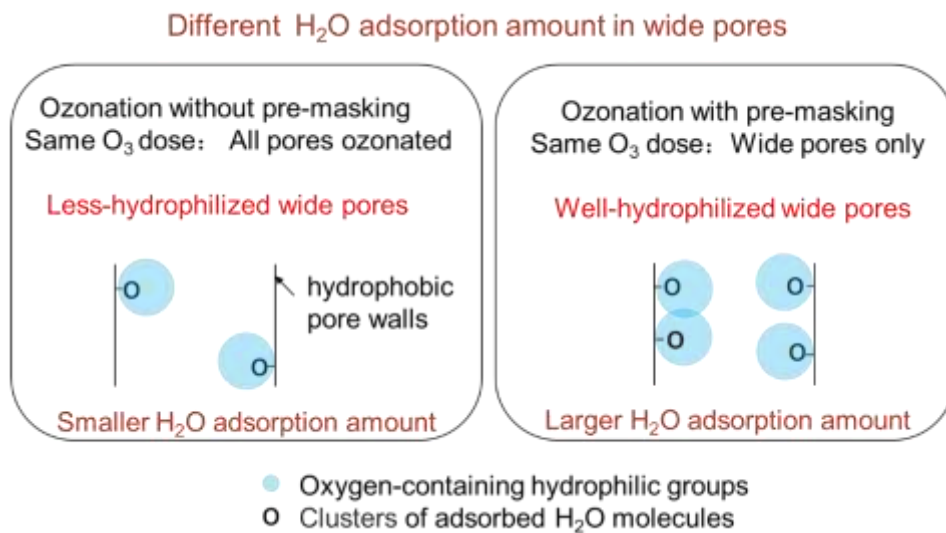


**Figure A11.** How the hydrophilization degree (amount of introduced oxygen-containing groups) of pore surface influence the H<sub>2</sub>O adsorption amount.

## References

- [1] Rivera-Utrilla J, Sánchez-Polo M, Gómez-Serrano V, Álvarez PM, Alvim-Ferraz MCM. Activated carbon modifications to enhance its water treatment applications. An overview. *J Hazard Mater* 2011;187:1–23.

## Chapter 5 General conclusions

Porous carbon (activated carbon), a versatile material as sorbents and storage media, catalyst/catalyst supports, electrodes, etc., was investigated here from the two main aspects, porosity and surface chemistry, that largely govern its properties and performance. Both are tunable to make porous carbon an attractive and promising material.

As for the porosity, the controlling the specific surface area, pore volume, and more importantly, the pore size distribution (PSD) are the keys to improve the performance in many applications. To narrowing the commonly PSD in activated carbons, a more homogeneous activation process was aimed by multistep activation. KOH second-step activation with and solution mixing method and/or lower heating rate induced uniform distribution of activating agent on overall carbon surface in already introduced micropores of once-activated starting sample. By carefully adjusting the mixing and activation conditions in second activation, development of AC with narrow PSD centered at optimized average pore size, which exhibits maximized effective adsorption amount, is highly expected.

Together with the porosity, the other key aspect, surface chemistry governs the performance especially for porous carbons working as catalyst support/catalyst and adsorbents. Although there are abundant methods to realize entire-surface modifications, ideally, to exhibit the best performance, each pore should have its own custom surface property depending on its size. Based on the molecular pre-masking, a three-step pore-size-selective surface modification strategy was proposed, and demonstrated to be effective to selectively introducing specific surface-bound species into pores within a desired pore size range. As the first demonstration, *n*-nonane was chosen as pre-masking agent and room-temperature ozonation as modification method. What's more, the controllability and universality of this strategy were further verified by adjusting the pre-masking degree through 1) Different vacuuming heating temperature,  $T_{VH}$ , for the removal of excess adsorbed *n*-nonane; 2) Other pre-masking agents with different boiling point; and by applying this method to a commercial microporous activated carbon. The controllability of the proposed strategy allows a flexible and precise control of the pore size range that the pores whose size falls within it are to be selectively surface modified. By employing a variety of molecular masking agents and/or surface-modification methods, based on the proposed set of criteria, thereby allowing the design of specific surface properties in pores within a desired pore size range. Therefore, diversified surface properties are able to simultaneously appear within random target pore-size ranges.

By combining the porosity control (especially PSD control) and pore-size selective surface modifications, we can customize a porous carbon material with a proper porosity and designed multi-surface-properties co-existing within the different target pore size ranges, respectively. the performance of such a porous carbon (activated carbon) for their application in catalyzing and adsorption fields will be checked and an obvious performance-upgrade was largely expected. What's more, new functionalities of customized porous carbon can be exploited.

## Acknowledgements

I'd like to express my gratitude to my supervisor, Prof. Jin Miyawaki, an interesting person having his own insistences, like climbing the steps instead of elevator, use the air conditioner only when room-temperature climbed up to 30°C; and his well-known obsession to Ebisu beer. I have to say that the Ebisu is indeed a bit bitter to me in my age, but from him, I learned his many insistences in research, and the way he get up with nice ideas as a researcher. To me, he is not just a supervisor who helped me a lot to get a Ph.D. degree, but also an impressive friend in daily life.

Dr. Hyun-Sig Kil, my gentle and kind senior, he gave me many supports and selflessly shared many considerations and tips in doing experiments in my first year of doctor course. Without him, I couldn't independently finish my research smoothly.

Other lab members also gave me help in their own ways and in every sense. I will keep what I learned or was reminded in mind.

I will always remember the company of the cats with diverse "personalities" in campus and the good time we spent together. From them, I learned a lot.

The biography of Vincent Willem van Gogh also accompanied me when I was writing the draft of this dissertation. From the protagonist, once again, I realized and derived the power of the sincerity and "awkward" endeavors.

Most of all, I'd like to give my thanks to my parents. Although I think they may not fully understand my insistence of being a researcher, maybe nor myself at the beginning, they chose to give me full support to get an "entrance ticket" to the fantastic world of academic research.

August 28, 2020  
YU Yao